NEW METHODS FOR NULL STEERING IN THE FIELD OF ADAPTIVE BEAMFORMING

By

MUHAMMAD ZAFAR ULLAH KHAN
Reg. No. 13-FET/PhD (EE)/F07

A dissertation submitted to I.I.U. in partial fulfillment of the requirements for the degree of

DOCTOR OF PHILOSOPHY

Department of Electronic Engineering
Faculty of Engineering and Technology
INTERNATIONAL ISLAMIC UNIVERSITY
ISLAMABAD

2014

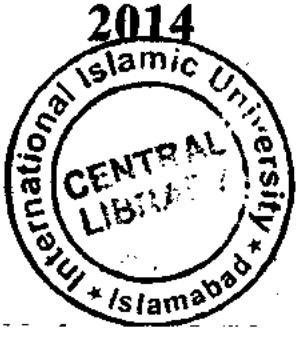

Adaptive control system

Intelligent control system

DEDICATED TO

My Parents, Teachers,
Wife and Children

CERTIFICATE OF APPROVAL

Title of Thesis:	New Methods for Null Steering in the Field of Adaptive Beamforming
Name of Student:	Muhammad Zafar Ullah Khan
Registration No:	13-FET/PHDEE/F-07

Accepted by the Department of Electronic Engineering, INTERNATIONAL ISLAMIC UNIVERSITY, ISLAMABAD, in partial fulfillment of the requirements for the Doctor of Philosophy Degree in **Electronic Engineering**.

Viva Voce Committee

Dr. Muhammad Usman (External Examiner)
DCM, AWC, Wah Cantt.

Dr. Aamer Saleem Chaudhry (External Examiner)
Associate Professor
Department of Electrical Engineering,
University of Lahore, Islamabad

Dr. Muhammad Amir (Internal Examiner)
Chairman, Department of Electronic Engineering
International Islamic University, Islamabad

Prof. Dr. Aqdas Naveed Malik (Supervisor)
Dean, Faculty of Engineering & Technology
International Islamic University, Islamabad

Thursday, 27th March, 2014

ABSTRACT

In this dissertation two categories of adaptive beamforming algorithms have been studied. In first category the adaptive beamforming has been applied for null steering whereas in second category it has been applied for direction of arrival mismatch problem to avoid performance degradation of the beamformers. New algorithms have been contributed in both categories.

In case of first category a specific structure has been proposed which provides independent steering of all the available nulls present in the radiation pattern of an array antenna. The idea is based on decoupling of the complex weights employed with each antenna element to provide adaptively by controlling their values. This results in a proposed specific structure. The proposed structure is further improved by incorporating sidelobe suppression capability. Second Order Cone Programming has been used to get the appropriate set of weights to be utilized in the proposed structure. Similarly, the method for improving beam symmetry around the desired signal direction is also incorporated. These additional features are included over the cost of number of steerable nulls. A tailored Genetic Algorithm is proposed to compute the weight vector required to incorporate the proposed structure for beam symmetry.

The second part of dissertation is meant for the second category of adaptive beamformers applied for direction of arrival mismatch problem. Performance of these beamformers degrades severely whenever there is a mismatch between the presumed and actual direction of desired signal impinging on an antenna array. A Robust Generalized Sidelobe Canceller has been proposed in this domain as remedial measure to restore the performance. The major advantage of proposed algorithm is that it provides improved results without broadening the main beam. This feature is an

added advantage in comparison with the previously existing techniques. For this purpose the blocking matrix present in GSC has been modified without disturbing the quiescent weight vector. This results in robustness against signal look direction error without broadening the main beam. The simulation results confirm the improved performance of the beamformer.

Another approach in this domain is based on diagonal loading of signal and data covariance matrices, involved in subsequent computations. The amount of this diagonal loading level is very critical which must not exceed a specific level to ensure the positive definite behavior of signal covariance matrix. This is a standard requirement for the convergence of existing general rank algorithms. Currently, there exists no reliable criterion for deciding the amount of diagonal loading level. In this context a new algorithm has been contributed to decide the amount of diagonal loading. Proposed algorithm is iterative in nature and uses the beam symmetry around the presumed signal direction to decide the level.

LIST OF PUBLICATIONS

[1] **Z. U. Khan**, A. Naveed, I. M. Qureshi, and F. Zaman, "Independent Null Steering by Decoupling Complex Weights," *IEICE Electronics Express*, vol. 8, no. 13, pp. 1008-1013, July 10, 2011. **ISI Impact Factor Journal**

[2] **Z. U. Khan**, A. Naveed, I. M. Qureshi, and F. Zaman, "Robust generalized sidelobe canceller for direction of arrival mismatch," *Archives Des Sciences*, vol. 65, no. 11, pp. 483–497, Nov. 2012. **ISI Impact Factor Journal**

[3] **Z. U. Khan**, A. Naveed, A.Safeer, and F. Zaman, "Diagonal loading of robust general-rank beamformer for direction of arrival mismatch," *Research J. Applied Sc., Eng., Tech.* vol. 5, no. 17, pp. 4257-4263, May, 2013.

[4] **Z. U. Khan**, A. Naveed, I. M. Qureshi, and F. Zaman, "Comparison of Adaptive Beamforming Algorithms Robust Against Directional of Arrival Mismatch," Journal of Space Technology, vol. 1, 28-31, 2012.

[5] F. Zaman, I. M. Qureshi, A. Naveed, and **Z. U khan**, "Real Time Direction of Arrival Estimation in Noisy Environment Using Particle Swarm Optimization with Single Snapshot," *Research Journal of Applied Sc., Engineering & Tech.*, 4(13): pp. 1949-1952, Jul 2012.

[6] Fawad Zaman, I.M.Qureshi, A. Naveed,and **Z.U. Khan** , "Joint Amplitude, Range and Direction of Arrival Estimation of near Field Sources using Hybrid Differential Evolution and Hybrid Particle Swarm Intelligence," Archives Des Sciences, vol. 65, pp. 671-685, 2012.

[7] Shahid Mehmood, **Z.U Khan** and Fawad Zaman "Performance Analysis of the Different Null Steering Techniques in the Field of Adaptive Beamforming" *Research Journal of Engineering and Technology (Maxwell Scientific organization)*, vol. 5(15) pp. 4006-4012, 2013.

[8] Fawad Zaman, J. A. Khan, **Z.U.Khan**, and I.M.Qureshi, "An application of hybrid computing to estimate jointly the amplitude and Direction of Arrival with single snapshot," Presented in IEEE, 10th-IBCAST, 15-19 Jan, 2013, pp. 364-368.

[9] Fawad Zaman, I.M.Qureshi, Fahad Munir and **Z.U. Khan**, "4D parameters estimation of plane waves using swarming intelligence," Chinese Physics B, vol. 23, no.7, 0784028, 2014. **ISI Impact Factor Journal**

[10] Fawad Zaman, I.M.Qureshi, A. Naveed,and **Z.U. Khan**, "An Application of Artificial Intelligence for the Joint Estimation of Amplitude and Two Dimensional Direction of Arrival of far field sources using 2-L shape array," International Journal of Antennas and Propagation, Article ID 593247, 10 pages, vol. 2013. **ISI Impact Factor Journal**

[11] Fawad Zaman, I.M.Qureshi, A. Naveed,and **Z.U. Khan**, "joint estimation of amplitude, direction of arrival and range of near field sources using memetic computing" *Progress in Electromagnetic research-C (PIER-C)* ,vol. 31, pp. 199-213, 2012. **Indexed in Elsevier's SCOPUS and Compendex**

LIST OF SUBMITTED PAPERS

[1] **Z. U. Khan**, A. Naveed, I. M. Qureshi, and F. Zaman, "Sidelobe Suppression with Null Steering by Independent Weight Control," *IEEE Trans. Antennas Prop.* **ISI Impact Factor Journal**

[2] S. Azmat Hussain, A.Naveed, **Z. U. Khan**, I. M. Qureshi, " Spectrum Sharing in Cognitive radio using GSC with suppressed sidelobes," International Journal of Distributed Sensor network (Hindawi Publication), **ISI Impact Factor Journal**

[3] Fawad Zaman, I.M.Qureshi, M. Zubair, and **Z.U. Khan**, "Multiple target localization with bistatic radar using heuristic computational intelligence" Paper key: 13052307, PIER, 2013. **ISI Indexed**

[4] Fawad Zaman, I.M.Qureshi, A. Naveed, and **Z.U. Khan**, "Hybrid Differential Evolution and hybrid Particle swarm optimization for the joint estimation of amplitude and Direction of Arrival of far field sources using L shape arrays," *Iranian journal of Science and Technology, Transaction of Electrical engineering,* Paper key: 1311-IJSTE, 2013.**ISI Impact Factor Journal**

ACKNOWLEDGEMENTS

I humbly thank Almighty Allah, the most gracious and merciful Who blessed me much more than my wishes. I offer my praises to Hazrat Muhammad (Peace be upon him) whose life is the glorious model for humanity.

I present my sincere thanks and appreciation to my supervisor Dr. Aqdas Naveed Malik who's continuous and motivating guidance, beneficial suggestions and affectionate supervision remained with me throughout the research work.

I offer special thanks to Dr. Ijaz Mansoor Qureshi who has the role of a grandfather in our research group. Despite his hyper-dimensional commitments, his dynamic guidance was always with me. I would like to thank the teachers like Dr. Aamer Saleem Ch., Dr. T. A. Cheema and Dr. Ihsan Ul Haq for their collaboration during my PhD studies.

I am thankful to university administration for kind cooperation and administrative support. I acknowledge the role of Higher Education Commission of Pakistan to uplift education standards in the country. I also acknowledge my departmental policy to facilitate the employees for higher studies.

I am greatly thankful to my foreign evaluators Dr. Ibrahim Develi, Erciyes University Kayseri, Turkey, and Prof. Dr. Amir Hussain, University of Stirling, UK for their significant suggestions and corrections to refine this research work.

I am really grateful to my retired director Mr. Khawar Javaid and Director Incharge Mr. Saud Saeed Akhtar for their generous cooperation in my studies. I am also greatly indebted to my Dy. Director Dr. Arshad Munir for his encouraging behavior towards research.

I have no words to thank Mr. Fawad Zaman for his sincere suggestions and help in this research work. I offer my sincere gratitude to my group fellows, Mr. Muhammad Siddique, Mr. Ishtiaq Akbar, Mr. Azmat Ali Shah and Mr. Shahid Mahmood whose good wishes enabled me to complete my studies successfully.

I have no words to express my sincere feelings to my parents who always wished for my qualification improvement and success. I also cannot forget the sincere wishes and prayers of my father-in-law Mr. Rao Ashiq Ali for the completion of my PhD.

I am proud of expressing my gratitude to my wife for performing additional responsibilities and encouraging behavior during my studies. I have good wishes for her and our children.

(Muhammad Zafar Ullah Khan)

TABLE OF CONTENTS

LIST OF FIGURES

LIST OF TABLES

LIST OF ABBREVIATIONS

ACO	Ant Colony Optimization
AF	Array Factor
AGC	Automatic Gain Control
AOA	Angle of Arrival
AWGN	Additive White Gaussian Noise
DE	Differential Evolution
DL	Diagonal Loading
DLL	Diagonal Loading Level
DOA	Direction of Arrival
ESA	Electronically Scanning Array
ESPIRIT	Estimation of Signal Parameters via Rotation Invariant Techniques
FPON	Fully Phase Only Null Steering
GA	Genetic Algorithm
GSC	Generalized Sidelobe Canceller
INR	Interference to Noise Ratio
INS	Independent Null Steering
LCMV	Linearly Constrained Minimum Variance
LMS	Least Mean Square
LSMI	Loaded Sample Matrix Inversion
MUSIC	Multiple Signal Classification
MVDR	Minimum Variance Distortionless Response
NLMS	Normalized Least Mean Square
NS	Null Steering
OA	Optimal Adaptive
PPON	Partially Phase Only Null Steering
PSD	Positive Semi-definite
PSO	Particle Swarm Optimization
RFID	Radio Frequency Identification
RGSC	Robust Generalized Sidelobe Canceller
RLCMV	Robust Linearly Constrained Minimum Variance
SINR	Signal to Interference Plus Noise Ratio

SL	Sidelobe
SMI	Sample Matrix Inversion
SNR	Signal to Noise Ratio
SOI	Signal of Interest
SSLs	Suppressed Sidelobes
SVD	Singular Value Decomposition
ULA	Uniform Linear Array

LIST OF NOTATIONS

α	Progressive Phase Shift
B_i	Real weight for i^{th} null steering
$\mathbf{a}(\theta)$	Steering vector in the direction θ
$\mathbf{a}(\theta_s)$	Steering vector in the desired signal direction
J	Cost function
$\mathbf{R}_{i+n}$	Interference plus noise covariance matrix
$\mathbf{R}_s$	Signal covariance matrix
$\mathbf{R}_y$	Received signal covariance matrix
$\hat{\mathbf{R}}_y$	Estimated value of received signal covariance matrix
$\mathbf{R}_v$	Noise covariance matrix

CHAPTER 1

ADAPTIVE BEAMFORMING: AN OVERVIEW

Adaptive Beamforming is the branch of signal processing that has got applications in the field of wireless communications, radar, sonar, seismology, mobile communication and medical imaging etc [1]-[7].

A beamformer uses an array of sensors to perform spatial filtering for detection and enhancement of the signal arriving from desired direction in the presence of interferences and noise. This spatial filtering separates signals with overlapping frequency but different spatial locations.

The important areas of research in Adaptive Beamforming such as Time efficient Null Steering, Sidelobe Suppression, and Robustness against signal look direction error are the targets of this dissertation.

1.1 NULL STEERING

Null steering has been an important area of research in adaptive beamforming and is yet significant due to an increasing pollution of the electromagnetic environment. It aims to cancel out the plane waves arriving to the antenna from undesired directions by placing nulls in the array response pattern along those directions. In response of null steering, the main beam remains undistorted and keeps on pointing in the desired signal direction.

A continuous aperture antenna cannot steer the main beam electronically instead it requires mechanical movement. An adaptive array antenna system however, provides the capability of null steering and at the same time it also guarantees that the main beam keeps on pointing in the desired direction. This is achieved by searching an appropriate set of weights for the array elements. That is why an antenna array is an integral part of adaptive beamformer.

Synthesizing broad nulls or steering relatively sharp nulls in the array pattern are the techniques which are imperative in a specific situation i.e. when the direction of arrival of interferences may vary slightly with time [8]. The adaptive array can respond to such a time-varying environment by adaptive control of either the individual element or a set of auxiliary (selected) elements. In case of adaptive control of individual element, the array is called fully adaptive while the array with selected elements is called partially adaptive [9]. In case of partially adaptive array, the selected elements may be subdivided and controlled in groups known as sub-arrays.

The Adaptive control of elements provides the desired degree of freedom necessary for synthesizing array pattern having nulls to cancel out all the interferences. Null steering is basically the process of shifting the null to a new direction/angular position to encounter the angular movement or angular repositioning of the undesired signals. Null steering can be achieved by the proper weighting of the array elements while guaranteeing that the signals from desired direction are received un-distorted without attenuation. Null steering techniques are required to be adaptive due to the reason that the direction of desired signal or interferences may not be known a priori. Moreover the directions may be varying with time due to the relative motion of the array and sources. Adaptive null steering algorithms can broadly be classified into two catagories on the basis of weight adjustment criteria,[10] namely

1. Direction of Arrival Based Algorithms
2. Optimal Adaptive Beamforming Algorithms

Direction of Arrival Based Algorithms: These algorithms require direction of arrival (DOA) of both the desired signal and the interferences for their adaptive weight control. Unlike optimal adaptive beamformers, these algorithms do not face the signal cancellation problem and are less sensitive to convergence issues. They need array calibration and precise knowledge of DOA of the sources impinging on the array.

Optimal Adaptive Beamforming Algorithms: These algorithms keep on adjusting the weights of the beamformer based on the signal at the array output and do not require the knowledge of DOA of interferences. These algorithms are more flexible and

robust against interference compared to DOA based algorithms. However, they face signal cancellation problem when there is even a slight mismatch between the presumed and the actual direction of the desired signal [11]. Optimal Adaptive beamformers have complicated structure and are expensive than their counterpart.
The following section presents a detailed overview of the development of DOA Based Adaptive Beamforming Algorithms and Optimal Adaptive Beamforming Algorithms.

1.1.1 DIRECTION OF ARRIVAL BASED BEAMFORMERS

DOA Based Algorithms utilize some direction finding techniques to estimate direction of arrival of signal of interest (SOI) and all the interferences impinging on the antenna array from different sources. This DOA information is then processed by the algorithm to adjust any or both of the following parameters to create the main beam in the desired direction and to place nulls in the direction of interferences [12].

1. The relative position of the elements.
2. The set of elemental weight.

Since direction finding techniques are also considered a subclass of beamforming, so first we have a look on these algorithms.

Direction Finding Techniques: MUSIC, ESPIRIT and their variants are the popular direction finding techniques [13]-[15]. Both the algorithms are computationally heavy because they require twice the number of snapshots as compare to the number of elements in the array [16]. Matrix Pencil method is time efficient that works on complex data of single snapshot [17] and uses singular value decomposition technique (SVD) for DOA estimation. SVD with complex data is time expensive. Unitary matrix pencil method reduces the computational burden to one fourth by converting the complex data matrix into real [18]. Another method for the conversion of the complex data matrix into real one is the Beam Space Method [19] that further reduces the computational burden. H. Karim and M. Viberg present various signal parameter estimation techniques and their performance comparison in [20].

Recently, efficient direction finding algorithms are being developed that utilize heuristic approaches on single snapshot [21]-[23]. Direction finding algorithms belong to the family of 'Optimal Adaptive Beamforming Algorithms'. The rest of the work is focused on different null steering techniques.

Elemental Position Algorithms: These null steering techniques are available with fully and partially adaptive arrays. Fully adaptive arrays are slow due to the movement of all the elements [24], [25]. Fast partially adaptive algorithms, hence developed, move the selected elements for null steering [26], [27]. Modern position perturbation null steering algorithms utilize meta-heuristic and hybrid meta-heuristic approaches [28] [29]. Both fully and partially adaptive position perturbation null steering techniques are slow for large arrays because new position perturbations of the elements are required to be recalculated even if the change in position of a single interference takes place. Furthermore, the techniques are efficient as long as the number of nulls is small as compared to the number of sensors in the array. Another drawback with these techniques is the requirement of servo-motors for the movement of each element.

Adaptive Weight Control Algorithms: These algorithms are the counterpart of elemental position perturbation techniques for array pattern synthesis. The adaptive weight can be real, imaginary or complex. That is why the popular adaptive weight control methods include controlling the excitation amplitude, the excitation phase and the complex weights having both the amplitude and the phase control.

Schelkenoff polynomial is a popular method for synthesizing array pattern with nulls along desired directions [30]. It utilizes both amplitude and phase excitations, that is the complex weights for the pattern synthesis. In this case, the array factor is considered as a polynomial whose roots are located on the unit circle in the complex weight plane. The method is computationally heavy, especially for large arrays with the inherent problem, that is, the whole set of elemental weights is required to be recalculated even if a single jammer changes its position.

Phase-Only Algorithms: In 1979, E. Mendelovicz and E. T. A. Oestreich presented the Phase-only adaptive nulling with discrete value, [31]. An electronically scanning array (ESA) that varies only the phase of the elements in discrete steps is used to obtain optimal phase settings for jammer cancellation. Giusto and Vincenti presented the phase only pattern nulling method for a phased array antenna that generates wide deterministic nulls in the sidelobe region [32]. Another method assumes the phase perturbations to be small so that the nonlinear problem may be linearized to derive an analytic solution by performing Taylor expansion of the array factor (AF). For this algorithm, the number of nulls must be much less than the number of array elements. Another problem with this algorithm is that it is incapable of cancelling a pair of interferences that are perfectly symmetrical about the main beam [33]. Cancellation of such interferences is possible if the phase perturbations are not restricted in size. Shore devised the computational method for obtaining phases required for symmetric nulling using nonlinear programming techniques [34].

Su showed that a couple of phases must be adjusted to achieve null steering [35]. In a situation when a couple of phases cannot form deep nulls in some directions, pattern with deep null steering can be achieved by adjusting more couples of phases.

D-C. Chang et al. showed the superiority of partially phase-only null steering (PPON) over full phase-only null steering (FPON) for a large phase array antenna equipped with low resolution phase shifters because the desired change in phase for PPON is larger than FPON [36]. This relatively large change in phase can be incorporated with available low resolution phase shifters.

Amplitude Control Algorithms: In 1977, Hicks presented amplitude control technique for null steering in linear arrays [37]. His system is capable of steering all of the available nulls independently in an array of any size.

Vu, in 1984 introduced another method in which he forced the zeros of the array factor to occur in conjugate pairs [38]. Under this condition, the coefficients of the array factor polynomial become real and symmetric about the center of the array. The advantage of this symmetry is that the half of the coefficients is required to be

calculated and also the null steering is carried out using real weight control. Thus Vu dedicated phase shifters for the steering of the main beam only and the null steering was carried out by controlling the real weights. His technique computes the coefficients iteratively, however, computation time is reduced to half due to symmetry of the coefficients. The price paid for this time efficiency is that the number of steerable nulls becomes less than half of the number of elements in the array.

Double Symmetry of Coefficients: Vu introduced another method [39] that introduces double symmetry of the coefficients about the center of the array to reduce the number of coefficients to quarter and the coefficients are calculated directly i.e. without using any iteration. The price for this achievement is the reduction in the number of steerable nulls that becomes slightly less than quarter of the number of antenna elements in the array.

Structure Based Algorithms: Ibrahim presented a structure [40] that provides independent null steering with real weight control in a number of stages. The technique combines three consecutive outputs of the previous stage by applying an adaptive weight on the central one. For a particular stage, the set of adaptive weights corresponds to the steering of a particular null and each member of the set has the same value. The major contribution of this technique is that if a single jammer changes its position, only the set of weights in the corresponding stage is required to be readjusted. The problem with this technique is that the steerable nulls are reduced to slightly less than half of the total number of elements in the linear array. Another technique presented in [41] regarding independent steering of maximum number of available nulls by decoupling complex weights is a recent development in the field. The previous stage outputs are combined in a group of two with an adaptive weight on one of them. The set of weight for a stage is responsible for steering of a particular null and each member of the set of weights for that particular stage has the same value.

Recently, meta-heuristic optimization techniques have been widely used for phase-only, amplitude-only, and complex weights adjustment and also elemental position

perturbations. These techniques include the evolutionary computing based algorithms such as Genetic Algorithms (GAs), Particle Swarm Optimization (PSO), Ant Colony Optimization (ACO), Differential Evolution (DE), TABU Search Algorithm, and Clonal Selection Algorithm [8], [42]-[47]. Hybrid approaches for these algorithms are also available in the literature. These techniques provide null steering with suppressed sidelobes but the number of steerable nulls is much less than the number of elements in the array.

1.1.2 OPTIMAL ADAPTIVE BEAMFORMERS

These beamformers do not require the direction of arrival of interferences for their operation. Optimal adaptive weight vector is determined by minimizing a cost function. This cost function is inversely proportional to the performance of the beamformer [48] and the minimization of the cost function maximizes the quality of signal of interest.

History of OA Beamformers: The history of optimal adaptive beamformers dates back to adaptive arrays which had been a growing and attractive field for the researchers in 1960s. At that time, retrodirective systems and self-steering or self-focusing arrays were the major advancements in antenna systems called adaptive arrays [49]. Those adaptive array systems were mainly based on phase-lock loops and phase-conjugate network schemes.

Retrodirective Arrays: Retrodirective systems were used to radiate a wave in the direction of a received wave without a priori knowledge of its direction [50], [51]. Van Atta array is their simplest form. Unlike conventional phased-array antennas where beam steering is carried out by exciting the elements with phase shifters, retrodirective arrays steer their beams automatically without need for any computationally heavy algorithms or hardware based phase shifters [52]. Retrodirective arrays after years are still equally important due to their unique feature i.e. automatically responding in the direction of a pilot signal. They have got application for automatic pointing and tracking systems, radar, radiofrequency

identification (RFID), solar power satellites, microwave power transmission, crosslink for small-satellite networks and complex communication systems.

Adaptive Interference Cancellation: Adaptive interference nulling capability was not available in the open literature since 1964. Howells Intermediate Frequency Sidelobe Canceller [53] is a major achievement towards adaptive beamforming. This sidelobe canceller is proficient of receiving a signal and automatically cancelling the effect of a strong jammer. It uses a high gain directional antenna and a low gain Omni-directional antenna for primary and reference inputs respectively. A null is placed in the direction of jammer anywhere in the sidelobe region. The sidelobe canceller was basically developed for the radar applications. Radar signal power density is inversely proportional to the fourth power of distance between the target and the radar, while the jammer power density at the radar antenna is inversely proportional to the square of distance between jammer and radar.

Another major contribution towards adaptive beamforming was made by Applebaum in 1966 [54], reprinted in 1976 Special Issue of IEEE Transactions on Antennas and propagation. He developed the method for adaptively optimizing the SNR of an array antenna. The method is useful when the direction of desired signal is available. Simple hardware and fast convergence time are the main advantages of this algorithm. Cascaded Applebaum arrays and AGC Applebaum algorithm are the variants of this technique to improve the convergence time for the situations when the eigenvalue spread of the input signal covariance matrix is large [55], [56].

LMS Based Algorithms: In 1967, Widrow and his coworkers developed independently an algorithm for weight adjustment in adaptive array antennas by applying adaptive filtering techniques [57]. A pilot signal is used to get the information of the desired response. The weights are adjusted adaptively by error minimization based on the least-mean-squares (LMS) algorithm. This makes the array to be trained so that the main beam is along the desired direction; hence the system has capability of rejecting interferences coming from different directions other than that of the desired source. Griffiths and Frost further improved the LMS algorithm to

retain a chosen frequency characteristic for the array along the desired direction in the presence of interfering noises using a set of linear equality constraints on the weights [58], [59]. To overcome the shortcomings of LMS algorithm, its several variants such as Normalized LMS (NLMS), Newton LMS, and Block LMS have been developed.

MVDR Beamformer: In 1969 Capon proposed a better method for array adaptive weights by minimizing the array output power subject to the linear constraint to guarantee that the desired signal suffers no distortion [60] i.e. distortionless response from the desired direction. The Capon beamformer also known as minimum variance distortionless response beamformer has improved resolution and better interference rejection capability compared to the standard beamformer. The array steering vector corresponding to the SOI is assumed to be precisely known. In practical situation, the knowledge of the SOI steering vector may be inaccurate i.e. there may be the difference between the presumed signal steering vector and the actual signal steering vector. In such situation, the performance of Capon beamformer degrades severely due to the suppression of the SOI as interference. To resolve this problem has been an active area of research in past and is equally attractive for the researchers even in recent years [61], [62].

SMI Beamformer: The sample matrix inversion (SMI) algorithm, developed by Reed et al. in 1974 provides rapid convergence and is an alternative to LMS algorithm. It uses an estimate of the Weiner weight solution to determine the optimum weight vector and overcomes many convergence problems of the optimum adaptive arrays [63]. For this algorithm, the noise covariance matrix must be nonsingular since the inverse of this matrix involves the expression for optimum weight vector.

LCMV Beamformer: Linearly constrained minimum variance (LCMV) is a popular beamforming algorithm first proposed by Frost in 1972 [59]. In 1982, Griffiths and Jim developed Generalized Sidelobe Canceller as an alternative approach to LCMV beamformer [64]. Van Veen and Buckley describe signal processing perspective and overview of optimal adaptive beamformer design [65]. H. Singh and R. M. Jha

provide comprehensive report and performance comparison of various adaptive beamforming algorithms [66].

Due to the development of the above discussed techniques, adaptive antennas had achieved automatic null steering and sidelobe reduction capability in an unknown interference environment while retaining desired signal characteristics [67].

W. F. Gabriel presented a brief review of sidelobe cancellers, fully adaptive arrays and super-resolution techniques in 1992 [68].

Limitations of OA Beamformers: Optimal adaptive (OA) beamformers are data dependent and their optimized weights are function of received data at the array subject to various constraints. The performance of these beamformers may get degraded if the array parameters are disturbed from ideal conditions under which the theoretical development of the system has been considered. Signal look direction error and small sample size are a few examples [61], [62]. [69]. Given the desired signal present in the data snapshots, and a mismatch between the presumed and actual signal direction, the desired signal is treated as interference. In such situation, the desired signal is also cancelled and the performance of the beamformer degrades severely [61], [62]. Efforts are being made to develop robust algorithms to cater for such mismatches.

Robust Beamformers: In [59], [61], [70], [71] (1972 to 1986) linear constraints have been incorporated to mitigate the direction of arrival mismatch problem. However these constraints cause the broadening of the main beam.

Takao and Boon [72] incorporated a notch filter into the conventional GSC that leads to the exclusion of the desired signal component from the beamformer auxiliary input. The auxiliary input is attached with variable weight vector while primary input is attached with fixed weight vector. The variable weights are adjusted to minimize the interfering signals of the primary channel. The proposed notch filter design is complicated and requires a large number of elements. The proposed GSC structure lessens the deviation of adaptive

weights from the optimum value and thus improves the convergence rate. The disadvantage of the structure is its complexity. It requires a sharp notch filter and a slave array for recovery of the desired signal.

Eigen space-based beamformer [73], [74] is another robust adaptive beamforming approach, but it is inefficient at low SNRs.

Robust Minimum Variance Beamforming: R. G. Lorentz and S. P. Boyd presented Robust Minimum Variance beamforming algorithm for direction of arrival mismatch. This algorithm clearly models the uncertainty in the array manifold via an ellipsoid for a particular look direction. The weights are chosen such that the array output power is minimized, subject to the constraint that the gain should exceed unity for all array responses in this ellipsoid [75]. The desired gain in the mismatch region is achieved at the cost of broadening of the main beam.

Robust GSC: Null broadening of blocking matrix for robustness of GSC against signal look direction is another popular approach. In order to avoid the broadening of the main beam, Z. U. Khan et al. proposed to utilize presumed signal steering vector to find quiescent weight vector and a cluster of steering vectors from signal mismatch region for blocking matrix respectively [76].

Robust Diagonal Loading Algorithms: Many techniques such as convex quadratic constraints Bayesian approach [77] and uncertainty set based method [78] have been proposed to mitigate DOA mismatch problem. These approaches belong popular Diagonal loading method that addresses efficiently all types of mismatches including signal look direction error problem [79], [80]. The shortcoming of diagonal loading method is the unavailability of the reliable criteria for choosing the proper loading factor and hence is an active area of research even in recent years [81], [82].

Robust General-Rank Beamformer: This beamformer is important for the situations where propagation effects cause the dispersion of the sources. Such dispersions are of significant interest in radio communication and sonar [83]-[85]. General-rank beamformer [86] incorporates signal look direction error for general-rank signal models and the array imperfections, such as source signal dispersion etc., by explicit

modeling of uncertainties in the desired signal covariance matrix and in the sample data covariance matrix respectively. The beamformer then solves the worst-case optimization based minimum variance problem. The solution results in negative diagonal loading of desired signal covariance matrix and positive diagonal loading of the sample data covariance matrix for robustness against signal look direction error and array imperfections respectively. Negative diagonally loaded signal covariance matrix must remain positive definite for the proper functioning of the algorithm. The expression for the positive definiteness of the negative diagonally loaded signal covariance matrix is given in [87] where diagonal loading level depends on the specified signal mismatch region.

Beam Symmetry Criterion for Diagonal Loading: Another approach presented by Wang and Wu, uses the practical fact that the peak of the main beam moves towards the presumed signal direction for the robust beamformers that utilize positive diagonal loading [82]. Diagonal loading level is increased iteratively till desired compromise on the left-right beam symmetry bout the presumed signal direction is achieved. Z. U. Khan et al. used the same approach for the positive and negative diagonal loading of the general-rank beamformer [88].

1.2 MOTIVATION OF THE THESIS

Linear antenna array provides option to place the main beam in the desired signal direction and nulls in the direction of interferences. The direction of arrival based beamformers can perform null steering by controlling the element positions. These techniques are efficient as long as the steerable nulls are small in number [24]-[29]. Similarly, another drawback of existing techniques is that the new positions of all the elements are needed to be re-evaluated even in case of steering of a single null. That is time consuming and becomes un-affordable when dealing with large arrays.

Though the time efficient techniques for evaluating elemental weights are proposed in [38]-[40] however, the problem with them is the number of steerable nulls which is reduced to less than half of the maximum number of available nulls. Hence the prime

motivation behind this work is the time efficient techniques capable of steering maximum available nulls.

The beam pattern and the sidelobe level for the beamformers depend on the relative position of the interferences. That is the reason for sufficiently low sidelobe level and the symmetry of the beam about the desired signal direction in these parameters are not always guaranteed. To incorporate sidelobe suppression and beam symmetry capabilities in time efficient null steering techniques is an additional motivation of this research.

In case of optimal adaptive beamformers, the direction of arrival mismatch in the presumed and actual signal causes the performance degradation. Robust LCMV based beamformers utilize MVDR with additional constraints in signal mismatch region. This causes the broadening of the main beam which is the major drawback of these beamformers. To devise a robust technique for DOA mismatch without broadening the main beam of LCMV based beamformer is another incentive to this effort.

Another approach for the robustness of the beamformer against signal look direction error is the diagonal loading. Robust General-Rank beamformer utilizes both negative and positive diagonal loading for signal covariance matrix and received data covariance matrix respectively. The negative diagonal loading is meant for robustness against signal look direction error while positive diagonal loading is intended for array imperfections. The suitable diagonal loading criteria is not available in the literature. Hence it is a further motivation to devise some suitable criteria for diagonal loading of Robust General-Rank Beamformer.

1.3 CONTRIBUTION OF THE THESIS

The summary of the contribution of the thesis is as given under

DOA Based Beamformers

1. A new structure for independent null steering by decoupling complex weights has been proposed. This structure is capable of steering the

maximum possible number of nulls, which for an array of N elements, is N-1. The structure is also time efficient due to the reason that if a single jammer changes its position, then only the corresponding set of weight is required to be changed. All the remaining weights are kept unchanged. This work has been published in *IEICE Electronics Express* [41].

2. The above mentioned structure is further improved by incorporating sidelobe suppression capability. The optimization problem to evaluate weight vector for sidelobe suppression is proved to be the second order cone. This weight vector does not need to be re-evaluated and changed as long as the desired signal direction does not change.
3. The proposed structure is further enhanced by introducing improvement in the left-right beam symmetry around the desired signal direction. For this purpose, the weight vector is computed using Genetic Algorithm. A few weights are suggested to be used for this purpose and remaining weights will be available for independent null steering.

Optimal Adaptive Beamformers

1. A new Robust Generalized Sidelobe Canceller (RGSC) is proposed which is an improved version Robust LCMV based GSC. RGSC modifies the blocking matrix of GSC without disturbing quiescent weight vector. This gives robustness against signal look direction error without broadening the main beam. The work has been published in *Archives Des Sciences* [76].
2. An iterative method for diagonal loading of Robust General-Rank beamformer is proposed that utilizes the difference in left-right beam symmetry around the desired signal direction. The negative diagonal loading level is increased iteratively until the difference in left-right

beam symmetry is within the desired limit. Corresponding to the negative diagonal loading level, suitable value of positive diagonal loading level is selected that guarantees the convergence of the algorithm. The work has been published in *Research Journal of Applied Sciences, Engineering and Technology* [88].

1.4 THESIS OUTLINE

The thesis explores the null steering techniques in the field of adaptive beamforming by using adaptive weight control methods for the elemental weights of the array. The techniques are broadly divided into two classes namely, Direction of arrival based beamformers and optimum adaptive beamformers. The thesis layout is as under:

Following the null steering techniques and literature review, chapter 2 describes the mathematical model for direction of arrival based beamformers. Two beamformers of this category, closely related to our research, have also been studied comprehensively.

Chapter 3 deals with our contributions in direction of arrival based beamformers. A new structure based technique for steering the maximum available nulls with independent weight control is presented here. The enhancement in structure capability for sidelobe control and beam symmetry about the desired signal direction is also part of this chapter.

Chapter 4 presents mathematical model for optimal adaptive beamformers and includes some popular beamforming techniques and their performance degradation in case of signal direction of arrival mismatch. Furthermore some robust adaptive beamforming techniques and their limitations are also part of this chapter.

Chapter 5 contributes improvement in two optimum adaptive beamforming algorithms. Firstly, Robust Generalized Sidelobe Canceller for direction of arrival mismatch provides robustness against signal look direction error without broadening of the main beam. Secondly, Diagonal loading of General-Rank beamformer provides an iterative approach, by utilizing beam symmetry, to select proper diagonal loading level.

In Chapter 6, the main conclusions of the thesis and the ideas for future research work are given.

CHAPTER 2

MATHEMATICAL MODEL FOR DOA BASED BEAMFORMERS

DOA based adaptive beamformers are proficient when directions of desired signal and interferences are exactly known. Array adaptive weights are calculated on the basis of the directional information which are used to form main beam along the desired direction and to place nulls in the direction of interferences. The reason behind the name is that instead of actual array output, the directional information of the desired signal and interferences is involved in their weight adaptation criterion. For large arrays, the conventional null steering algorithms are slow to change the complex weights adaptively. This chapter deals with the mathematical model for DOA based adaptive beamformers and presents the comprehensive study of two selected time efficient algorithms of this family. The behavior of the algorithms is demonstrated by simulation of a few illustrative examples. The material presented in this chapter is related to [41] and references therein.

2.1 MATHEMATICAL MODEL

Consider a uniform linear array of N antenna elements with constant inter-element spacing d and progressive phase shift α as shown in Fig. 2.1.

Taking element-1 as reference and let θ be the angle of arrival. The path difference of the impinging wave on adjacent elements is given as:

$$x = d\cos\theta$$

Let the array factor for this arrangement be AF' which is given by [38]

$$AF' = \sum_{i=1}^{N} e^{j(i-1)\psi} \tag{2.1.1}$$

where

$$\psi = \alpha + (2\pi/\lambda) d\cos\theta \tag{2.1.2}$$

Let $e^{j\psi} = z$, then

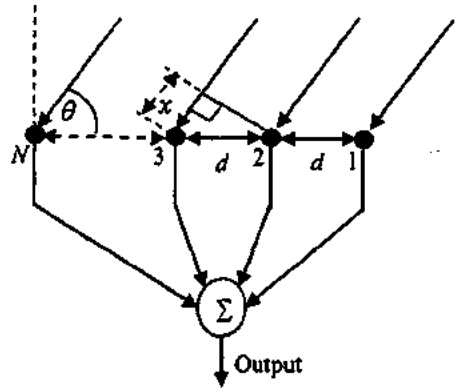

Figure 2.1: An *N*-element uniform linear array with fixed nulls

$$AF' = \sum_{i=1}^{N} z^{(i-1)} = 1 + z + ... + z^{(N-1)} = (1 - z^N)/(1 - z) \tag{2.1.3}$$

In expression(2.1.3), all the roots of $1 - z^N = 0$ except $z = 1$ are the zeros of the array factor and these zeros are equally spaced on the unit circle in the complex plane. The polynomial in expression (2.1.3) is of $(N-1)$ degree and hence with $(N-1)$ roots. It can also be written in factors form as:

$$AF' = \sum_{i=1}^{N} z^{(i-1)} = (z - z_1')(z - z_2')...(z - z_{N-1}') \tag{2.1.4}$$

This means, there exist zeros at $z_1', z_2', ..., z_{N-1}'$ and these zeros correspond to nulls in the pattern along fixed directions $\theta_1', \theta_2' ... \theta_{N-1}'$. It must be noted that for equation(2.1.4), if $\alpha = 0$ then the beam-pointing direction will be perpendicular to the line joining the elements of the array (along the broad side to the array) because the output of each element will be added without applying any delay or gain [89].

In order to steer nulls along arbitrary directions $\theta_1, \theta_2 ... \theta_{N-1}$, the array factor should be modified as shown in Fig. 2.2 and is given in relation(2.1.5).

$$AF = A_0 + A_1 z + ... + A_{N-1} z^{(N-1)} \tag{2.1.5}$$

This array factor is also a polynomial of degree $(N-1)$ and has $(N-1)$ adjustable

roots dependent on the suitable selection of coefficients $A_0, A_1, ..., A_{N-1}$. These coefficients (weights) correspond to the excitation of each element in the linear array and are complex quantities in general. In factorized form (2.1.5) can be written as

$$AF = (z - z_1)(z - z_2)...(z - z_{N-1}) \tag{2.1.6}$$

Where $z_1, z_2, ...z_{N-1}$ are the zeros on the unit circle in the complex plane and their position on the circle depends on the coefficients $A_0, A_1, ..., A_{N-1}$. Expression (2.1.6) is the basic tool for array pattern synthesis [90].

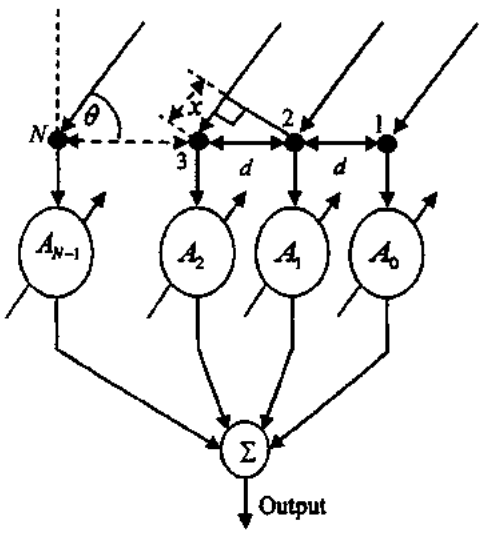

Figure 2.2: An *N*-element uniform linear array with steerable nulls

The progressive phase shift α is meant for steering of the main beam in the desired direction and is given as under

$$\alpha = -(2\pi / \lambda) d \cos\theta_s \tag{2.1.7}$$

In above expression, θ_s represents the desired direction of the main beam.

In expression(2.1.5), z is dependent on inter-element spacing d. To achieve null steering solely by the coefficients $A_0, A_1, ..., A_{N-1}$, we limit the inter-element distance to $d = \lambda/2$.

2.2 NULL STEERING ALGORITHMS (NS ALGORITHMS)

In this section following two time efficient null steering algorithms are being discussed

- Null Steering Without Using Phase Shifters
- Independent Null Steering by Real Weight Control

Null steering without phase shifters and independent null steering by real weight control are abbreviated in a same way as NS W/O using phase shifters and INS by real weight control respectively.

2.2.1 NS WITHOUT USING PHASE SHIFTERS

T. B. Vu presented the method of null steering without using phase shifters [38]. In general, complex coefficients $A_0, A_1, ..., A_{N-1}$ as given in (2.1.5) are used for the purpose of array pattern nulling i.e. both amplitude and phase of the currents are involved. T. B. Vu dedicated phase shifters for steering of main beam only and real coefficients (weights) are used to achieve null steering. That means only the amplitudes of the inputs are needed to be varied for null steering. This condition results in the symmetry of the coefficients about the centre of the array and thus the number of coefficients to be calculated reduces to half.

The real coefficients of array are achieved by choosing the zeros of the AF, as in expression(2.1.6), to exist in conjugate pairs on the unit circle in the complex plane. The technique is slightly different for even and odd number of antenna elements in linear array. The expressions for both cases are given below.

Array Factor for Even Number of Elements

Let $N = 2k$, where k is integer

There will be odd number of zeros in A.F. i.e. $2k-1$ and accordingly the expression (2.1.6) becomes

$$AF = (z+1)(z-z_1)(z-z_1^*)...(z-z_{k-1})(z-z_{k-1}^*) \quad (2.2.1)$$

In(2.2.1), the factor $(z+1)$ forces one unpaired zero to exist at $z=-1$.

Array Factor for Odd Number of Elements

Let $N = 2k+1$, where k is integer

There will be even number of zeros in AF i.e. $2k$ and the equation (2.1.6) becomes

$$AF = (z-z_1)(z-z_1^*)...(z-z_k)(z-z_k^*) \quad (2.2.2)$$

In expressions (2.2.1) and(2.2.2), $z_i = e^{j\psi_i}$ with $\psi_i = \alpha + (2\pi/\lambda)d\cos\theta_i$ and θ_i is the position of the i^{th} null. Since it is assumed that $d = \lambda/2$, this gives $\psi_i = \alpha + \pi\cos\theta_i$.

It has been proved [38] that these real coefficients of the array factor are symmetric about the centre of the array. Thus the calculation time for the coefficients of AF is effectively reduced to the half. The cost to be paid is in the form of reduction of the number of steerable nulls, slightly less than half of the elements in the array. This cost is paid due to the existence of the zeros in conjugate pairs. For example, an array of eight elements can steer 3 nulls at most and its array factor will be as given under.

$$AF = 1 + A_1 z + A_2 z^2 + A_3 z^3 + A_3 z^4 + A_2 z^5 + A_1 z^6 + z^7$$

Similarly the AF for nine element linear array is given below to show the symmetry of coefficients

$$AF = 1 + A_1 z + A_2 z^2 + A_3 z^3 + A_4 z^4 + A_3 z^5 + A_2 z^6 + A_1 z^7 + z^8$$

The iterative approach for finding AF and the coefficients

Let $AF^{(M)}$ represent array factor for M steerable nulls for a uniform linear array with odd number of elements, then

$$AF^{(M+1)} = AF^{(M)}(1 + Bz + z^2) \quad (2.2.3)$$

In expression(2.2.3), $(1+Bz+z^2)$ is the product of factors for conjugate pair of zeros corresponding to $(M+1)^{th}$ null. It should be noted that $AF^{(1)}$, the array factor for

single steerable null, will be the product of factors for conjugate pair of zeros corresponding to that null.

Similarly if $A_i^{(M)}$ is the i^{th} coefficient of the linear array with M steerable nulls, then the i^{th} coefficient of the linear array with $M+1$steerable nulls will be $A_i^{(M+1)}$ and is given as under

$$A_i^{(M+1)} = A_i^{(M)} + BA_{i-1}^{(M)} + A_{i-2}^{(M)} \tag{2.2.4}$$

For an array with even number of elements ($N = 2k+2$), the array factor is given as

$$(AF)_{2k+2} = (AF)_{2k+1}(1+z) \tag{2.2.5}$$

For large arrays, this iterative approach for finding AF coefficients is time consuming and real weights reduce the steerable nulls to half of the maximum. T. B. Vu presented another technique using sum and difference patterns [39] which gives faster computing speed for coefficient finding but reduces the steerable nulls to the quarter of the maximum due to double symmetry of the coefficients. But the problem for his both algorithms is that if a single jammer changes its position, all the coefficients have to be recalculated.

2.2.1.1 SIMULATION RESULTS FOR NS W/O USING PHASE SHIFTERS

Simulations have been performed in MATLAB to elaborate the features and shortcomings of the algorithm. Since AF for even and odd number of elements has different mathematical form, two examples are given. Example 1 utilizes a uniform linear array with odd number of elements while example 2 considers an array with even number of elements.

Example 1:

In this example the uniform linear array with 7 Omni-directional elements is considered. This array can steer three arbitrary nulls. The main beam is taken along $\theta_s = 110^\circ$and the corresponding progressive phase shift $\alpha = 1.074$. Three interferences are taken in the directions $\theta_1 = 40^\circ$, $\theta_2 = 60^\circ$ and $\theta_3 = 150^\circ$. Fig. 2.3

shows the radiation pattern for the AF of this array. It is clear from the fig that main beam appears along θ_s and the nulls in the direction of interferences i.e. along θ_1, θ_2 and θ_3.

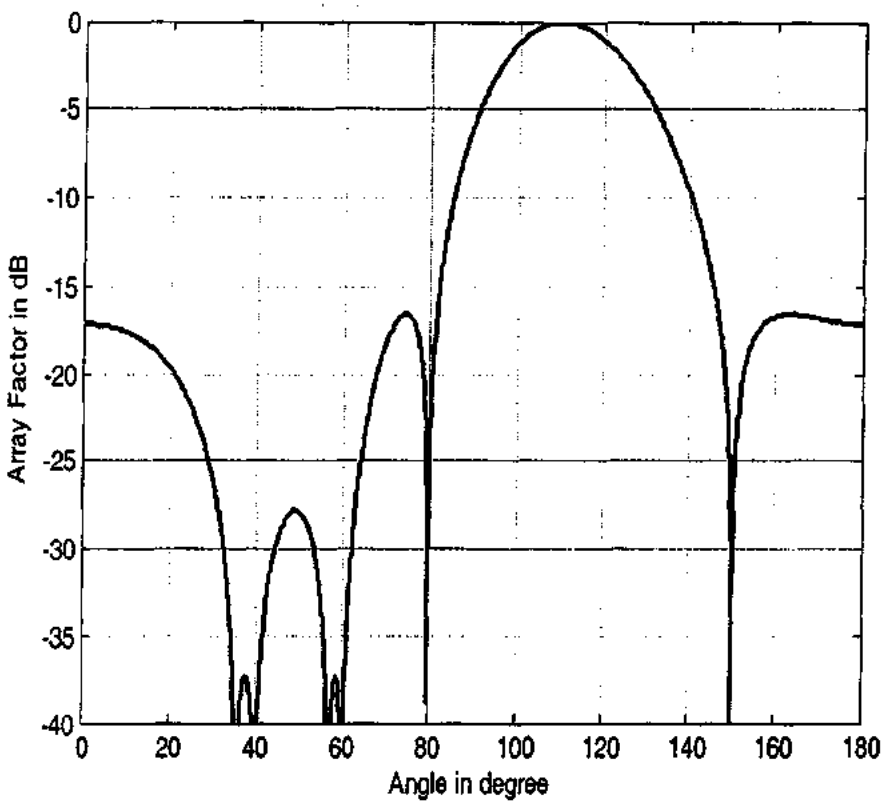

Figure 2.3: NS w/o using phase shifters for 7-element ULA with $\theta_s = 110°$ and $\theta_i = \{40°, 60°, 150°\}$

Example 2:

This example shows the AF for a uniform linear array with 8 antenna elements. This array can steer three nulls by using real weight control. The desired signal is taken along $\theta_s = 90^\circ$ and the corresponding progressive phase shift $\alpha = 0$. Three interferences are taken in the directions $\theta_1 = 30^\circ$, $\theta_2 = 60^\circ$ and $\theta_3 = 110^\circ$. Fig. 2.4 shows the radiation pattern for this array.

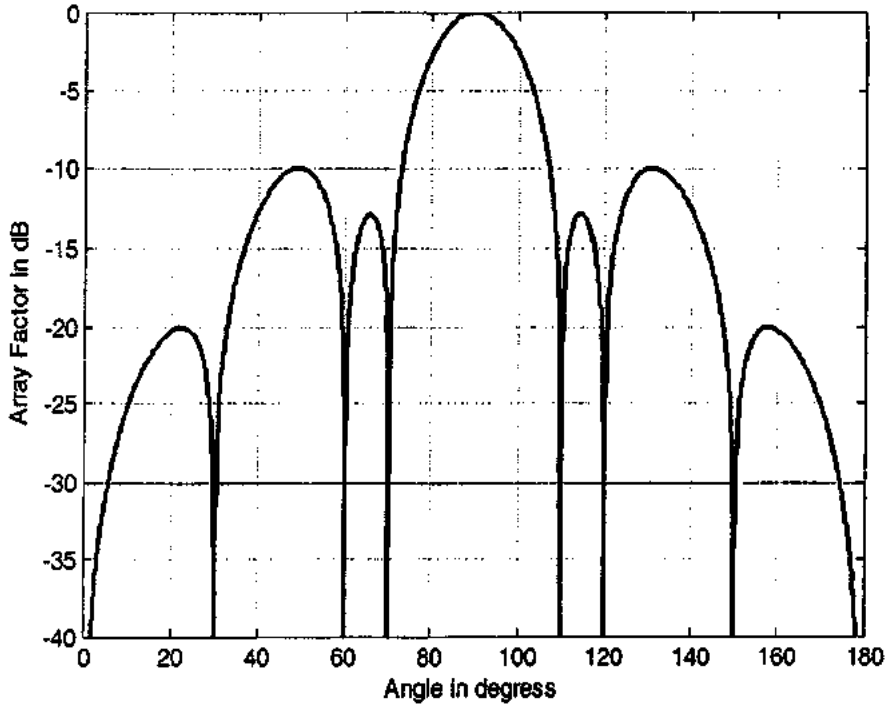

Figure 2.4: NS w/o using phase shifters for 8-element ULA with $\theta_s = 90°$ and $\theta_i = \{30°, 60°, 110°\}$

Effect of variation in θ_s and θ_i on A_i and α

Table 2.1 contains simulation results, to indicate the effect mentioned above. Consider the situations when the position of the desired signal θ_s does not change. Clearly by changing the position of one or more interferences θ_i, the progressive phase shift α remains unchanged but all the coefficients A_i, except first and the last, which are always equal to 1, change. On the other hand with the change in position of the desired signal θ_s, both α and A_i change. An important feature of the algorithm is that the coefficients A_i are always symmetric about the centre of the array.

In the table, maximum number of interferences has been utilized for each case. By observing the number of elements and the corresponding number of interferences, it is clear that the number of steerable nulls is always slightly less than the half of the number of elements in the array.

Table 2.1: Performance of "Null Steering without Using Phase Shifters"

S. No.	N	θ_s	α	θ_i	Coefficients A_i
1	7	110°	1.074	40°, 60°, 150°	1, 3.795, 6.866, 8.090, 6.866, 3.795,1
2	7	110°	1.074	35°, 60°, 150°	1, 3.658, 6.605, 7.780, 6.605, 3.658,1
3	7	100°	0.546	35°, 60°, 150°	1, 4.174, 8.527, 10.706, 8.527,4.174,1
4	8	90°	0	30°, 60°, 110°	1, 1.873, 2.135, 3.008, 3.008, 2.135, 1.873,1
5	8	90°	0	30°, 55°, 150°	1, 2.331, 2.993, 3.528, 3.528, 2.993, 2.331,1
6	8	95°	0.274	30°, 55°, 150°	1, 2.554, 2.366, 1.254, 1.254, 2.366, 2.554, 1
7	9	100°	0.546	50°, 80°,130° 150°	1, 1.696, 2.943, 3.464, 4.226, 3.464, 2.943, 1.696,1
8	9	100°	0.546	50°, 80°,130° 155°	1, 1.895, 3.054, 3.724, 4.508, 3.724, 3.054, 1.895, 1
9	9	105°	0.813	50°, 80°,130° 155°	1, 1.665, 2.829, 3.904, 4.169, 3.904, 2.829, 1.665, 1

2.2.2 INDEPENDENT NULL STEERING BY REAL WEIGHT CONTROL

H. M. Ibrahim presented a technique to implement expressions (2.1.5), (2.2.1) and (2.2.2) using a structure such that each null can be steered independently by using real weights [40]. In case of change in position of a single interference, only the weight set corresponding to that interference has to be changed while the weight sets corresponding to remaining interferences does not change. Each element of a weight set has a particular fixed value depending on the location of the corresponding zero in the array pattern. The structure of this time efficient technique is discussed below.

The product of each conjugate pair of zeros corresponding to a particular null is real and AF_i represents the product for the i^{th} conjugate pair as given below

$$AF_i = (z - z_i)(z - z_i^*) = 1 + B_i z + z^2 \tag{2.2.6}$$

In above expression, z_i is the position of i^{th} zero on the unit circle in the direction θ_i of the corresponding interference.

$$B_i = -(z_i + z_i^*) = -(e^{jw_i} + e^{-jw_i}) \tag{2.2.7}$$

$$B_i = -2\cos(\alpha + (2\pi/\lambda)d\cos\theta_i) \tag{2.2.8}$$

The special structure to implement (2.2.6) is shown in Fig. 2.5 and is capable of steering single null in the direction θ_i.

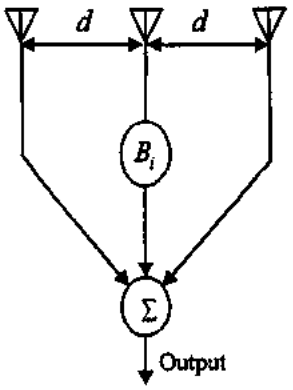

Figure 2.5: Basic structure for INS by real weight control using 3-element ULA to steer single null [40].

Normalized Array Factor for i^{th} Null

Let $B_i = -(e^{j\psi_i} + e^{-j\psi_i})$ and $z = e^{j\psi}$ then (2.2.6) becomes

$$AF_i = 1 - 2\cos\psi_i(\cos\psi + j\sin\psi) + (\cos\psi + j\sin\psi)^2$$

$$= 1 - 2\cos\psi_i\cos\psi - 2j\cos\psi_i\sin\psi + \cos^2\psi - \sin^2\psi + 2j\cos\psi\sin\psi$$

$$= \cos^2\psi + \sin^2\psi - 2\cos\psi_i\cos\psi - 2j\cos\psi_i\sin\psi + \cos^2\psi - \sin^2\psi + 2j\cos\psi\sin\psi$$
$$= 2\cos^2\psi - 2\cos\psi_i\cos\psi - 2j\cos\psi_i\sin\psi + 2j\cos\psi\sin\psi$$

$$= 2\cos\psi(\cos\psi - \cos\psi_i) + 2j\sin\psi(\cos\psi - \cos\psi_i)$$

$$= 2(\cos\psi + j\sin\psi)(\cos\psi - \cos\psi_i)$$

The normalized array factor is given by

$$(AF_i)_n = F_i(\theta) = (\cos\psi - \cos\psi_i)$$

$$= \cos\psi + \frac{1}{2}(-2\cos\psi_i) = \cos\psi + \frac{1}{2}B_i$$

$$F_i(\theta) = \cos[(2\pi/\lambda)d\cos\theta + \alpha] + \frac{B_i}{2} \qquad (2.2.9)$$

Now we will draw the corresponding structures for arrays with seven and eight elements respectively. Both the structures can steer three nulls independently. The difference in two structures is that when the number of elements is even, there exists

an unpaired zero that cannot form conjugate pair. Therefore, that zero is fixed at $z=-1$ to cater the unavailability of conjugate pair problem.

Structure for Seven-Element linear Array

Using expression(2.2.2), the AF for a linear array with seven elements is given below

$$AF=(z-z_1)(z-z_1^*)(z-z_2)(z-z_2^*)(z-z_3)(z-z_3^*) \qquad (2.2.10)$$

$$=(1+B_1z+z^2)(1+B_2z+z^2)(1+B_3z+z^2)$$

The structure corresponding to this AF is shown in Fig 2.6

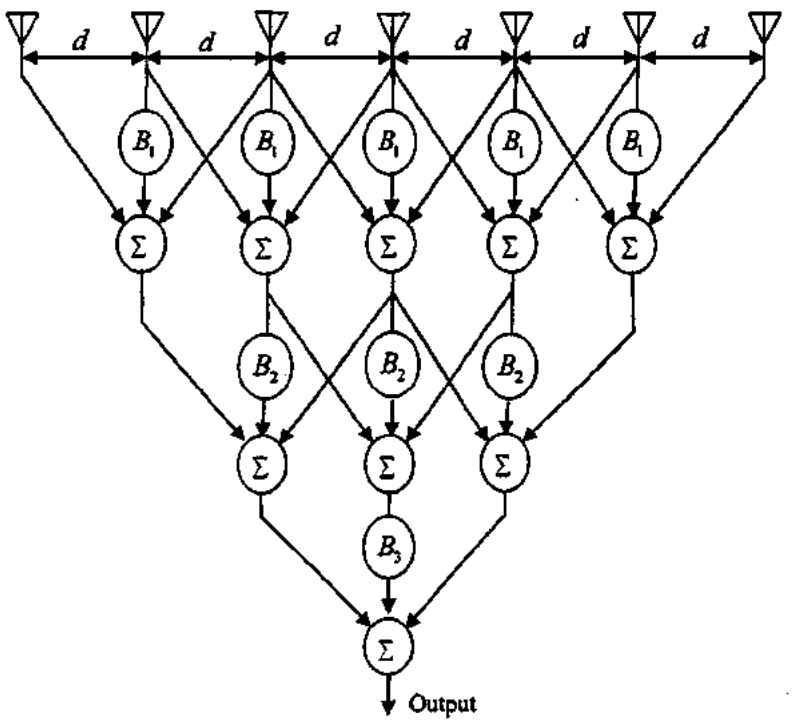

Figure 2.6: Structure for INS by real weight control using 7-element ULA to steer 3 nulls independently [40]

Structure for Eight-Element Linear Array

Using expression (2.2.1), the AF for eight-element linear array is given below by equation (2.2.11)

$$AF = (z+1)(z-z_1)(z-z_1^*)(z-z_2)(z-z_2^*)(z-z_3)(z-z_3^*) \qquad (2.2.11)$$

$$= (z+1)(1+B_1 z+z^2)(1+B_2 z+z^2)(1+B_3 z+z^2)$$

The AF in expression (2.2.11) contains a factor $(z+1)$ to fix the unpaired zero at $z=-1$.

Fig. 2.7 shows the structure to implement expression (2.2.11). This structure is also capable of steering 3 nulls independently by varying the real weights B_1, B_2 and B_3.

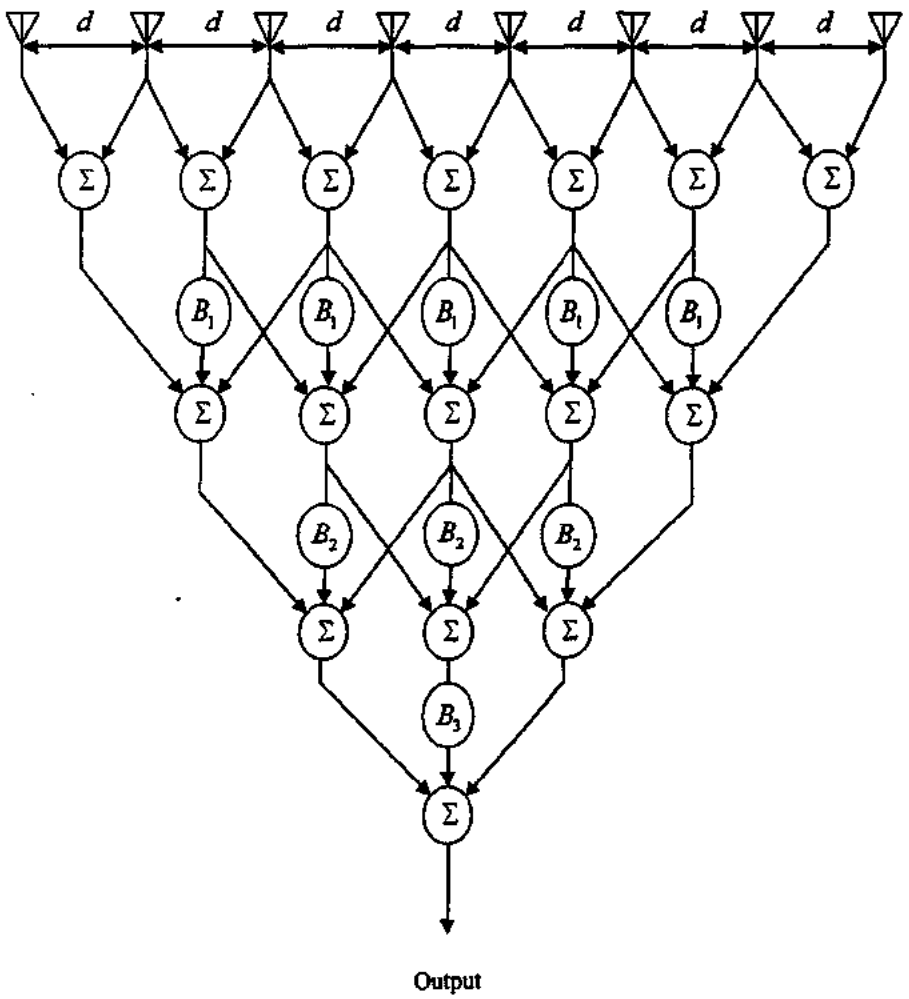

Figure 2.7: Structure for INS by real weight control using 8-element uniform linear array to steer 3 nulls independently [40]

Position of null corresponding to $z=-1$

It can be seen from expression (2.2.1) and (2.2.11) that the AF for even number of elements contains the factor $(z+1)$ that forces one unpaired zero to exist at $z=-1$. The angular position of this zero is derived as follows

Since $z=e^{j\psi}=-1$

$\Rightarrow \cos\psi=-1,$

$\Rightarrow \psi=\pi$

$\Rightarrow \alpha+(2\pi/\lambda)d\cos\theta=\pi$

$\Rightarrow \cos\theta=(\pi-\alpha)\lambda/(2\pi d)$

$\Rightarrow \theta=\cos^{-1}[(\pi-\alpha)\lambda/(2\pi d)]$

When $d=\lambda/2,$

$$\theta=\cos^{-1}[(\pi-\alpha)/\pi] \qquad (2.2.12)$$

Expression (2.2.12) shows the position of unpaired zero on the unit circle in the complex plane.

2.2.2.1 SIMULATION RESULTS FOR INS BY REAL WEIGHT CONTROL

Simulations have been performed in MATLAB to indicate the features and limitations of the algorithm. Two examples are being presented here for demonstration. Example 1 shows the situation when the number of elements in array is odd while example 2 is for an array with even number of elements.

Example 1:

In this example the uniform linear array with 7 elements has been considered. The spacing between the adjacent elements is taken to be $d=\lambda/2$. This array is capable of steering three nulls independently. The main beam is taken along $\theta_s=110^\circ$ and the three interferences are taken in the directions $\theta_1=40^\circ$, $\theta_2=60^\circ$ and $\theta_3=150^\circ$. The progressive phase shift α is related to $\theta_s=110^\circ$ as $\alpha=-\pi\cos\theta_s$. Fig. 2.8 shows the radiation pattern for the AF of this array.

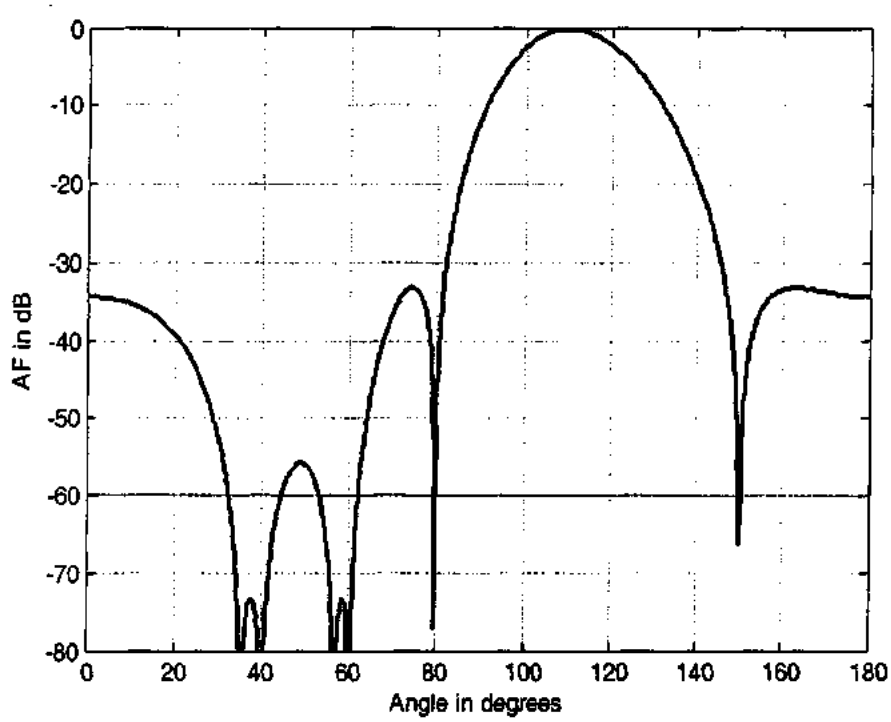

Figure 2.8: INS by real weight control using 7-element uniform linear array with $\theta_s = 110°$ and $\theta_i = \{40°, 60°, 150°\}$

Example 2:

This example shows the AF for a uniform linear array with 8 antenna elements. The desired signal is taken along $\theta_s = 90^\circ$ and the three interferences are considered in the directions $\theta_1 = 30^\circ$, $\theta_2 = 60^\circ$ and $\theta_3 = 110^\circ$. The progressive phase shift $\alpha = 0$ is chosen in accordance with the desired signal $\theta_s = 90^\circ$. Fig. 2.9 shows the radiation pattern for this AF.

Effect of variation in θ_s and θ_i on B_i and α

Table 2.2 contains illustrative simulation results, performed in MATLAB, in order to examine the above mentioned effect i.e. variation in θ_s and θ_i on B_i and α. It can be observed from table 2.2 that change in position of any interference θ_i changes only the corresponding coefficient B_i and has no effect on the remaining coefficients and

the progressive phase shift α. On the other hand, if θ_s changes, progressive phase shift α also changes along with all the coefficients B_i. Thus weights are decoupled for independent null steering when θ_s does not change.

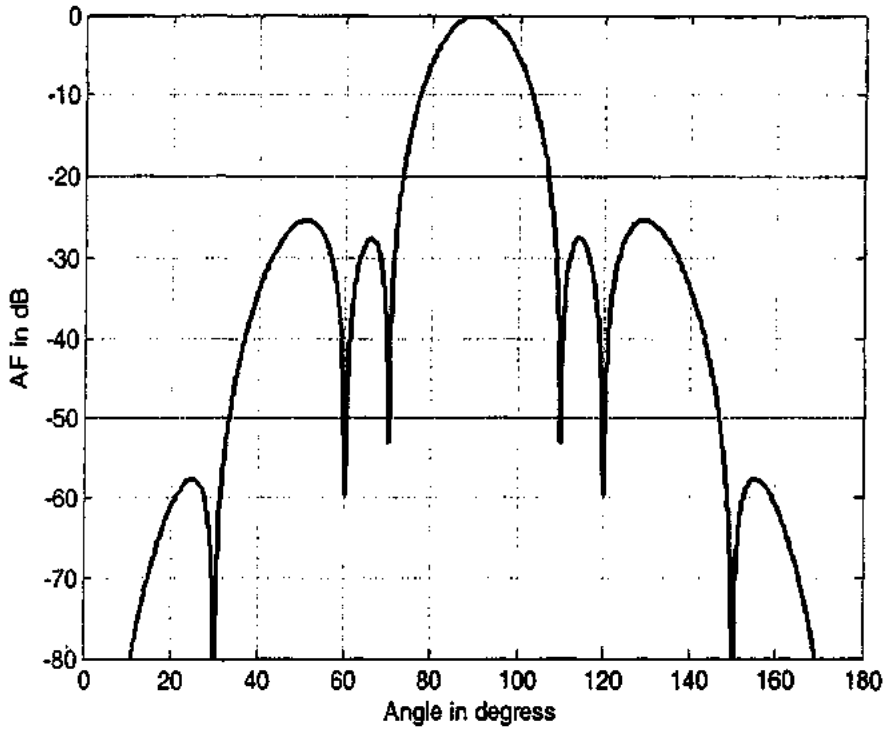

Figure 2.9: INS by real weight control using 8-element ULA with $\theta_s = 90°$ and $\theta_i = \{30°, 60°, 110°\}$

Table 2.2: Performance of "Independent Null Steering by Real Weight Control".

S. No.	N	θ_s	α	θ_i	Coefficients B_i
1	7	100°	0.546	30°, 70°, 150°	1.985, 0.098, 1.136
2	7	100°	0.546	35°, 70°, 150°	1.999, 0.098, 1.136
3	7	110°	1.074	35°, 60°, 150°	1.749, 1.093, 0.151
4	8	90°	0	50°, 65°, 130°	0.867, -0.481, 0.867
5	8	90°	0	50°, 63°, 130°	0.867, -0.288, 0.867
6	8	95°	0.274	50°, 63°, 130°	1.322, 0.258, 0.348
7	9	100°	0.546	30°, 70°,130° 160°	1.984, 0.098, -0.194, 1.484
8	9	100°	0.546	35°, 70°,130° 160°	1.999, 0.098, -0.194, 1.484
9	9	105°	0.813	35°, 70°,130° 160°	1.940, 0.623, -0.713, 1.076

2.3 CONCLUSION

The prominent features of the two null steering algorithms discussed in this chapter are summarized as below.

Null Steering Without Using Phase Shifters

1. Half of the weights are required to be computed because real weights are symmetric about the center of the array. This makes the algorithm relatively time efficient in comparison to the techniques that require computation of all the weights to steer even a single null.

2. The problem with this scheme is that if a null changes its position, the whole set of symmetric weights (half of the total weights) will have to be changed to steer null along that interference. This is the reason, it is not yet time efficient for large arrays.
3. The steerable nulls are very limited. Specifically that is slightly less than half the number of elements in the array. Therefore it is expensive from hardware point of view.

Independent Null Steering by Real Weight Control

4. This scheme is time efficient because it has a well defined and direct weight finding formula(2.2.8).
5. Moreover, if a single interference changes its position, only the corresponding set of weights is required to be updated to steer the corresponding null along that interference. The remaining set of weights will be undisturbed. That is why, the title of independent null steering has been allocated.
6. The cost for time efficiency is the requirement of extra components that is weights and adders to implement the proposed structure, which makes it hardware wise inefficient.
7. Number of steerable nulls is slightly less than half the number of elements in the array. Hence regarding the hardware requirements to attain certain fixed

number of nulls, the proposed scheme is comparable with the previous one, i.e., the scheme using real weights without Using Phase Shifters.

CHAPTER 3

NOVEL INDEPENDENT NULL STEERING ALGORITHM IN DOA BASED BEAMFORMERS

An overview of DOA based adaptive beamformers was given in Chapter 1 while some algorithms of this category were also discussed in Chapter 2. Processing time, Number of steerable nulls and Sidelobe level are important parameters of the beamformers lying in this category. In this chapter we have contributed the following three new DOA based beamforming algorithms.

- Independent Null Steering by Decoupling Complex Weights
- Independent Null Steering with Suppressed Sidelobes
- Independent Null Steering with Suppressed Sidelobes and Symmetric Beam

Independent Null steering by Decoupling Complex Weights, Independent Null Steering with Suppressed Sidelobes and Independent Null Steering with Suppressed Sidelobes and Symmetric Beam are abbreviated as INS by Decoupling Complex Weights, INS with Suppressed SLs and INS with Suppressed SLs and Symmetric Beam respectively.

First algorithm is time efficient that presents a structure to steer maximum available nulls by independent weight control. For this algorithm, there is no control on high sidelobe levels. Second algorithm mitigates sidelobe level problem and provides independent null steering with suppressed sidelobes. Finally, the third algorithm provides improved beam symmetry along with the independent null steering with suppressed sidelobes. Most of the material in this chapter is from [41].

3.1 INS BY DECOUPLING COMPLEX WEIGHTS

The independent Null Steering Structure for a uniform linear array of N elements will be discussed. Initially N is taken as 6 which is then generalized for an array with variable number of antenna elements. Finally simulation examples will be given to evaluate the performance of the beamformer.

3.1.1 INS STRUCTURE FOR 6-ELEMENT ULA

The proposed structure for a uniform linear array of $N=6$ elements is shown in Fig. 3.1

In chapter 2, the expression for z was developed which is being reproduced here i.e.

$$z = e^{j\psi} \tag{3.1.1}$$

The expression for the structure components z_i can be obtained from the above expression if ψ is replaced by ψ_i i.e.

$$z_i = e^{j\psi_i} \tag{3.1.2}$$

Where

$$\psi_i = \alpha + (2\pi/\lambda) d\cos\theta_i \tag{3.1.3}$$

With α as given in expression (2.1.7) is the progressive phase shift and d is the inter-element spacing while θ_i is the desired position of the i^{th} null.

In the structure two input summers are used. The summer output $y_{i,j}$ represents j^{th} output of i^{th} stage. Each stage of the structure steers a particular null independently without disturbing the others.

The outputs of first stage are given as

$y_{1,1} = z - z_1$, $y_{1,2} = z(z - z_1)$, $y_{1,3} = z^2(z - z_1)$, $y_{1,4} = z^3(z - z_1)$, $y_{1,5} = z^4(z - z_1)$

The second stage steers 2nd null independently and its outputs are given as

$y_{2,1} = z - z_2$, $y_{2,2} = z(z - z_2)$, $y_{2,3} = z^2(z - z_2)$, $y_{2,4} = z^3(z - z_2)$

The steering of third null is carried out by stage-3 with the following outputs

$y_{3,1} = z - z_3$, $y_{3,2} = z(z - z_3)$, $y_{3,3} = z^2(z - z_3)$

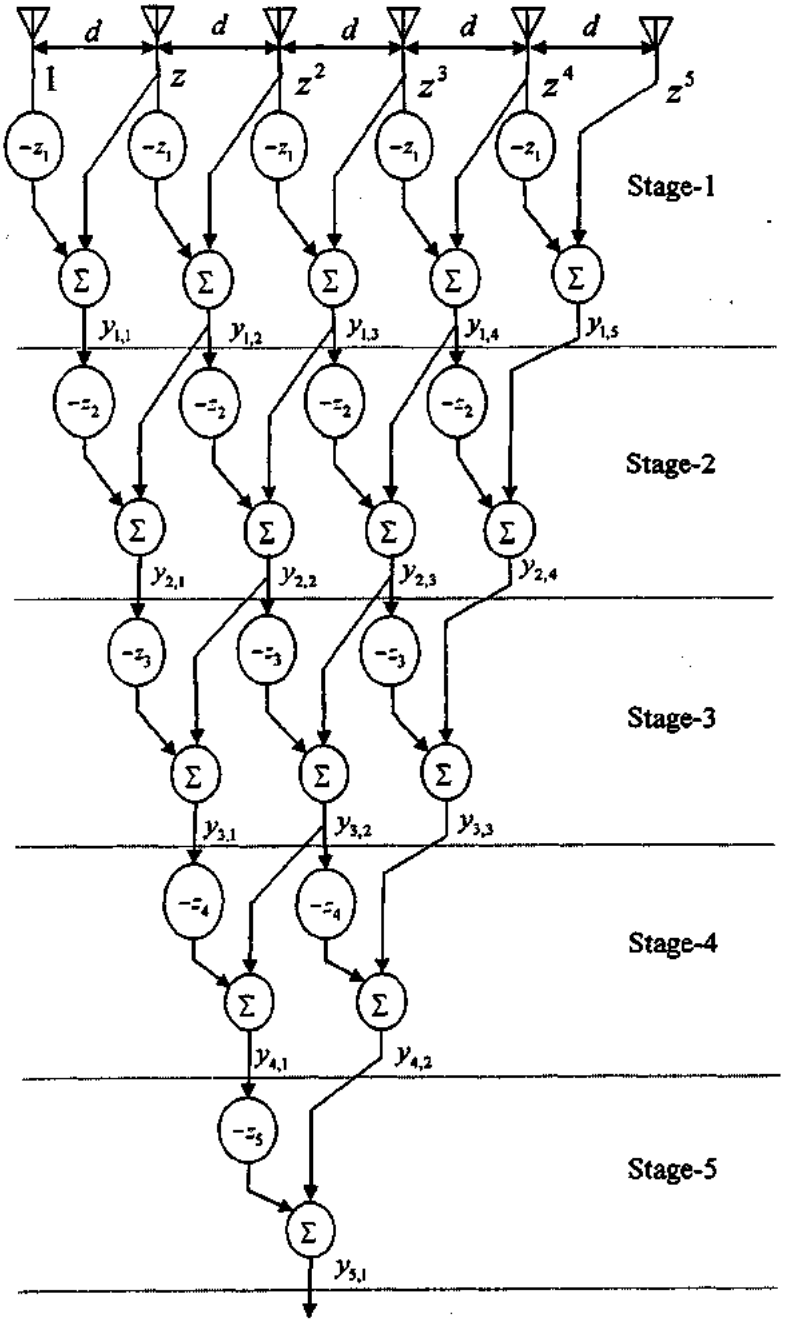

Figure 3.1: Structure for independent null steering by decoupling complex weights.

Similarly the stage-4 is responsible for the steering of the 4th null and creates the following outputs

$y_{4,1} = z - z_4$, $y_{4,2} = z(z - z_4)$

Finally the stage-5 is meant for the steering of fifth null and creates the only output i.e. $y_{5,1} = z - z_5$.

It can be seen that first stage has maximum number of outputs as compare to any other stage and this number is one less than the total number of elements in the array. The number of outputs in $(i+1)^{th}$ stage is one less than that of i^{th} stage and the last stage has single output.

3.1.2 INS BY DECOUPLING COMPLEX WEIGHTS FOR *N*-ELEMENT ULA

The comprehensive study of the independent null steering structure for 6-element linear array (shown in Fig. 3.1) has enabled us to extend it for N-element linear array. It will have $N-1$ stages and will incorporate the following array factor.

$$AF = \prod_{i=1}^{N-1}(z - z_i) \tag{3.1.4}$$

Expression (3.1.4) is equivalent to

$$AF = A_0 + A_1 z + \ldots + A_{N-1} z^{(N-1)} \tag{3.1.5}$$

Where the coefficients $A_0, A_1, \ldots, A_{N-1}$ are complex and the structure decouples them.

The first stage will have $(N-1)$ outputs. The general formula for the j^{th} output of this stage is

$$y_{1,j} = z^{j-1}(z - z_1) \text{ for } j = 1, \ldots, N-1 \tag{3.1.6}$$

The general formula for the j^{th} output of i^{th} stage is given as

$$y_{i,j} = z^{j-1}(z - z_1)(z - z_2)\ldots(z - z_k) \tag{3.1.7}$$

Where $i = 1, \ldots N-1$, $j = 1, \ldots, N-i$, and $k = 1, \ldots i$

The final output of the array is obtained by putting $i = N-1$, $j = 1$ and $k = 1, \ldots, N-1$ in expression (3.1.7) and is equivalent to the array factor given as

$$y_{N-1,1} = \prod_{i=1}^{N-1}(z - z_i) \tag{3.1.8}$$

3.1.3 HARDWARE FOR INS STRUCTURE USING N-ELEMENT ULA

It is clear from Fig.3.1 that an N-element array will have $N-1$ stages. First stage will have $N-1$ weights each of value z_1. Similarly, each weight of stage-2 will be of value z_2 and there will be $N-2$ weights in this stage. The last stage will have only weight with value z_{N-1}. Each stage utilizes the same number of summers as that of weights. Thus the structure uses $N-1$ types of weights that are $z_1, z_2, \ldots, z_{N-1}$. Let the array uses n weights in total, the number of summers will also be the same. This n can be obtained by summing the number of weights in each stage i.e.

$$n = (N-1)+(N-2)+\ldots+1 = \sum_{i=1}^{N-1} i$$

The general formula for n comes out to be

$$n = \frac{N(N-1)}{2} \tag{3.1.9}$$

3.1.4 SIMULATION RESULTS FOR INS BY DECOUPLING COMPLEX WEIGHTS

In this section a few examples are presented to show the capabilities of the proposed structure. In all the examples, the inter-element spacing d is $\lambda/2$.

Example 1:

This example demonstrates the independent null steering capability of the technique given in section 3.1.1 and 3.1.2. A uniform linear array of 5-elements is considered for this purpose. It can steer four nulls independently. The main beam is taken along $\theta_s = 100°$ and the four interferences are placed at $\theta_{i1} = 55°, \theta_{i2} = 80°, \theta_{i3} = 120°$ and $\theta_{i4} = 160°$. The value of α is determined by (2.1.7) which comes out to be 0.5455 and the weights z_i can be computed by using (3.1.2). Fig. 3.2 and 3.3, indicate the change in the patterns of single null by changing only the corresponding weight in the structure.

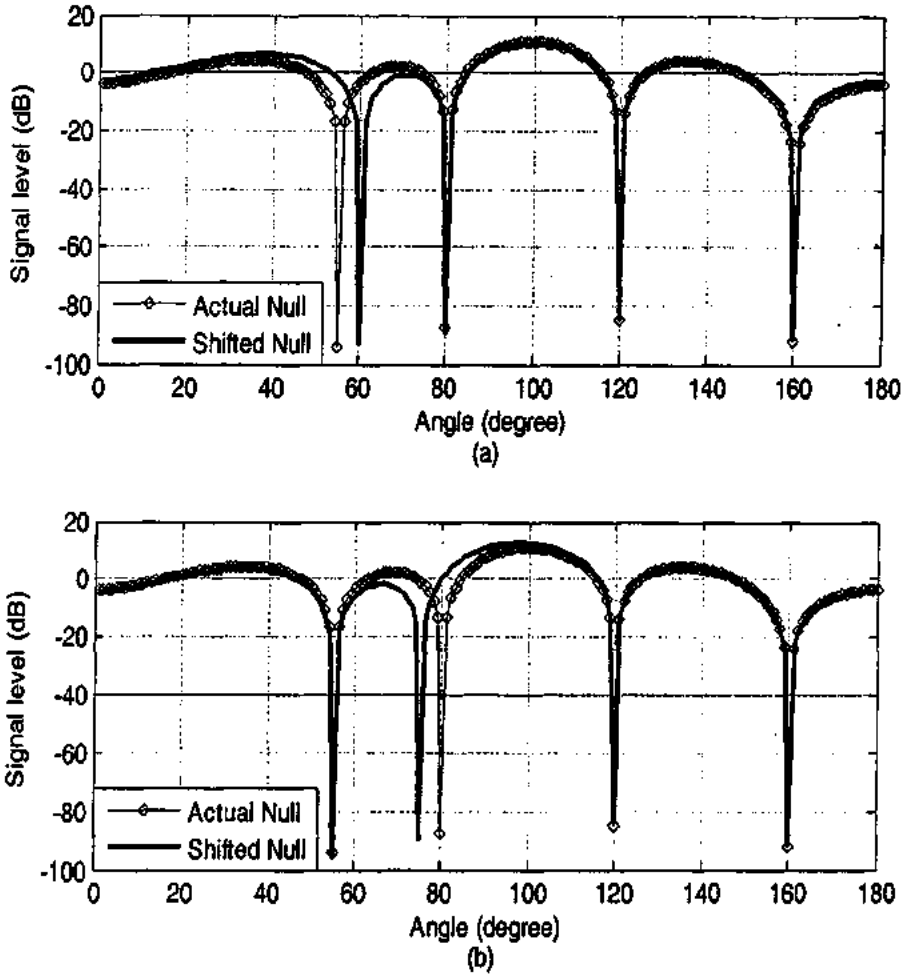

Figure 3.2: INS by decoupling complex weights (a) First null shifts from 55° to 60° when z_1 is changed. (b) Second null shifts from 80° to 75° when z_2 is changed

Let the first interference changes its position from 55° to 60°. In order to steer the first null along the new direction of the interference, z_1 is changed from -0.7009 + 0.7132i to -0.5189 + 0.8549i while z_2, z_3 and z_4 remain unchanged and this change in null position is shown in Fig 3.2 (a). Fig 3.2 (b) shows the steering of 2nd null from 80° to 75° by changing z_2 without disturbing z_1, z_3 and z_4.

Similarly, the steering of 3rd and 4th nulls is shown in Fig 3.3 (a) and Fig 3.3 (b) respectively by changing the corresponding weight only.

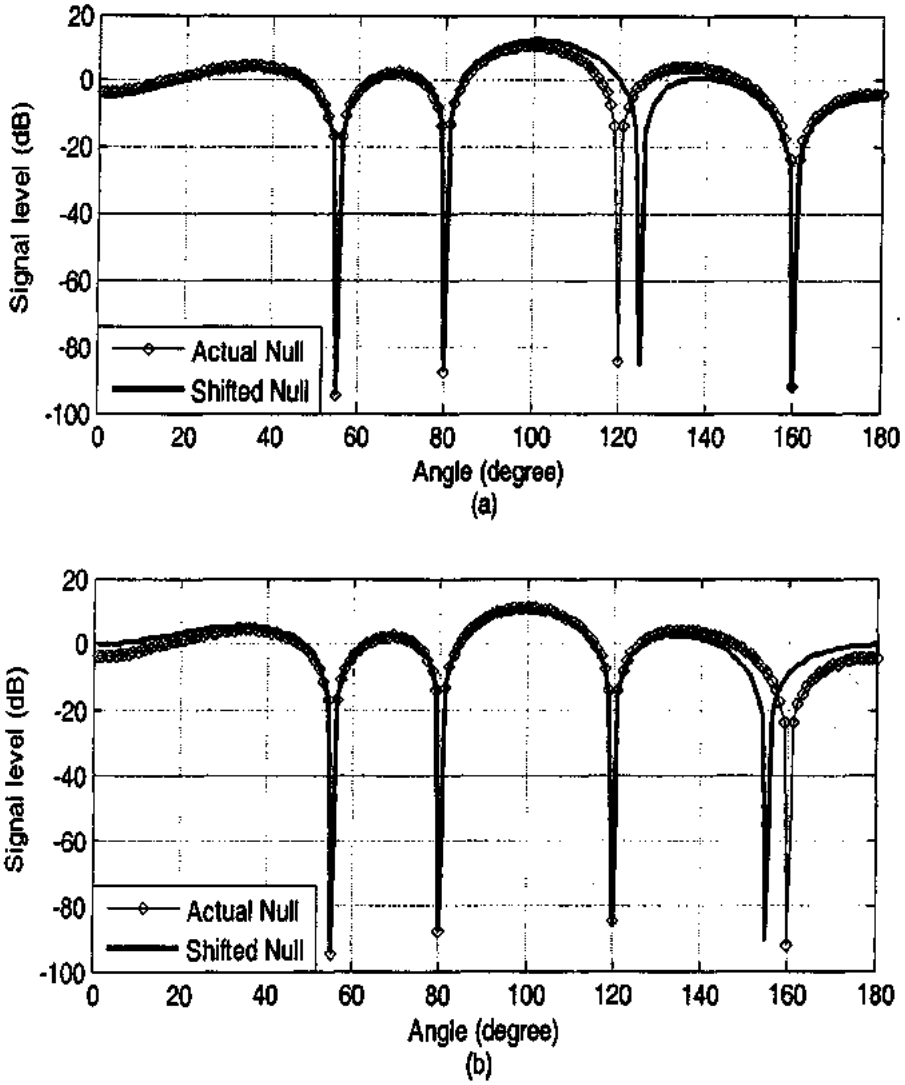

Figure 3.3: INS by decoupling complex weights (a) Third null shifts from 120° to 125° when z_3 is changed. (b) Fourth null shifts from 160° to 155° when z_4 is changed.

Table 3.1 shows that in order to move a null, only the corresponding weight is required to be changed while remaining weights remain unchanged. In order to steer multiple nulls, the same number of corresponding weights are required to be changed. Bold entries of the table show the changed position of the nulls and the corresponding changed weights.

Table 3.1: Performance of Independent Null Steering Algorithm for $\theta_s = 100°$, $N = 5$

S. No.	θ_i	z_1	z_2	z_3	z_4
1	55°, 80°, 120°, 160°	-0.7009 + 0.7132i	0.4615 + 0.8871i	0.5189 - 0.8549i	-0.7418 - 0.6706i
2	**60°**, 80°, 120°, 160°	**-0.5189 + 0.8549i**	0.4615 + 0.8871i	0.5189 - 0.8549i	-0.7418 - 0.6706i
3	55°, **75°**, 120°, 160°	-0.7009 + 0.7132i	**0.2106 + 0.9776i**	0.5189 - 0.8549i	-0.7418 - 0.6706i
4	55°, 80°, **125°**, 160°	-0.7009 + 0.7132i	0.4615 + 0.8871i	**0.3092 - 0.9510i**	-0.7418 - 0.6706i
5	55°, 80°, 120°, **155°**	-0.7009 + 0.7132i	0.4615 + 0.8871i	0.5189 - 0.8549i	**-0.6676 - 0.7446i**
6	**60°**, 80°, 120°, **155°**	**-0.5189 + 0.8549i**	0.4615 + 0.8871i	0.5189 - 0.8549i	**-0.6676 - 0.7446i**
7	55°, **75°**, **125°**, 160	-0.7009 + 0.7132i	**0.2106 + 0.9776i**	**0.3092 - 0.9510i**	-0.7418 - 0.6706i
8	**60°**, **75°**, **125°**, 160	**-0.5189 + 0.8549i**	**0.2106 + 0.9776i**	**0.3092 - 0.9510i**	-0.7418 - 0.6706i
9	**60°**, **75°**, **125°**, **155°**	**-0.5189 + 0.8549i**	**0.2106 + 0.9776i**	**0.3092 - 0.9510i**	**-0.6676 - 0.7446i**

Example 2:

This example considers a uniform linear array of 6-elements. It can steer five nulls independently. The main beam is taken along $\theta_s = 140°$ and the five interferences are placed at $\theta_{i1} = 15°, \theta_{i2} = 45°, \theta_{i3} = 70°, \theta_{i4} = 120°$ and $\theta_{i5} = 160°$.

Table 3.2: Performance of Independent Null Steering Algorithm for $\theta_s = 140°$, $N = 6$

S. No.	θ_i	z_1	z_2	z_3	z_4	z_5
1	15°, 45°, 70°, 120°, 160°	0.6659 - 0.7460i	-0.0842 - 0.9964i	-0.9429 - 0.3330i	0.6706 +0.7418i	0.8549-0.5189i
2	**20°**, 45°, 70°, 120°, 160°	**0.6023 - 0.7983i**	-0.0842 - 0.9964i	-0.9429 -0.3330i	0.6706 +0.7418i	0.8549-0.5189i
3	15°, **40°**, 70°, 120°, 160°	0.6659 - 0.7460i	**0.1006 - 0.9949i**	-0.9429 -0.3330i	0.6706 +0.7418i	0.8549-0.5189i
4	15°, 45°, **75°**, 120°, 160°	0.6659 - 0.7460i	-0.0842 - 0.9964i	**-0.9970 -0.0780i**	0.6706 +0.7418i	0.8549-0.5189i
5	15°, 45°, 70°, **115°**, 160°,	0.6659 - 0.7460i	-0.0842 - 0.9964i	-0.9429 -0.3330i	**0.4723 + 0.8814i**	0.8549-0.5189i
6	15°, 45°, 70°, 120°, **165°**	0.6659 - 0.7460i	-0.0842 - 0.9964i	-0.9429 -0.3330i	0.6706 +0.7418i	**0.8092-0.5875i**

For $\theta_s = 140°$, α comes out to be 2.4066. Table 3.2 shows the independent steering of a null by changing only the corresponding weight. The changed position of the nulls and the corresponding weights are shown by the bold entries of the table.

The null steering given in table 3.2 can also be observed in Fig. 3.4 and Fig. 3.5. In these figures all the nulls maintain their positions except the one that changes its position by changing the corresponding weight. The actual and changed positions of the nulls are evident and are also indicated in these figures clearly.

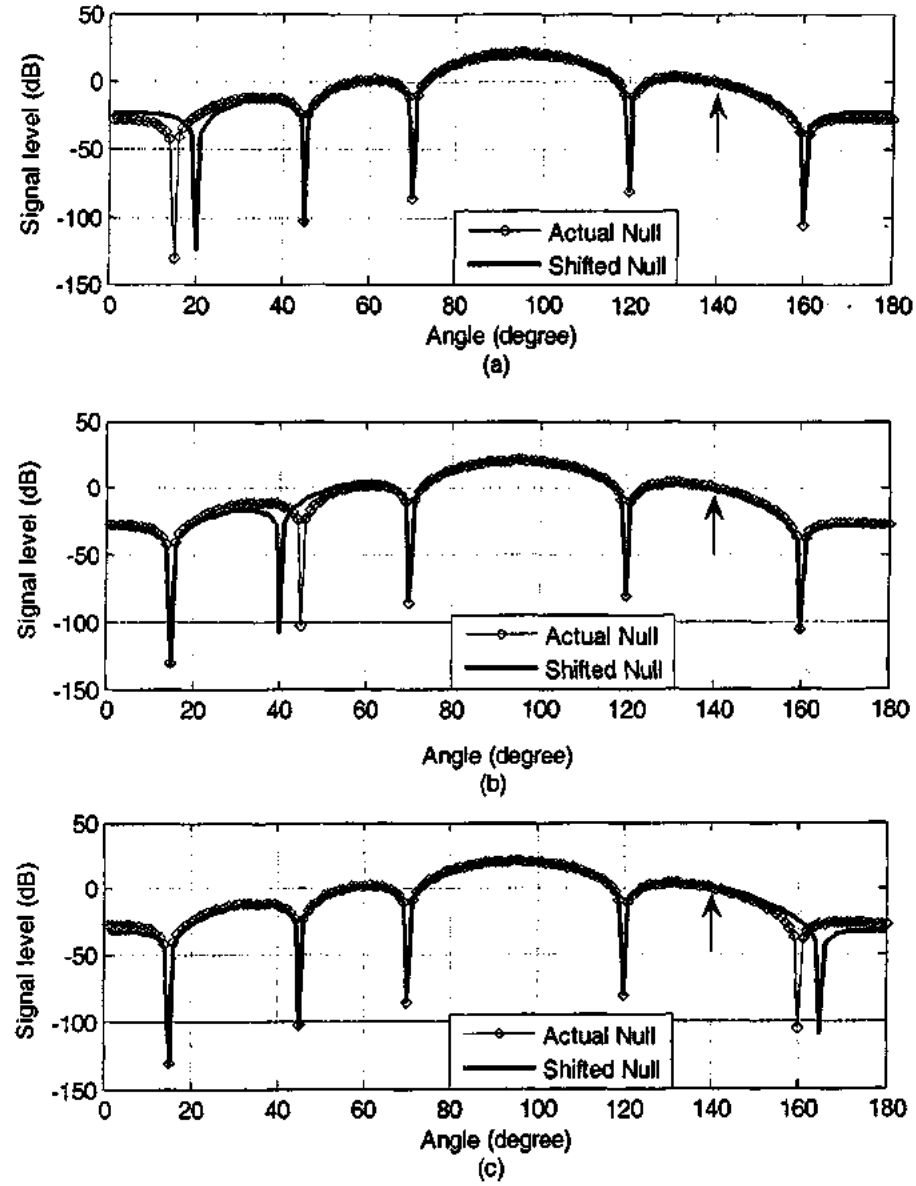

Figure 3.4: INS by decoupling complex weights, (a) First null shifts from 15° to 20° when z_1 is changed. (b) Second null shifts from 45° to 40° when z_2 is changed. (c) Fifth null shifts from 160° to 165° when z_5 is changed.

In these figures, the main beam is approximately at 100° which is deviated from the desired position i.e. 140° or in other words the side lobe level is higher than the beam

at the desired position. The desired position is indicated by the arrow in the Figs. This deviation of the main beam or equivalently the high sidelobe level is the problem with the DOA based beamformers. The reason for this abnormality is that the array pattern depends on the relative position of the interferences. In the next section, the independent null steering algorithm will be modified to solve this problem.

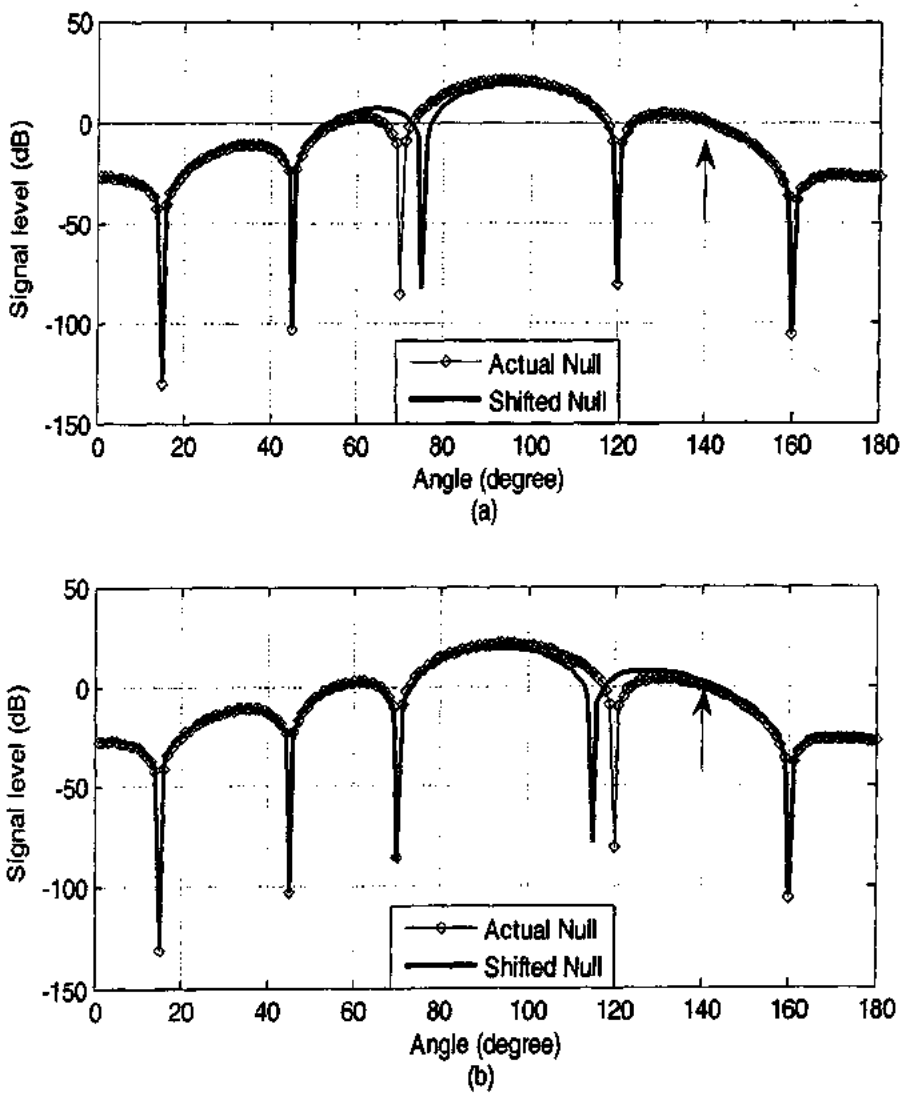

Figure 3.5: INS by decoupling complex weights (a) Third null is shifted from 70° to 75° when z_3 is changed. (b) Fourth null is shifted from 120° to 115° when z_4 is changed.

3.2 INS WITH SUPPRESSED SIDELOBES

The beam pattern of a uniform linear array depends on the relative positions of the interferences. The position of the main beam along the desired direction is not guaranteed to be preserved (sidelobe looks like main beam due to dominant levels). In this section the independent null steering technique is improved by introducing an additional feature of sidelobe suppression at the cost of an optional number of steerable nulls. For this purpose, the array factor is obtained by multiplying two polynomials. One polynomial is used for independent null steering and utilizes the existing structure, discussed in the previous section. Second polynomial is meant for the sidelobe suppression. The coefficients of this polynomial are obtained by utilizing convex optimization.

3.2.1 PROPOSED ALGORITHM FOR INS WITH SSLS

According to Schelkenoff [30] the product of two or more polynomials is also a polynomial and there exists a linear array with AF equal to the resultant polynomial. Utilizing the same fact, consider the following AF

$$AF = AF_1 AF_2$$

Where AF_1 is meant for independent steering of N_1 nulls using the technique discussed in section 3.1 and represented by the following expression

$$AF_1 = \prod_{i=1}^{N_1}(z - z_i) \tag{3.2.1}$$

The purpose of AF_2 is to suppress sidelobes and the expression for this array factor is given as

$$AF_2 = b_0 + b_1 z + ... + b_{N_2-1} z^{N_2-1} = \mathbf{s}_{N_2}\mathbf{b} \tag{3.2.2}$$

Where $\mathbf{b} = [b_0, b_1, ..., b_{N_2-1}]^T$ is the complex weight vector and $\mathbf{s}_{N_2} = [1\, z ... z^{N_2-1}]$ is the steering vector. The condition on vector $\mathbf{b}$ is that it guarantees the sidelobe suppression and the procedure to find out $\mathbf{b}$ is given as under:

First of all, sidelobe region S_R is selected. It is the region outside the main beam with width θ_{mb} and is represented as below

$$S_R = \left\{0 < \theta \le \theta_s - \frac{\theta_{mb}}{2}\right\} U \left\{\theta_s + \frac{\theta_{mb}}{2} < \theta \le 180^\circ\right\} \tag{3.2.3}$$

A set containing p discrete angles is selected from the sidelobe region S_R and this set is named as A_{SR}

$$A_{SR} = \{\theta_i \mid \theta_i \in S_R \wedge \theta_i = \theta_0 + i\delta\theta\} \subseteq S_R \tag{3.2.4}$$

Where $i = 0, 1, ..., p-1$ and θ_0 is the starting angle and $\delta\theta$ is the step size.

Since,

$z = \exp(j(\alpha + (2\pi/\lambda)d\cos\theta))$,

$z(\theta_i) = \exp(j(\alpha + (2\pi/\lambda)d\cos\theta_i))\ \forall\ \theta_i \in \mathrm{A}_{SR}$

And

$$\mathbf{A} = \left[\mathbf{s}_{N_2}(\theta_0)\mathbf{s}_{N_2}(\theta_1)...\mathbf{s}_{N_2}(\theta_{p-1})\right]^T$$

with

$$\mathbf{s}_{N2}(\theta_i) = [1, \exp(j(\alpha + (2\pi/\lambda)d\cos\theta_i)), ..., \exp(j(N_2 - 1)(\alpha + (2\pi/\lambda)d\cos\theta_i))]$$

Hence the requirement is to minimize the array output power along the angles $\theta_i \in \mathrm{A}_{SR}$ subject to the unit output along desired signal direction θ_s as shown in Fig. 3.6. The requirement is fulfilled if we restrict the maximum output power in the sidelobe region (sidelobe level) to minimum value. Minimizing this power along the angles $\theta_i \in \mathrm{A}_{SR}$ is the same as minimizing the absolute output along these angles i.e.

$$\min_{\mathbf{b}} \max(|\mathbf{s}_{N_2}(\theta_i)\mathbf{b}|), \theta_i \in \mathrm{A}_{SR} \quad \text{Subject to } \mathbf{s}_{N_2}(\theta_s)\mathbf{b} = 1$$

The steering vectors along these angles are contained in matrix $\mathbf{A}$ and the absolute output along these angles is $|\mathbf{Ab}|$. Therefore, the problem becomes as

$$\min_{\mathbf{b}} \max|\mathbf{Ab}| \text{ subject to } \mathbf{s}_{N_2}(\theta_s)\mathbf{b} = 1 \tag{3.2.5}$$

In (3.2.5) the objective function controls the sidelobe level and the constraint forms the main beam in the desired direction shown in Fig 3.6. This problem can be cast as the Second-Order Cone Program in the following manner

$$\begin{aligned} &\min imize\ t \\ &subject\ to\ |\mathbf{Ab}| \le t \\ &\qquad \mathbf{s}_{N_2}(\theta_s)\mathbf{b} = 1 \end{aligned} \tag{3.2.6}$$

The inequalities are called second-order cone constraints and $(\mathbf{Ab}, t) \in$ second-order cone in $\mathbf{R}^{\rho+1}$ [91]

Second-order cone program is the sub class of convex optimization hence the problem (3.2.5) can be solved using convex optimization technique [92].

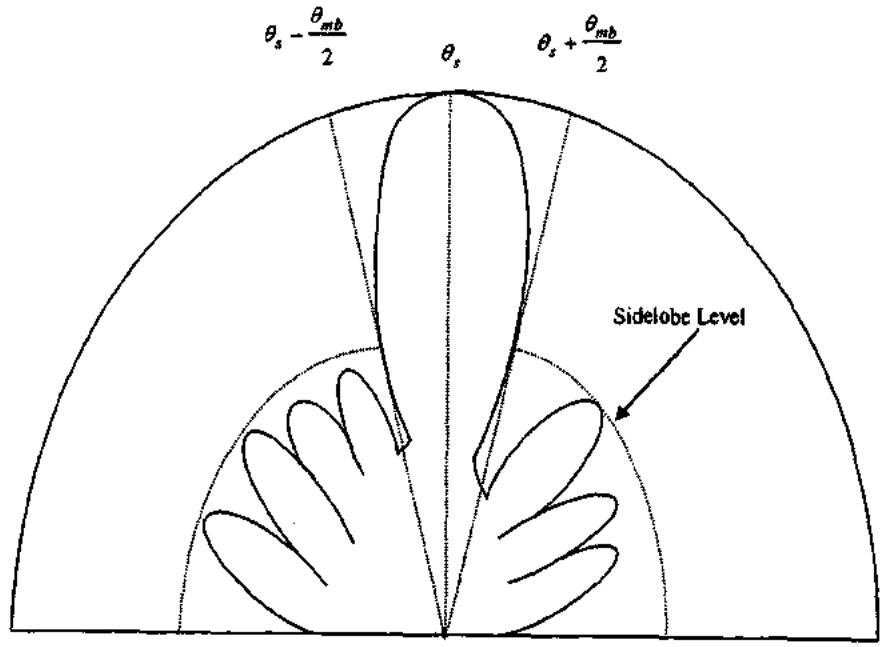

Figure 3.6: Main beam and sidelobe level for AF2

The array factor AF_2 suppresses sidelobelevels and has overlapping main beam with that of AF_1. Due to pattern multiplication, $AF = AF_1.AF_2$ will give the independent null steering capability with suppressed sidelobes. The array factor AF_2 is required to be calculated once and remains unchanged as long as the position of the main beam is unchanged. However, if the position of main beam is required to be changed, then both of the array factors AF_1 and AF_2 will have to be recalculated and changed.

3.2.2 PROPOSED STRUCTURE FOR INS WITH SSLS

Consider a uniform linear array of $N_1 + N_2$ elements. If we apply the structure of Fig. 3.1 on these elements, we will get N_2 outputs after N_1 stages. These N_1 stages will give AF_1 and steer N_1 nulls independently and the resulting N_2 outputs are weighted and summed to give AF_2 for sidelobe suppression. As mentioned earlier, convex optimization is used to find the N_2 complex weights. These N_2 weights remain unchanged even if one or more nulls change their position. On the other hand, if the main beam changes its position, the whole set of INS weights for N_1 stages and the N_2 weights for sidelobe control are changed. The structure is shown in Fig. 3.7.

3.2.3 SIMULATION RESULTS FOR INS WITH SSLS

In this section some simulation examples are given to verify the performance of the proposed algorithm for independent null steering with suppressed sidelobes. For these examples independent null steering algorithm (section 3.1) faces the problem of dominant levels of sidelobes

Two examples are being presented here in order to demonstrate the validity of the proposed algorithm.

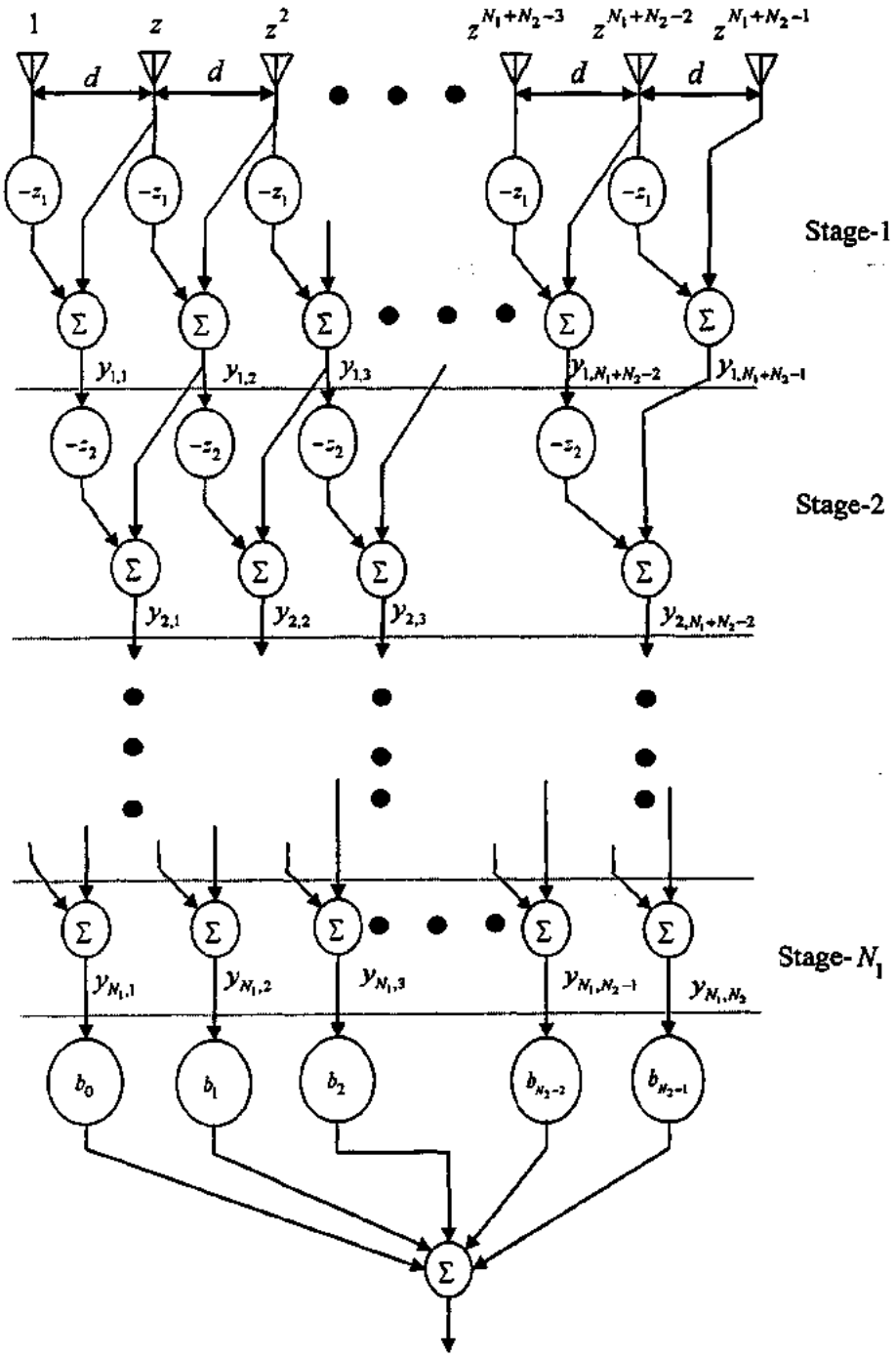

Figure 3.7: Structure for independent null steering with suppressed sidelobes

Example 1:

This example shows the effect of main beam width θ_{mb} of AF_2 on the sidelobe level. We considered interferences along $\theta_{i1}=15°, \theta_{i2}=40°, \theta_{i3}=65°, \theta_{i4}=100°$ and $\theta_{i5}=130°$ and the main beam is along $\theta_s=115°$. Since five nulls are to be steered, therefore $AF_1=\prod_{i=1}^{5}(z-z_i)$. Seven coefficients are dedicated to AF_2 i.e.

$$AF_2=b_0+b_1z+...+b_6z^6=\mathbf{s}_{N_2}\mathbf{b}.$$

Sidelobe level is observed by varying the width of the main beam. A linear array of 12 elements is required to implement these array factors. The AF_2 coefficients for $\frac{\theta_{mb}}{2}=15°,20°,25,30$ are shown in table 3.3

In simulation results, it is observed that on the average sidelobe level decreases as θ_{mb} increases. The performance of the algorithm for $\frac{\theta_{mb}}{2}=15°$ and $\frac{\theta_{mb}}{2}=30°$ is being discussed here under.

Fig 3.8 (a) shows the output power pattern for AF_1, which is the independent null steering by decoupling complex weights. It can be seen from the Fig. that the signal power from desired direction ($\theta_s=115°$) is approximately 3 dB down the highest power in the sidelobe region of the radiation pattern.

Fig 3.8 (b) shows the output power pattern of AF_2 for $\frac{\theta_{mb}}{2}=15°$ with main beam at 115°. Here the output power from desired direction is approximately 13 dB above the highest power in the sidelobe region.

The overall power pattern of the array factor ($AF=AF_1AF_2$) is shown in Fig 3.8 (c) where the power from desired direction is 11 dB above the highest power in the sidelobe region.

The comparison of Fig 3.8 (a) and (c) show that the proposed algorithm has improved the desired signal relative to the highest power in the sidelobe region.

Next the beam width θ_{mb} is increased and its effect on sidelobe level is observed. Fig 3.9 utilizes broader beam in the desired direction in comparison to Fig 3.8.

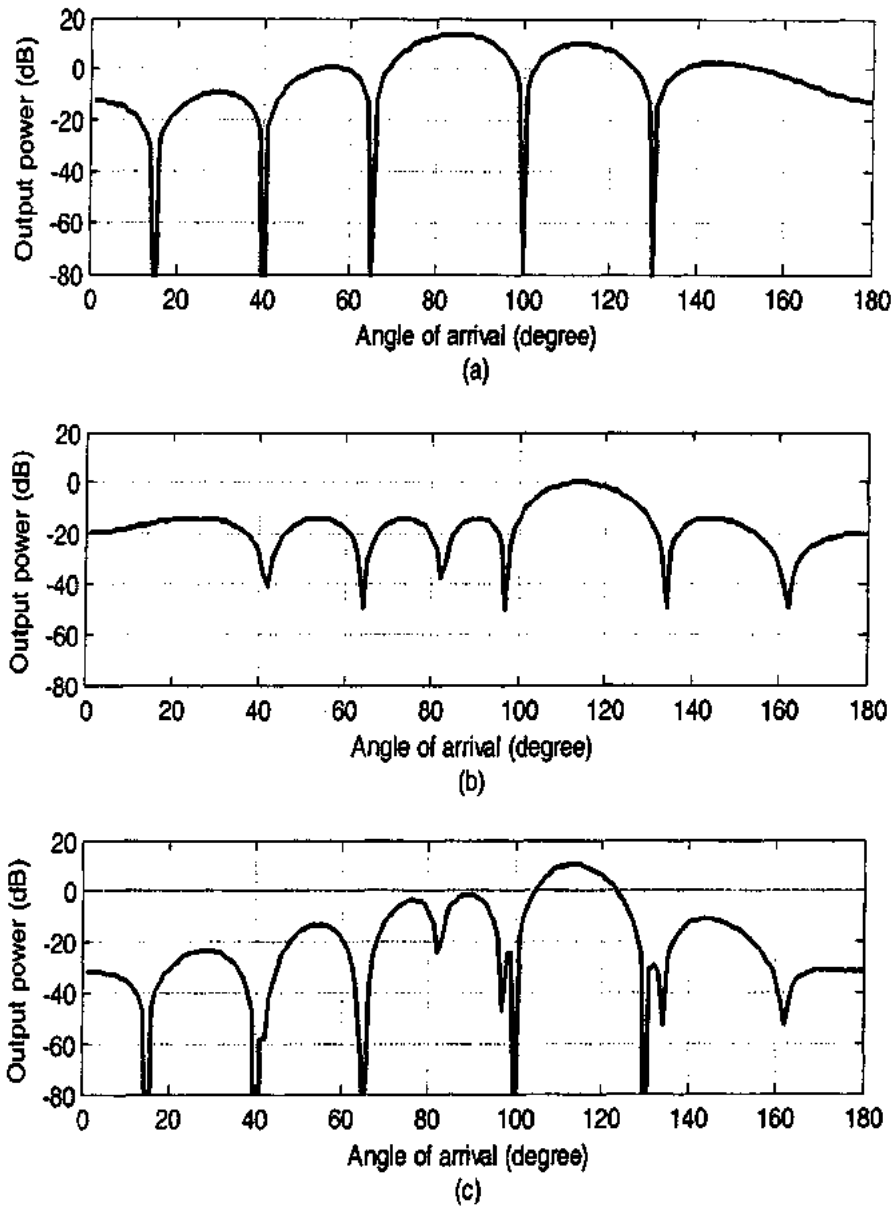

Figure 3.8: (a) Pattern for AF_1 when $\theta_s = 115°$ and $\theta_i = \{15°, 40°, 65°, 100°, 130°\}$ (b) Pattern for AF_2 when $\theta_s = 115°$ and $\frac{\theta_{mb}}{2} = 15°$ (c) Pattern for $AF = AF_1 AF_2$

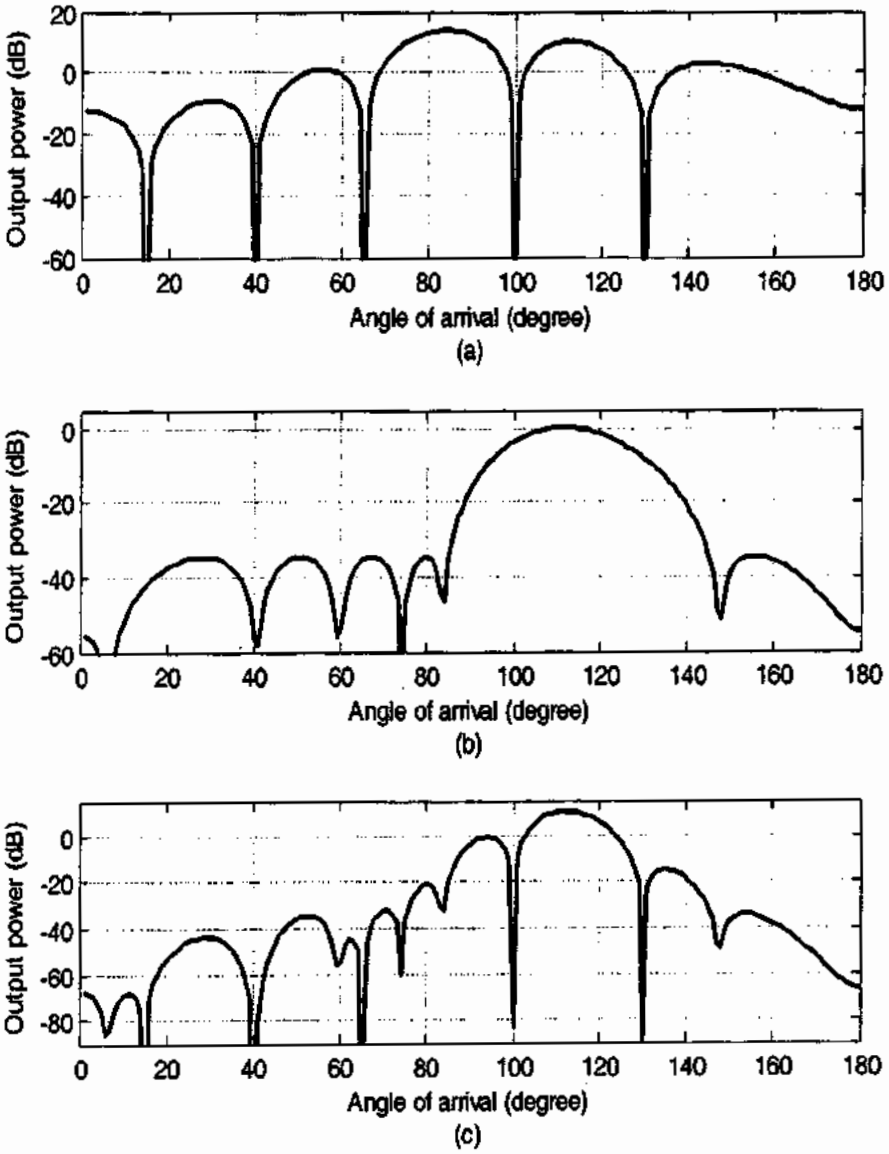

Figure 3.9: (a) Pattern for AF_1 when $\theta_s = 115°$ and $\theta_i = \{15°, 40°, 65°, 100°, 130°\}$. (b) Pattern for AF_2 when $\theta_s = 115°$ and $\frac{\theta_{mb}}{2} = 30°$ (c) Pattern for $AF = AF_1 AF_2$

Fig 3.9 (a) and Fig 3.8 (a) are the same and show the output power pattern for AF_1. Fig 3.9 (b) shows the pattern for AF_2 when $\frac{\theta_{mb}}{2} = 30°$ and $\theta_s = 115°$. Here the signal

from desired direction is 34 dB above the highest power in the sidelobe region and a portion of the main beam of AF_2 overlaps with the segment of the highest power region of AF_1 (between 85° and 100°).

Fig 3.9 (c) shows the performance of the proposed algorithm and is the product of patterns of Fig 3.9 (a) and 4.9 (b). It is clear from the Fig that the highest sidelobe is 10.7 dB down the main beam and hence no improvement is there in comparison to Fig 3.8 (c). Reason is again the same i.e., the overlapping discussed above. However the rest of the sidelobes are suppressed significantly.

Table 3.3: AF_2 coefficients with different beam width when $\theta_s = 115°$

b	$\frac{\theta_{mb}}{2} = 15°$	$\frac{\theta_{mb}}{2} = 20°$	$\frac{\theta_{mb}}{2} = 25°$	$\frac{\theta_{mb}}{2} = 30°$
b_0	0.1555 + 0.0214i	0.0979 + 0.0240i	0.0644 + 0.0253i	0.0437 + 0.0259i
b_1	0.1216 + 0.0109i	0.1307 + 0.0211i	0.1289 + 0.0328i	0.1219 + 0.0453i
b_2	0.1457 + 0.0066i	0.1752 + 0.0141i	0.1953 + 0.0244i	0.2099 + 0.0378i
b_3	0.1545 + 0.0000i	0.1924 - 0.0000i	0.2227 + 0.0000i	0.2489 + 0.0000i
b_4	0.1457 - 0.0066i	0.1752 - 0.0141i	0.1953 - 0.0244i	0.2099 - 0.0378i
b_5	0.1216 - 0.0109i	0.1307 - 0.0211i	0.1289 - 0.0328i	0.1219 - 0.0453i
b_6	0.1555 - 0.0214i	0.0979 - 0.0240i	0.0644 - 0.0253i	0.0437 - 0.0259i

Example 2:

This example shows the effect of number of AF_2 coefficients on the sidelobe level. For this purpose, $\frac{\theta_{mb}}{2}$ is kept constant and the number of coefficients N_2 is varied. These coefficients are evaluated by using convex optimization. The signal and interferences are the same as that of example 1. The coefficients are found for $\frac{\theta_{mb}}{2} = 20°$ and $N_2 = 10, 15, 20$. These coefficients are given in table 3.4. Fig 3.10 and 3.11 show the beam patterns for $\frac{\theta_{mb}}{2} = 20°$ and $N_2 = 10, 15$.

Fig. 3.10 (a) shows the pattern for AF_2 when $N_2 = 10$ where the signal power along desired direction ($\theta_s = 115°$) is approximately 33.5 dB above the highest power in the sidelobe region. Fig. 3.10 (b) shows the pattern for $AF = AF_1 AF_2$ where the signal power along desired direction is approximately 28 dB above the highest power in the sidelobe region.

Table 3.4: AF_2 coefficients when $\theta_s = 115°$, $\frac{\theta_{mb}}{2} = 20°$

S. No.	N_2	$\mathbf{b}^T$	Value of $\mathbf{b}^T$
1	10	$b_0 - b_9$	0.0300 + 0.0113i, 0.0608 + 0.0175i, 0.1027 + 0.0208i, 0.1415 + 0.0171i, 0.1650 + 0.0066i, 0.1650 - 0.0066i, 0.1415 - 0.0171i, 0.1027 - 0.0208i, 0.0608 - 0.0175i, 0.0300 - 0.0113i
2	15	$b_0 - b_{14}$	0.0040 + 0.0025i, 0.0129 + 0.0067i, 0.0295 + 0.0125i, 0.0540 + 0.0180i, 0.0835 + 0.0205i, 0.1122 + 0.0182i, 0.1334 + 0.0107i, 0.1411 - 0.0000i, 0.1334 - 0.0107i, 0.1122 - 0.0182i, 0.0835 - 0.0205i, 0.0540 - 0.0180i, 0.0295 - 0.0125i, 0.0129 - 0.0067i, 0.0040 - 0.0025i
3	20	$b_0 - b_{19}$	0.0005 + 0.0005i, 0.0023 + 0.0018i, 0.0066 + 0.0045i, 0.0151 + 0.0087i, 0.0288 + 0.0136i, 0.0479 + 0.0180i, 0.0705 + 0.0203i, 0.0934 + 0.0190i, 0.1122 + 0.0135i, 0.1228 + 0.0049i, 0.1228 - 0.0049i, 0.1122 - 0.0135i, 0.0934 - 0.0190i, 0.0705 - 0.0203i, 0.0479 - 0.0180i, 0.0288 - 0.0136i, 0.0151 - 0.0087i, 0.0066 - 0.0045i, 0.0023 - 0.0018i, 0.0005 - 0.0005i

Fig. 3.11 (a) shows the pattern for AF_2 when $N_2 = 15$ where the signal power along the desired direction is about 55 dB above the highest power in the sidelobe region. Fig. 3.11 (b) shows the pattern for $AF = AF_1 AF_2$ where the signal power along the desired direction is approximately 37 dB above the highest power in the sidelobe region.

In Fig. 3.12, the desired signal and interferences are along $\theta_s = 140°$ and $\theta_i = \{15°, 45°, 70°, 120°, 160°\}$. Fig 3.12 (a) and Fig 3.12 (b) shows the pattern for AF_1 and AF_2 respectively. For AF_2 where $N_2 = 20$ and $\frac{\theta_{mb}}{2} = 20°$, it can be seen from Fig that the desired signal is 50 dB above the highest power in the sidelobe region. This results in the sidelobe suppression for $AF = AF_1 AF_2$ where the desired signal is 30 dB

above the highest power in the sidelobe region as is clear from Fig. 3.12 (c). However in Fig 3.12, the beam symmetry around the desired direction is not available.

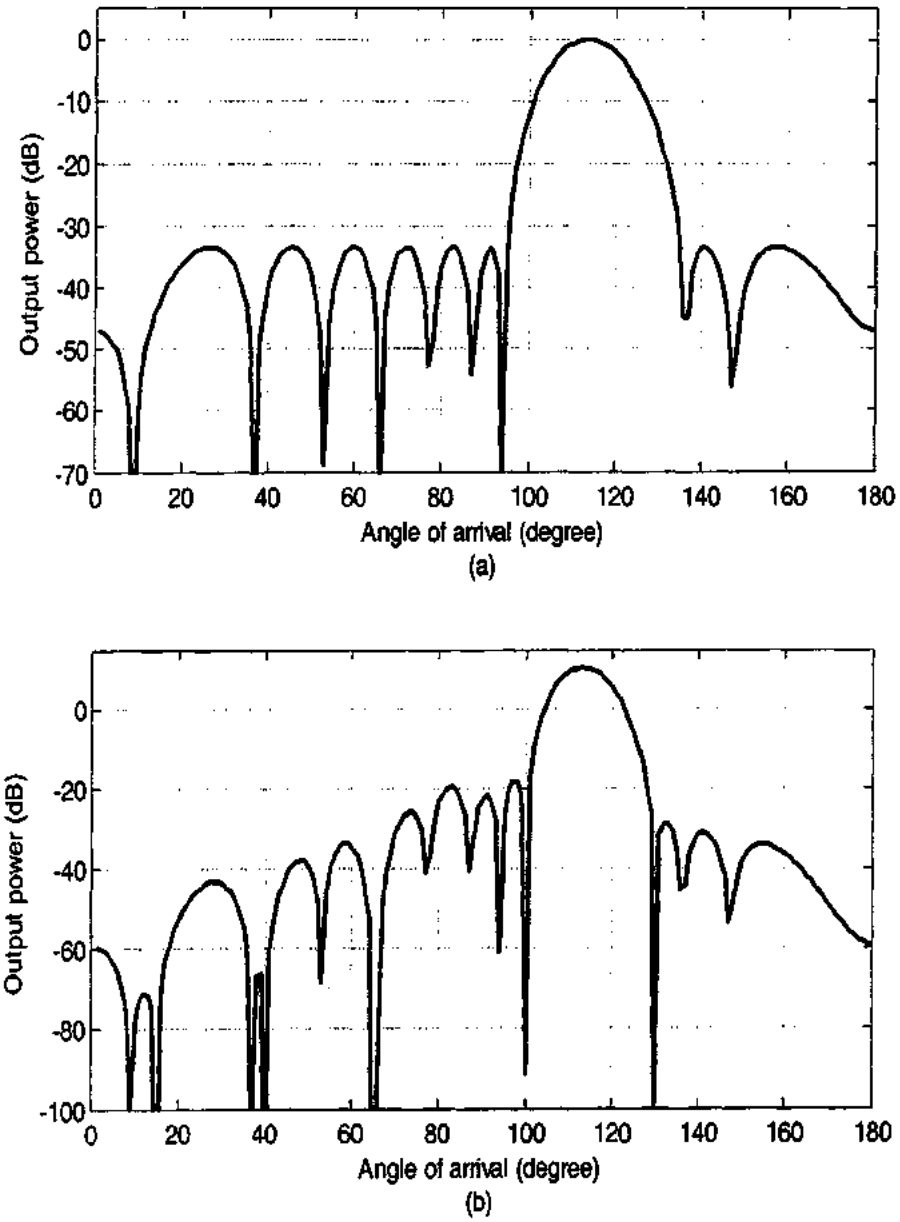

Figure 3.10: (a) Pattern for AF_2 when $\frac{\theta_{mb}}{2} = 20°$, $N_2 = 10$ (b) Independent null steering with suppressed sidelobes for $\theta_s = 115°$ and $\theta_i = \{15°, 40°, 65°, 100°, 130°\}$

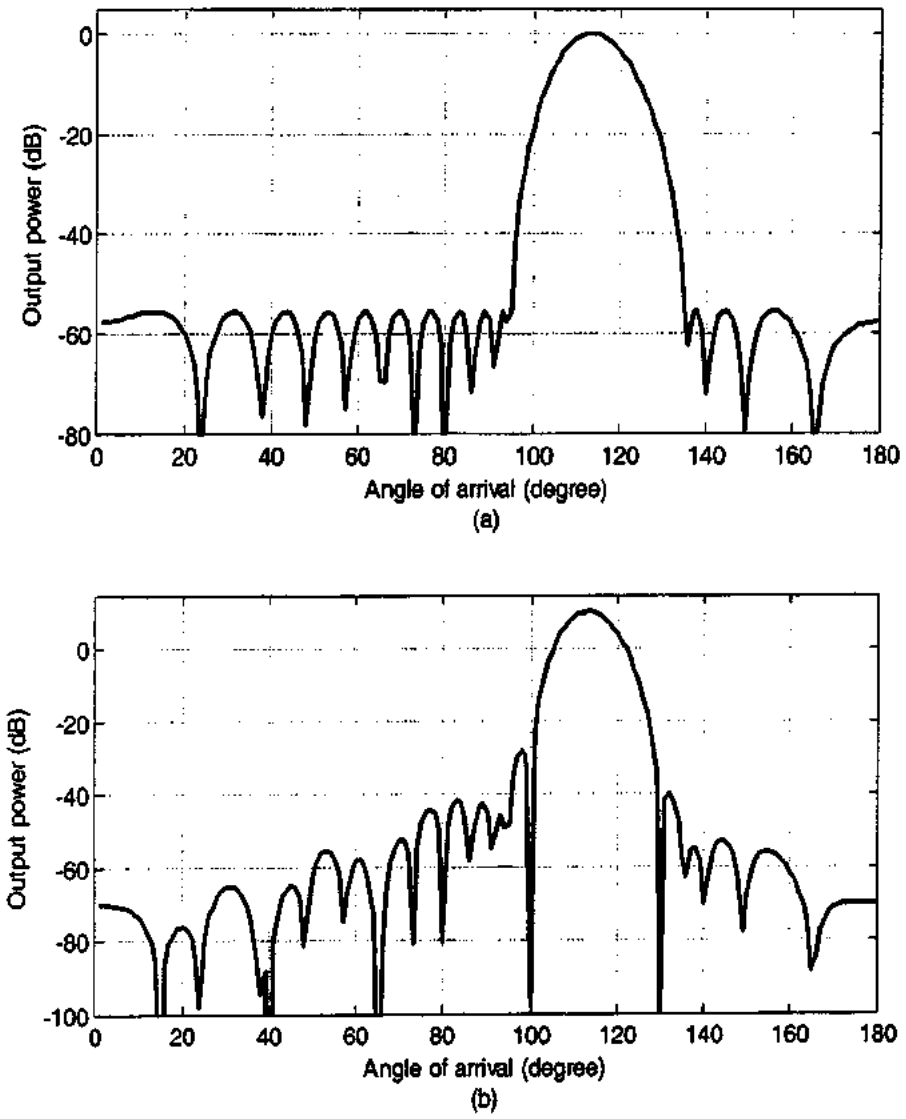

Figure 3.11: (a) Pattern for AF_2 when $\frac{\theta_{mb}}{2} = 20°$, $N_2 = 15$ (b) Independent null steering with suppressed sidelobes for $\theta_s = 115°$ and $\theta_i = \{15°, 40°, 65°, 100°, 130°\}$

It can be seen from Fig 3.8 through Fig 3.12 that though the proposed algorithm can provide independent null steering with suppressed sidelobes yet it is incapable to provide symmetric beam around the desired signal direction. This beam symmetry problem is solved in the next section.

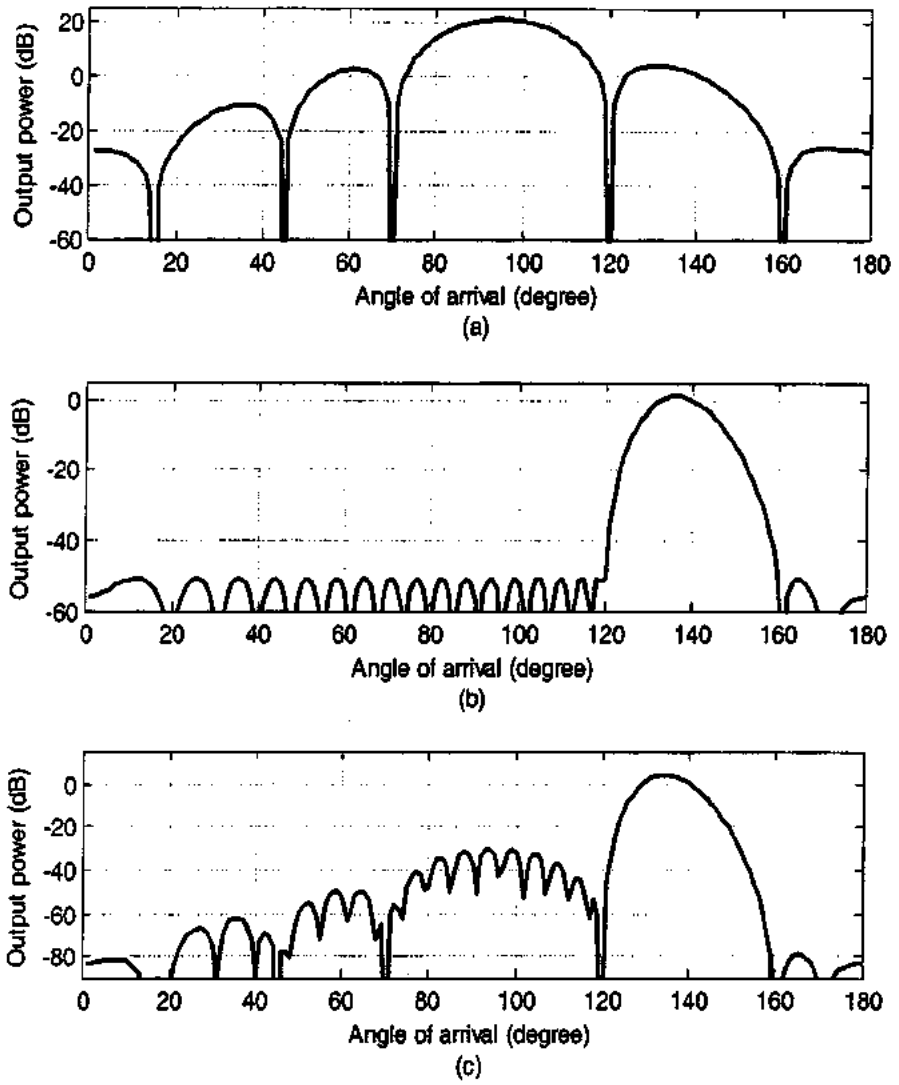

Figure 3.12: (a) Pattern for AF_1 when $\theta_s = 140°$ and $\theta_i = \{15°, 45°, 70°, 120°, 160°\}$. (b) Pattern for AF_2 when $\frac{\theta_{mb}}{2} = 20°$ $N_2 = 20$ (c) Independent null steering with suppressed sidelobes

3.3 INS WITH SUPPRESSED SLS AND SYMMETRIC BEAM

In order to achieve beam symmetry, the array factor for independent null steering is multiplied with the polynomial AF_3. The coefficients of this polynomial are

responsible for beam symmetry of AF_1 around θ_s. Thus the product AF_1AF_3 provides independent null steering with symmetric beam. In order to achieve sidelobe suppression along with INS with symmetric beam; AF_2 is also multiplied with the above product. Thus

$$AF = AF_1AF_3AF_2 \tag{3.3.1}$$

(3.3.1) Provides INS with symmetric beam and suppressed SLs, where

$$AF_3 = a_0 + a_1 z + ... + a_{N_3-1} z^{N_3-1} = \mathbf{s}_{N_3}\mathbf{a} \tag{3.3.2}$$

It is convenient to keep N_3 small so that the number of steerable nulls of the array factor is not affected to a greater limit.

3.3.1 COEFFICIENTS FOR AF_3

In order to find out the coefficients $a_0, a_1, ..., a_{N_3-1}$ we proceed as follows.

First of all select two angles θ_L and θ_R on left and right side of θ_s such that

$\theta_s - \theta_L = \theta_R - \theta_s$

Let P_L, P_s and P_R be the output power of AF_1 along θ_L, θ_s and θ_R respectively and

$P_L < P_s$ and $P_R < P_s$

Let $P_D = \frac{P_L + P_R}{2}$ be the desired power along θ_L and θ_R for symmetric beam of the array factor of expression (3.3.1) and

$$\begin{aligned} \psi_L &= \pi\cos(\theta_L) + \alpha \\ \psi_R &= \pi\cos(\theta_R) + \alpha \end{aligned} \tag{3.3.3}$$

Let $z_L = \exp(j\psi_L)$ and $z_R = \exp(j\psi_R)$ then

$$\begin{aligned} P_L &= \left|\prod_{i=1}^{N_1}(z_L - z_i)\right| \\ P_R &= \left|\prod_{i=1}^{N_1}(z_R - z_i)\right| \end{aligned} \tag{3.3.4}$$

Let P_{Ls} and P_{Rs} be the output power of the array factor AF_1AF_3 along θ_L and θ_R respectively, then

$$\begin{aligned} P_{Ls} &= \left|\prod_{i=1}^{N_1}(z_L - z_i)(a_0 + a_1 z_L + \ldots + a_{N_3-1} z_L^{N_3-1})\right| \\ P_{Rs} &= \left|\prod_{i=1}^{N_1}(z_R - z_i)(a_0 + a_1 z_R + \ldots + a_{N_3-1} z_R^{N_3-1})\right| \end{aligned} \tag{3.3.5}$$

$$error1 = |P_{Ls} - P_D| \tag{3.3.6}$$

$$error2 = |P_{Rs} - P_D| \tag{3.3.7}$$

$$error = |P_{Ls} - P_D| + |P_{Rs} - P_D| \tag{3.3.8}$$

The coefficients for beam symmetry can be found by minimizing the error i.e.

$$\min_{\mathbf{a}} |P_{Ls} - P_D| + |P_{Rs} - P_D| \tag{3.3.9}$$

Subject to $\prod_{i=1}^{N_1}(z_s - z_i)(b_0 + b_1 z_s + \ldots + b_{N_2-1} z_s^{N_2-1})(a_0 + a_1 z_s + \ldots + a_{N_3-1} z_s^{N_3-1}) = 1$

The minimization of the object function guarantees the main beam symmetry while the constraint forces the highest power in the main lobe to be equal to unity.

This problem can be solved using Genetic Algorithm (GA) [93], [94]. For this purpose we utilize the constraint given in (3.3.9) to define

$$error3 = \left|\prod_{i=1}^{N_1}(z_s - z_i)(b_0 + b_1 z_s + \ldots + b_{N_2-1} z_s^{N_2-1})(a_0 + a_1 z_s + \ldots + a_{N_3-1} z_s^{N_3-1}) - 1\right| \tag{3.3.10}$$

Then fitness function for GA is developed as given below

$$fins = error1 + error2 + error3 \tag{3.3.11}$$

The complex weight vector **a** is found through GA to minimize the fitness function given in(3.3.11).

3.3.2 STRUCTURE FOR INS WITH SSLS AND SYMMETRIC BEAM

Since multiplication is commutative i.e. $AF = AF_1AF_3AF_2 = AF_1AF_2AF_3$. That is why, the structure for $AF = AF_1AF_3AF_2$ has the same output as $AF = AF_1AF_2AF_3$.

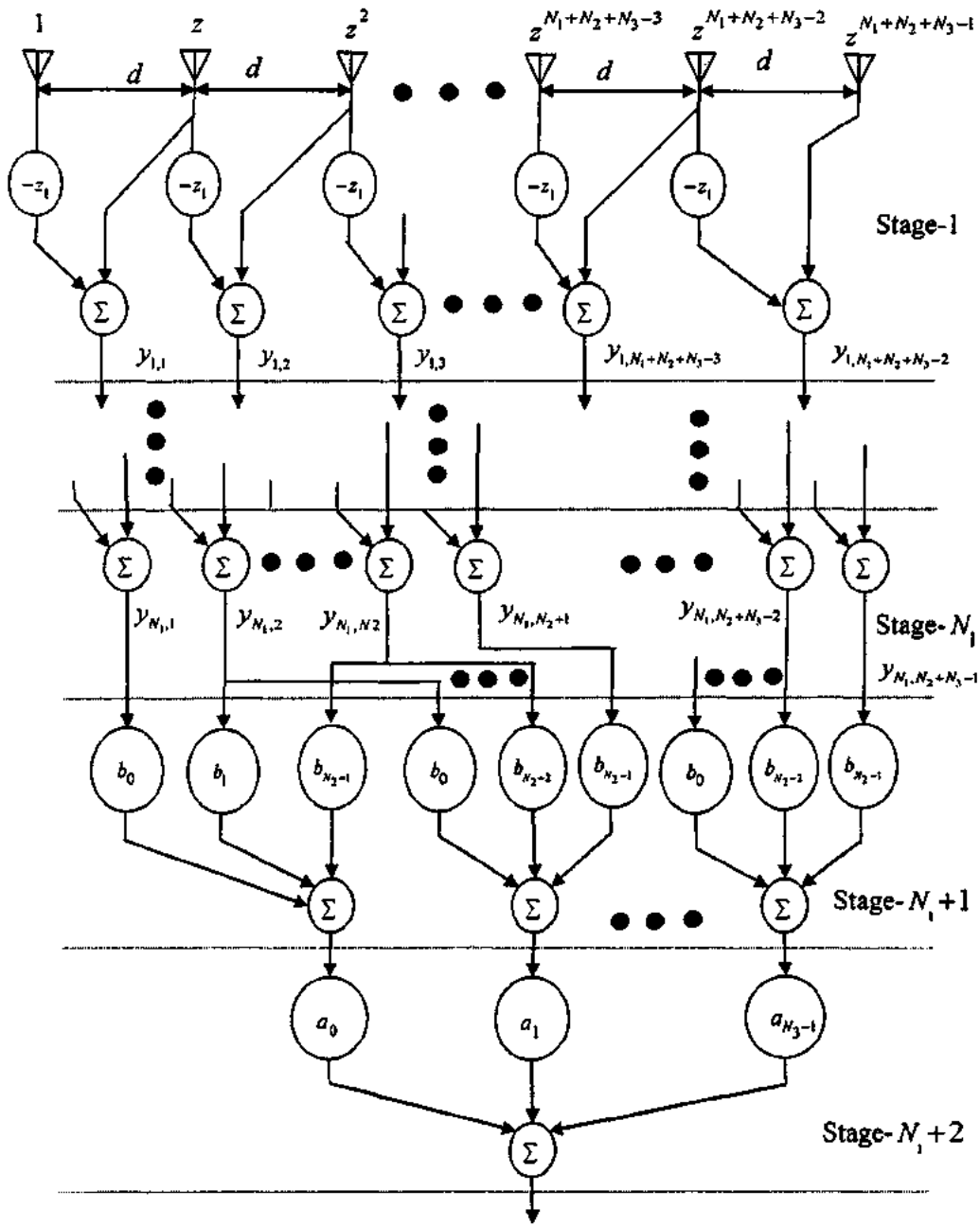

Figure 3.13: INS with suppressed sidelobes and beam symmetry

Then next set of outputs from 2 to N_2+1 is selected and multiplied by the same weight vector **b** and summed to result in AF_1AF_2z. The product AF_1AF_2 is the same as that the final output given in Fig 3.7. Same procedure is repeated until all of the outputs are utilized. The final stage will give N_3 outputs which are

$$AF_1AF_2, AF_1AF_2z, AF_1AF_2z^2, ..., AF_1AF_2z^{N_3-1}.$$

Finally this set of outputs is multiplied by the weight vector **a** and summed to result in $AF_1AF_2AF_3$. Vector **a** can be found by utilizing expression (3.3.9) and is responsible for beam symmetry. The structure for independent null steering with suppressed sidelobes and symmetric beam is shown in Fig 3.13.

3.3.3 Simulation Results for INS with SSLs and Symmetric Beam

In this section, beam symmetry for two algorithms namely, 'INS algorithm with suppressed sidelobes' and 'INS algorithm with suppressed sidelobes and symmetric beam' is compared. It must be noted that AF_1, AF_2 and AF_3 are the polynomials for independent null steering, sidelobe suppression and beam symmetry respectively.
Two illustrative examples are given to analyze the performance of the algorithm.

Example 1:

This example explains the steps involved to achieve beam symmetry and compares the beam pattern for $AF = AF_1AF_2$ and $AF = AF_1AF_2AF_3$.to match the beam symmetry for the algorithms namely

a. INS with SSLs
b. INS with SSLs and symmetric beam.

For this purpose, we have taken five interferences along $\theta_{i1} = 15°, \theta_{i2} = 45°$, $\theta_{i3} = 70°, \theta_{i4} = 120°$ and $\theta_{i5} = 160°$ and the main beam has been taken along $\theta_s = 140°$.

Since five nulls are to be steered, therefore $AF_1 = \prod_{i=1}^{5}(z - z_i)$. Ten coefficients are dedicated to AF_2 and three to AF_3 i.e.

$AF_2 = b_0 + b_1 z + ... + b_9 z^9 = \mathbf{s}_{N_2}\mathbf{b}$ with $\frac{\theta_{mb}}{2} = 30°$ and

$AF_3 = a_0 + a_1 z + a_2 z^2 = \mathbf{s}_{N_3}\mathbf{a}$.

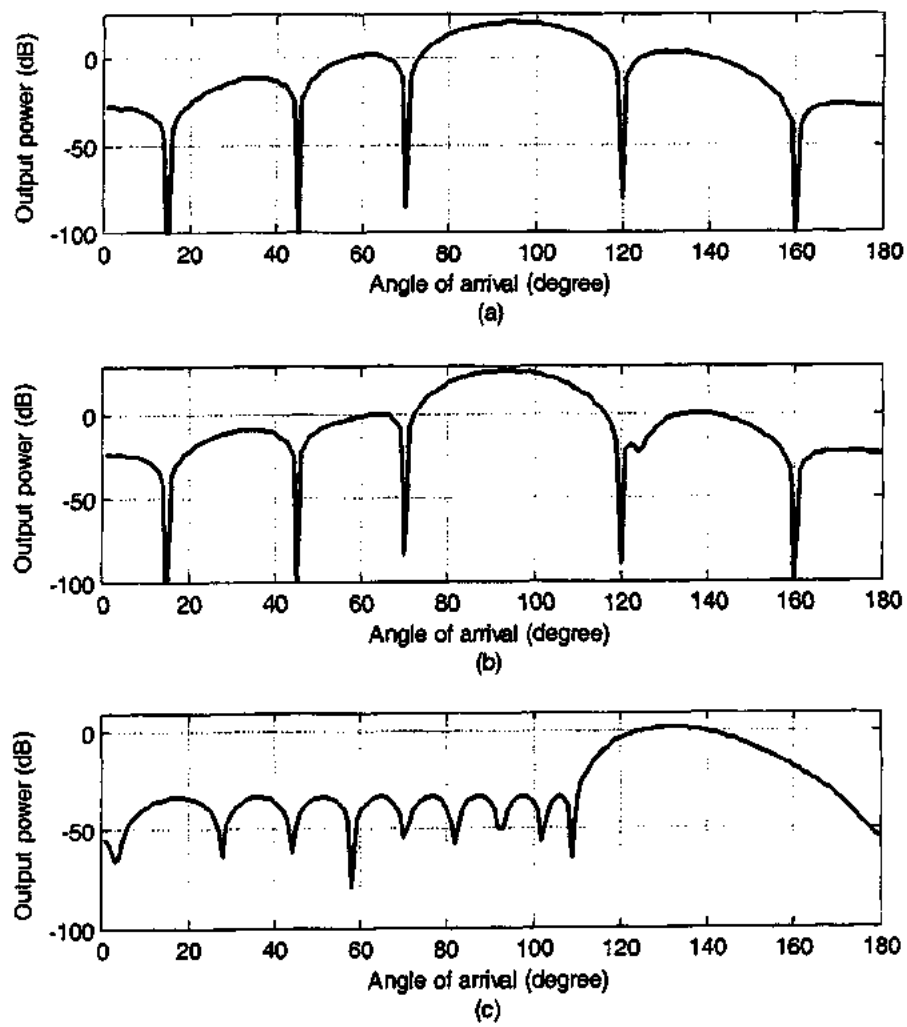

Figure 3.14: (a) INS i.e. $AF = AF_1$, (b) INS with beam symmetry around $\theta_s = 140°$ i.e. $AF = AF_1AF_3$, (c) Beam. Pattern of AF_3, meant for sidelobe suppression.

Fig 3.14 (a) shows the beam pattern for INS polynomial AF_1 where high sidelobe level and beam symmetry problem around the desired signal direction $\theta_s = 140°$ can be observed clearly. Since AF_3 is meant for improving the AF_1 symmetry, so $AF = AF_1 AF_3$ will have improved symmetry than AF_1 as is clear from the comparison of Fig 3.14 (a) and (b). Fig. 3.14 (c) shows the pattern for the sidelobe suppression polynomial AF_2 where the degradation in beam symmetry of the polynomial around $\theta_s = 140°$ is obvious. Fig 3.15 (a) shows the pattern for INS with SSLs i.e. $AF = AF_1 AF_2$ where two polynomials with beam symmetry problem multiply. Consequently, this problem is magnified in the resultant pattern of fig 3.15 (a).

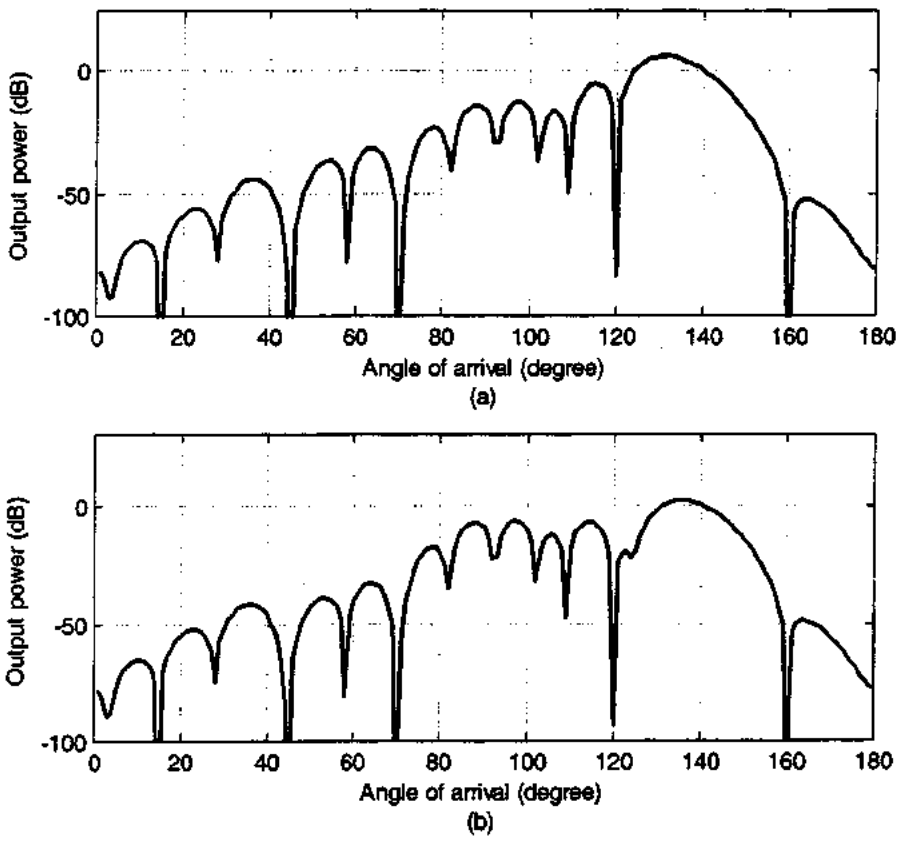

Figure 3.15: (a) INS with SSLs i.e. $AF = AF_1 AF_2$, (b) INS with suppressed sidelobes and beam symmetry i.e. $AF = AF_1 AF_2 AF_3$.

Fig 3.15 (b) shows the pattern for $AF = AF_1 AF_2 AF_3$ where the polynomial for INS with symmetric beam i.e. $(AF_1 AF_3)$ is multiplied with the polynomial AF_2 having degraded beam symmetry. Consequently the resultant pattern for $AF = AF_1 AF_2 AF_3$ has better symmetry than $(AF_1 AF_2)$ as is clear from the comparison of Fig 3.15 (a) and (b).

It is worth to mention that the symmetry can further be improved by improving the symmetry of AF_2. This can be achieved by multiplying AF_2 with another polynomial AF_4 whose coefficients will result in improved symmetry of $(AF_2 AF_4)$ as compared to AF_2 .and the corresponding structure can easily be developed like that shown in Fig 3.13.

Example 2:

This example deals with the same signals as those in example 1 above i.e main beam is along $\theta_s = 140°$ and

$$AF_1 = \prod_{i=1}^{5}(z - z_i)$$

However, AF_2 in this example utilizes 15 coefficients and is expressed below

$$AF_2 = b_0 + b_1 z + \ldots + b_{14} z^{14} = \mathbf{s}_{N_2}\mathbf{b} \text{ with } \frac{\theta_{mb}}{2} = 20°.$$

Fig 3.16 (a) and 3.16 (b) show the beam pattern for $AF = AF_1 AF_2$ and $AF = AF_1 AF_2 AF_3$ respectively.

It is evident from the comparison of Fig 3.16 (a) and (b) that beam symmetry improves in Fig 3.16 (b) due to the introduction of AF_3 in the corresponding array factor.

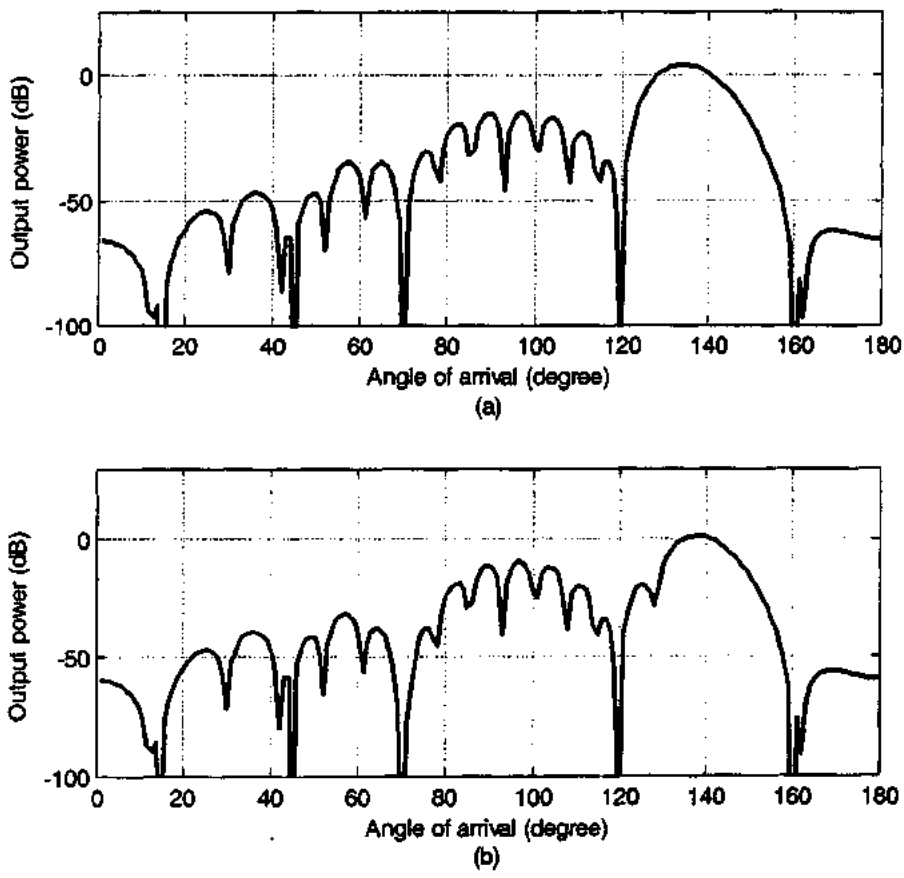

Figure 3.16: $N_2 = 15$, $\frac{\theta_{mb}}{2} = 20°$ **(a) INS with suppressed sidelobes i.e.** $AF = AF_1AF_2$, **(b) INS with suppressed sidelobes and beam symmetry i.e.** $AF = AF_1AF_2AF_3$.

3.4 CONCLUSION

In this chapter, three independent null steering structures have been presented. The key features of these algorithms are summarized below.

1. The first technique namely, Independent Null Steering by decoupling Complex Weights, has the capability of steering the maximum number of nulls independently. High sidelobe level and unsymmetric main beam along the desired direction may be there due to relative positions of desired signal and interferences.

2. Independent Null Steering with suppressed sidelobes is the structure that controls sidelobe level along with independent null steering. If the number of nulls to be steered independently is N_1 and the polynomial for sidelobe suppression is of degree N_2 then the required number of elements in the linear array will be $N_1 + N_2$. The additional feature of sidelobe suppression is obtained at the cost of $N_2 - 1$ nulls.
3. For the case of INS with suppressed sidelobes, the sodelobe level decreases as the degree N_2 of sidelobe suppression polynomial increases. However, with this algorithm the peak of the main beam is not guaranteed to lie in the desired signal direction.
4. The third structure provides independent null steering with suppressed sidelobes and symmetric main beam by multiplying three polynomials meant for independent null steering, sidelobe suppression and beam symmetry respectively. If the number of nulls to be steered independently is N_1 and the polynomial for sidelobe suppression and beam symmetry are of degree N_2 and N_3 respectively, then the required number of elements in the linear array will become $N_1 + N_2 + N_3$. The additional feature of sidelobe suppression and beam symmetry is obtained at the cost of $(N_2 + N_3 - 1)$ nulls.

CHAPTER 4

MATHEMATICAL MODEL FOR OPTIMAL ADAPTIVE BEAMFORMERS

Optimal adaptive (OA) beamformers have an advantage over the Direction of Arrival (DOA) based beamformers that they do not need the knowledge of DOA of interferences. Array adaptive weights are calculated by optimizing a cost function to form main beam along the desired direction and to place nulls in the direction of interferences. The cost function is developed in accordance with some specific criteria such as minimum variance, maximum SINR and maximum entropy [95], [96]. This chapter deals with the mathematical model for OA Beamformers and presents the comprehensive study of three popular algorithms in this domain.

The study of performance degradation of adaptive beamformers due to signal look direction errors is also included in this chapter. Simulation examples are given to depict the performance degradation of the beamformers caused by this problem. Finally some robust adaptive beamforming techniques for signal look direction errors are also discussed. The material presented in this chapter is mostly relevant to the publications [76], [86], [88], [97].

4.1 MATHEMATICAL MODEL FOR OA BEAMFORMERS

Consider a uniform linear array (ULA) of M antenna elements, shown in Fig. 4.1. The inter-element spacing is $\lambda/2$, with λ being the wavelength of incoming narrow band signal of interest.

For K signals, impinging on ULA, the output of the i^{th} antenna element $\{y_i(n)\}_{i=1}^{M}$ is given by

$$y_i(n)=\sum_{l=1}^{K} e^{j(i-1)\pi\sin\theta_l} s_l(n)+v_i(n) \tag{4.1.1}$$

With $s_l(n)$, the signal received from l^{th} source and $v_i(n)$, the additive white noise at this element.

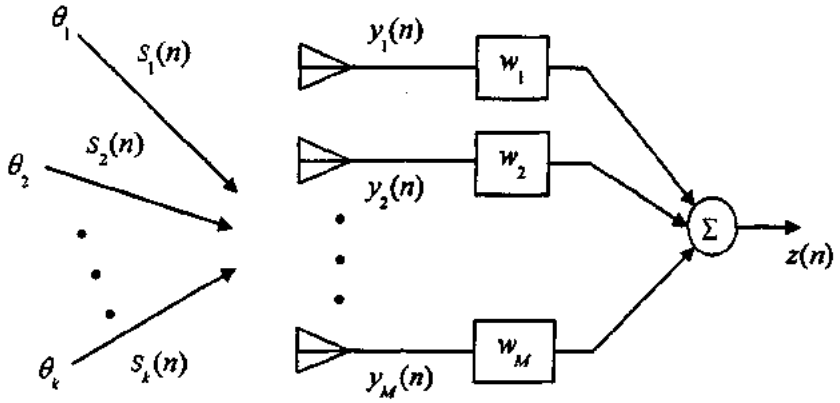

Figure 4.1: A ULA of *M*-antenna elements receiving signals from *K* sources.

Generally, expression (4.1.1) can be written in matrices form as given below

$$\mathbf{y}(n)=\mathbf{A}\mathbf{s}(n)+\mathbf{v}(n) \tag{4.1.2}$$

Where

$$\mathbf{y}(n)=\left[y_1(n)y_2(n)\ldots y_M(n)\right]^T$$

$$\mathbf{s}(n)=\left[s_1(n)s_2(n)\ldots s_K(n)\right]^T$$

$$\mathbf{A}=\left[\mathbf{a}(\theta_1)\ \mathbf{a}(\theta_2)\ \ldots\ \mathbf{a}(\theta_K)\right]$$

Also

$$\mathbf{a}(\theta_l)=\left[1\ e^{j\phi}\ e^{j2\phi}\ldots\ e^{j(M-1)\phi}\right]^T \tag{4.1.3}$$

Where $\phi_l=\pi\sin\theta_l$. The above expression represents the steering vector for l^{th} source [98].

The covariance matrix of source signals is given as

$$\mathbf{R}=E[\mathbf{s}(n)\mathbf{s}^H(n)]$$

$$= \begin{bmatrix} \sigma_{s_1}^2 & 0 \ldots & 0 \\ 0 & \sigma_{s_2}^2 \ldots & 0 \\ \vdots & \ddots & \vdots \\ 0 & \cdots & \sigma_{s_K}^2 \end{bmatrix} \tag{4.1.4}$$

$\{\sigma_{s_l}^2\}_{l=1}^{K}$ is the power of the signal received from l^{th} source. Similarly, the correlation matrix for noise is given as

$$\mathbf{R}_{\mathbf{v}} = E\left[\mathbf{v}(n)\mathbf{v}^H(n)\right] = \sigma_v^2 \mathbf{I}_M \tag{4.1.5}$$

Where $\mathbf{I}_M$ is identity matrix of order M and σ_v^2 is the noise variance. The covariance matrix $\mathbf{R}_{\mathbf{y}}$ of received signals from sources and noise is given by

$$\begin{aligned} \mathbf{R}_{\mathbf{y}} &= E\left[\mathbf{y}(n)\mathbf{y}^H(n)\right] \\ &= \mathbf{A}\mathbf{R}\mathbf{A}^H + \sigma_v^2 \mathbf{I}_M \end{aligned} \tag{4.1.6}$$

Where $\mathbf{A}$ is same as in (4.1.2). In practical situations, the covariance matrix $\mathbf{R}_{\mathbf{y}}$ of received signal is estimated from N snapshots and is expressed as

$$\hat{\mathbf{R}}_y = \frac{1}{N}\sum_{n=1}^{N} \mathbf{y}(n)\mathbf{y}^{\mathbf{H}}(n) \tag{4.1.7}$$

4.2 OA BEAMFORMING ALGORITHMS

In this section following optimal adaptive beamforming algorithms are discussed.

- MVDR Beamformer
- LCMV Beamformer
- Generalized Sidelobe Canceller

4.2.1 MVDR BEAMFORMER

This beamformer is also known as Capon beamformer since it was developed by Capon in 1969 [60]. This beamformer utilizes second order statistics of the array output $\mathbf{y}(n)$. It minimizes the variance i.e. the average output power of the

beamformer and maintains the distortionless response in the desired signal direction. The mathematical derivation for this beamformer is as given below.

Let $\mathbf{a}(\theta_s)$ be the steering vector in the desired direction and $\mathbf{R}_y$ is the received signal covariance matrix as given in expression(4.1.6). The optimization problem, cost function J and its solution in terms of beamformer weight vector $\mathbf{w}_{MV}$ are given in (4.2.1), (4.2.2) and (4.2.3) respectively.

$$\min_{\mathbf{w}} \mathbf{w}^H \mathbf{R}_y \mathbf{w} \text{ Subject to } \mathbf{w}^H \mathbf{a}(\theta_s) = 1 \tag{4.2.1}$$

$$J = \mathbf{w}^H \mathbf{R}_y \mathbf{w} + \lambda(\mathbf{w}^H \mathbf{a}(\theta_s) - 1) \tag{4.2.2}$$

$$\mathbf{w}_{MV} = \frac{\mathbf{R}_y^{-1}\mathbf{a}(\theta_s)}{\mathbf{a}^H(\theta_s)\mathbf{R}_y^{-1}\mathbf{a}(\theta_s)} \tag{4.2.3}$$

For practical situation

$$\mathbf{w}_{MV} = \frac{\hat{\mathbf{R}}_y^{-1}\mathbf{a}(\theta_s)}{\mathbf{a}^H(\theta_s)\hat{\mathbf{R}}_y^{-1}\mathbf{a}(\theta_s)} \tag{4.2.4}$$

Where $\hat{\mathbf{R}}_y$ is as given in (4.1.7).

The variants of MVDR Beamformer with sidelobe control are also available in the literature [99], [100].

4.2.1.1 SIMULATION RESULTS FOR MVDR BEAMFORMER

In order to show the performance of the MVDR Beamformer, two simulation examples are given. For this purpose we have considered a uniform linear array of 16 elements with inter-element spacing $\lambda/2$. INR is taken to be 30 dB.

Example 1:

This example shows the output power pattern for MVDR Beamformer with one desired signal and two interferences. The desired signal direction is $\theta_s = 0°$ with SNR=10 dB and the interferences are along $\theta_{i1} = 30°$ and $\theta_{i2} = 60°$. The direction of these interferences is represented as $\theta_i = \{30^0, 60^0\}$. The desired signal is always

present in the snapshot data. The simulation is performed in MATLAB utilizing expression (4.2.4) for adaptive weight vector of the beamformer. The performance of the beamformer for 500 snapshots is shown in Fig. 4.2.

From figure it is clear that the highest power of main beam is along 0° and the two nulls that are below -60 dB are along 30° and 60° .respectively Thus the radiation pattern of the beamformer is in accordance with θ_s and θ_i .

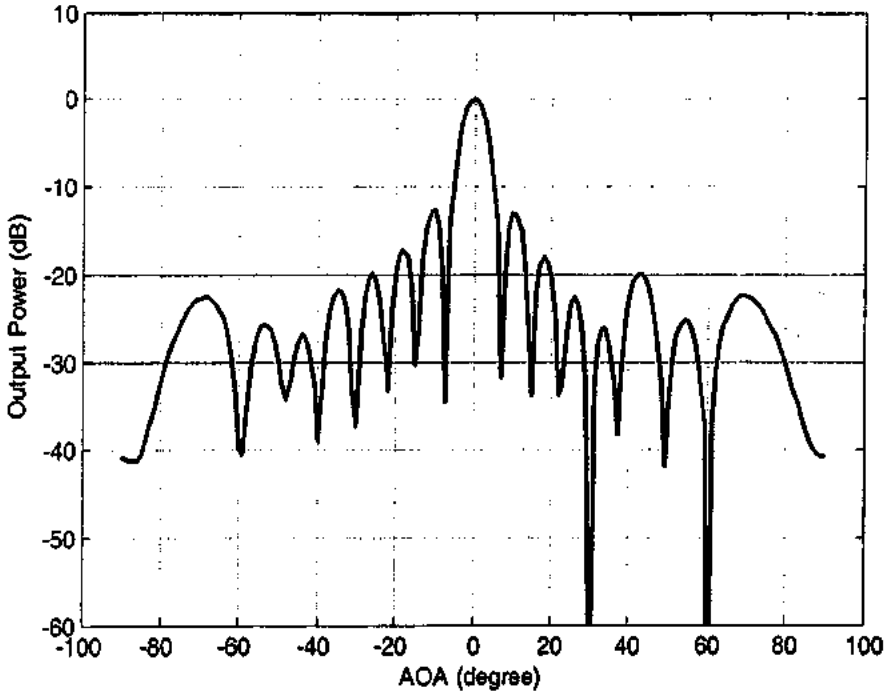

Figure 4.2: Radiation Pattern for MVDR Beamformer using 16-element ULA with $\theta_s = 0°$ and $\theta_i = \{30°, 60°\}$

Example 2:

This example shows the performance of MVDR Beamformer in terms of output SINR versus SNR. The desired signal has been taken at $\theta_s = 0°$. The interferences are placed at $\theta_{i1} = 30°$ and $\theta_{i2} = 60°$. Fig. 4.3 shows the performance of MVDR Beamformer for 500 snapshots averaged over 300 independent runs.

From figure it is clear that the output SINR of the beamformer is very close to the optimal value in the region of SNR ≤ 20 dB. The output SINR is approximately linear in the range of SNR ≤ 30 dB and saturates beyond that.

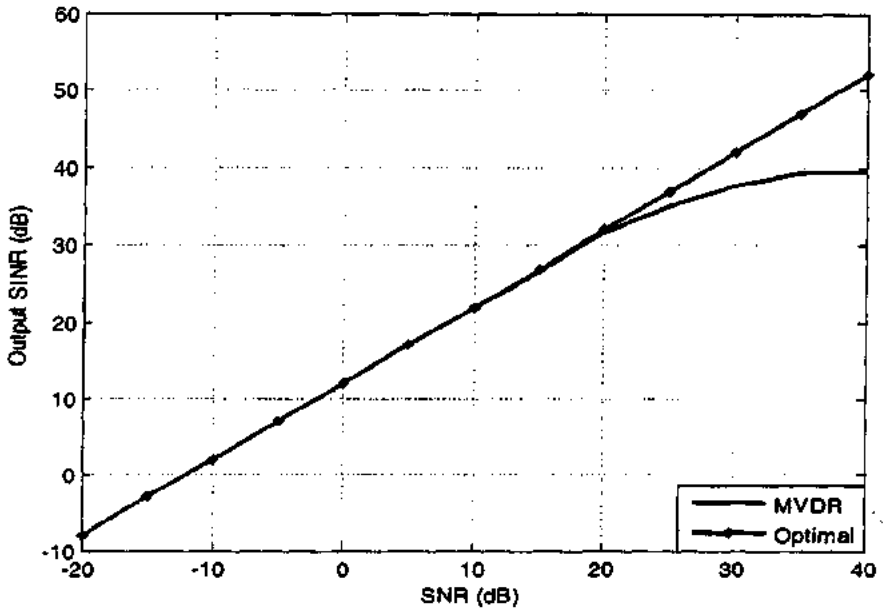

Figure 4.3: Performance of MVDR Beamformer in terms of Output SINR versus SNR

4.2.2 LCMV BEAMFORMER

Linearly Constrained Minimum Variance (LCMV) Beamformer determines the optimal weight vector that minimizes the output power while satisfying one or more linear equality constraints [101]. The optimization problem for this beamformer is given by (4.2.5).

$$\min_{\mathbf{w}} \mathbf{w}^H \mathbf{R}_y \mathbf{w} \text{ subject to } k \text{ linear constraints } \mathbf{C}^H \mathbf{w} = \mathbf{f} \tag{4.2.5}$$

The constraint matrix $\mathbf{C}$ contains k steering vectors and $\mathbf{f}$ is the gain vector corresponding to each steering vector contained in the matrix $\mathbf{C}$.

The solution to this optimization problem comes out to be

$$\mathbf{w}_{LC} = \mathbf{R}_y^{-1}\mathbf{C}(\mathbf{C}^H\mathbf{R}_y^{-1}\mathbf{C})^{-1}\mathbf{f} \tag{4.2.6}$$

For single constraint, LCMV beamformer becomes MVDR Beamformer given by (4.2.1), (4.2.2) and (4.2.3).

4.2.2.1 SIMULATION RESULTS FOR LCMV BEAMFORMER

For single constraint the LCMV beamformer becomes MVDR Beamformer mentioned above, hence we present the example with multiple constraints.

Example 1:

We have considered a uniform linear array of 16 Omni-directional elements with inter-element spacing $\lambda/2$. Two desired signals along $\theta_{s1} = -60°, \theta_{s2} = 0°$ with SNR=10 dB are considered. Two interferences, with INR=30 dB, are placed at $\theta_{i1} = 30°$ and $\theta_{i2} = 60°$. The corresponding correlation matrix $\mathbf{R}_y$ is given in expression(4.1.6). Fig. 4.4 shows the performance of LCMV beamformer for this example.

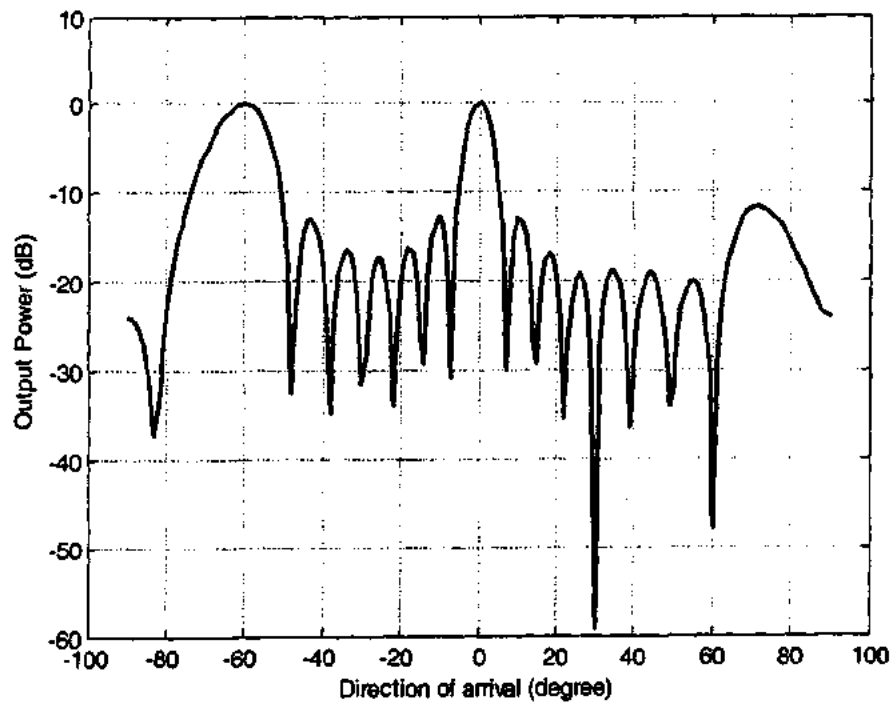

Figure 4.4: Output power pattern for LCMV Beamformer using 16-element ULA with $\theta_s = \{-60°, 0°\}$ and $\theta_i = \{30°, 60°\}$

4.2.3 GENERALIZED SIDELOBE CANCELLER (GSC)

Generalized sidelobe canceller (GSC) is a variant of linearly constrained minimum variance (LCMV) beamformer that converts constraint optimization problem into an unconstrained one.

The block diagram of GSC is shown in Fig. 4.5. GSC consists of two branches with quiescent beamformer in upper branch having weight vector $\mathbf{w}_q$ and sidelobe cancelling in lower branch having blocking matrix $\mathbf{B}$ followed by adaptive weight vector $\mathbf{w}_a$ [102]. The weight vector $\mathbf{w}_q$ in the upper branch preserves the desired signal. Matrix $\mathbf{B}$ blocks the desired signal and preservers interferences and noise i.e. undesired signal in the sidelobe cancelling branch which is the lower branch as indicated in Fig. 4.5.

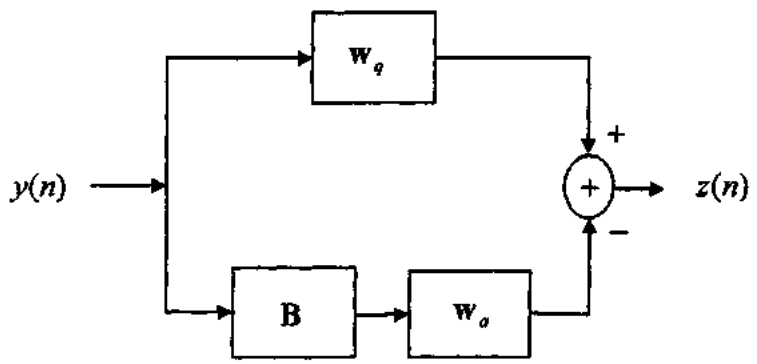

Figure 4.5: Generalized Sidelobe Canceller

Following are some well known results present in the literature

$$\mathbf{w}_q = \mathbf{C}(\mathbf{C}^H\mathbf{C})^{-1}\mathbf{f} \tag{4.2.7}$$

$$\mathbf{B} = null\{\mathbf{C}^H\} \tag{4.2.8}$$

Here $\mathbf{C}$ is constraint matrix containing steering vectors, $\mathbf{f}$ is gain vector containing gain corresponding to each steering vector of matrix $\mathbf{C}$. If $\mathbf{C}$ has k steering vectors, $\mathbf{B} = null\{\mathbf{C}^H\}$ represents null space such that

$$\mathbf{B}^H\mathbf{C}=\mathbf{O}$$

Where $\mathbf{O}$ is $M-k$ by M null matrix. Clearly the order of the null matrix indicates that $k<M$.

The unwanted signal which is preserved in the lower branch is subtracted from the, signal of upper branch which contains all the components i.e. the desired as well as undesired, signal components. The output $z(n)$ of GSC is given as:

$$\begin{aligned} z(n) &= \mathbf{w}_q^H\mathbf{y}(n)-\mathbf{w}_a^H\mathbf{B}^H\mathbf{y}(n) \\ &= \left(\mathbf{w}_q-\mathbf{B}\mathbf{w}_a\right)^H\mathbf{y}(n) \end{aligned} \tag{4.2.9}$$

The optimized adaptive weight vector $\mathbf{w}_a$, in the lower branch, denoted by $\mathbf{w}_{a\omega}$, is the one that minimizes the cost function

$$J(\mathbf{w}_a)=\left(\mathbf{w}_q-\mathbf{B}\mathbf{w}_a\right)^H\mathbf{R}_y(\mathbf{w}_q-\mathbf{B}\mathbf{w}_a)$$

$$\text{i.e. } \min_{\mathbf{w}_a}(\mathbf{w}_q-\mathbf{B}\mathbf{w}_a)^H\mathbf{R}_y(\mathbf{w}_q-\mathbf{B}\mathbf{w}_a)$$

The solution for this optimization problem comes out to be

$$\mathbf{w}_{a\omega}=(\mathbf{B}^H\mathbf{R}_y\mathbf{B})^{-1}\mathbf{B}^H\mathbf{R}_y\mathbf{w}_q \tag{4.2.10}$$

GSC is an alternative implementation of LCMV given by (4.2.5) and (4.2.6). GSC applies this problem discussed as below.

The objective function of the problem is applied by the subtraction of the outputs of two branches of GSC with the help of adaptive weight vector $\mathbf{w}_a$ to minimize the output power of the beamformer shown in Fig. 4.5. The constraint part is applied with the help of quiescent weight vector $\mathbf{w}_q$ in the upper branch and blocking matrix $\mathbf{B}$ in the lower branch. The $\mathbf{w}_q$ provides the required gain to the desired signal satisfying constraint and the blocking matrix $\mathbf{B}$ blocks the desired signal in the lower branch by creating sharp nulls. The weight vector $\mathbf{w}_a$ amplifies the interference and noise in the lower branch such that their combined effect in two branches results in minimum output power.

4.2.3.1 SIMULATION RESULTS FOR GSC

We have considered a uniform linear array of 16 Omni-directional elements with inter-element spacing $\lambda/2$. Three examples are presented here to elaborate the performance of the beamformer. Example 1 shows the beam pattern for single beam GSC, example 2 deals with multiple beam GSC and example 3 plots SINR versus SNR for single beam GSC.

Example 1:

In this example, one desired signal along $\theta_s = 0°$ with SNR=10 dB is considered. Two interferences, with INR=30 dB, are placed at $\theta_{i1} = 30°$ and $\theta_{i2} = -60°$. The covariance matrix $\mathbf{R}_y$ is used as given in expression(4.1.6). GSC weight vector is found using (4.2.7) and (4.2.10). for which the radiation pattern of the beamformer is plotted in Fig. 4.6/ The main beam appears in the desired signal direction and nulls appear along the directions of interferences respectively.

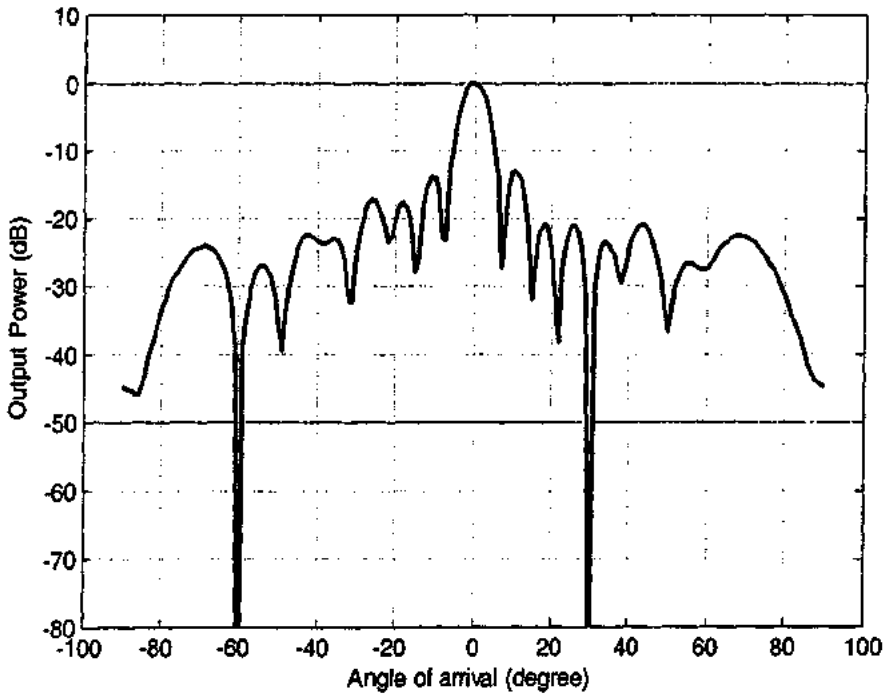

Figure 4.6: Single beam GSC using 16-element ULA with $\theta_s = 0°$ and $\theta_i = \{30°, -60°\}$

Example 2:

In this example two desired signals along $\theta_{s1} = -60°, \theta_{s2} = 0°$ with SNR=10 dB are considered for multiple beam GSC. Two interferences, with INR=30 dB, are placed at $\theta_{i1} = 30°$ and $\theta_{i2} = 65°$. The correlation matrix $\mathbf{R}_y$ is used as given in expression(4.1.6) . GSC weight vector is found using (4.2.7) and(4.2.10). The corresponding radiation pattern is plotted in Fig. 4.7. Clearly the main beam is in desired signal direction and nulls are in the directions of interferences respectively.

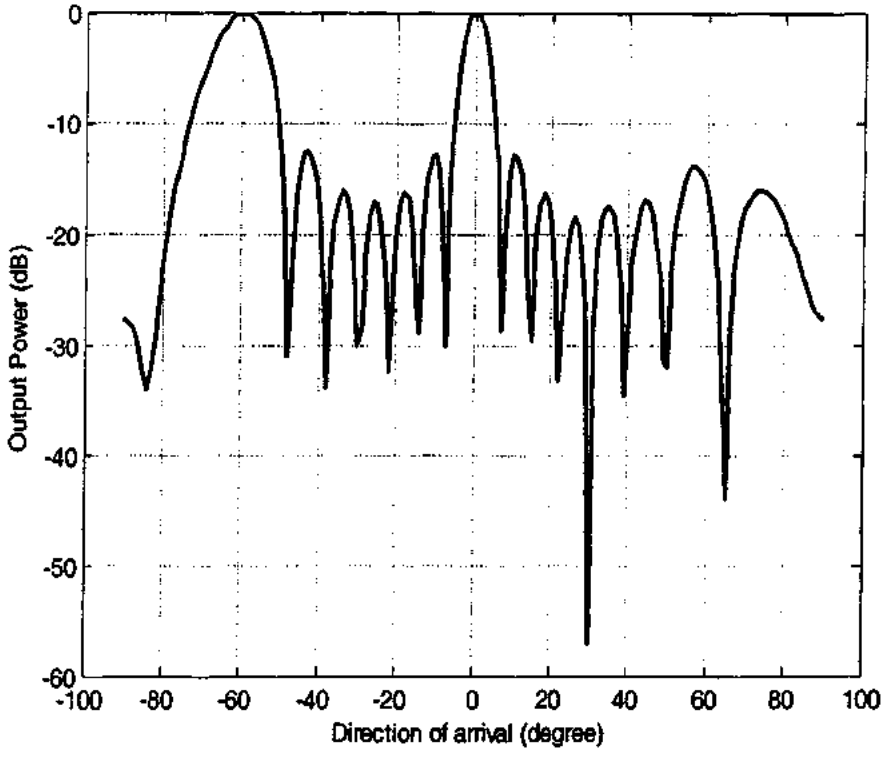

Figure 4.7: Multiple beam GSC using 16-element ULA with $\theta_s = \{-60°, 0°\}$ and $\theta_i = \{30°, 65°\}$

Example 3

In this example, we draw output SINR versus SNR for GSC. The desired signal has been taken at $\theta_s = 0°$. The interferences are placed at $\theta_{i1} = 30°$ and $\theta_{i2} = 60°$. INR is kept at 30 dB. Fig. 4.8 shows the performance of GSC regarding SINR versus SNR for 500 snapshots averaged over 300 independent runs.

From the Fig it is clear that the output SINR of GSC is close to optimal for SNR ≤ 20 dB. The output SINR is approximately linear for SNR ≤ 30 dB and SINR saturates for SNR > 30 dB.

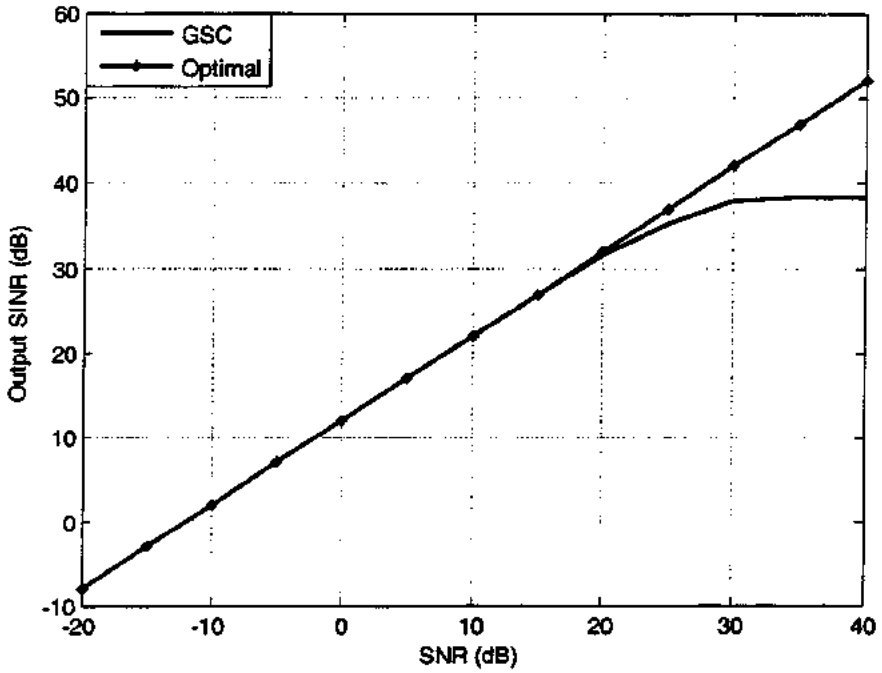

Figure 4.8: Performance of GSC in terms of Output SINR versus SNR

4.3 PERFORMANCE DEGRADATION OF OA BEAMFORMERS

The optimal adaptive (OA) beamforming algorithms such as MVDR, LCMV, GSC and SMI utilize second order statistics to minimize the output power subject to single or multiple linear constraints. The performance of these beamformers degrades severely due to number of reasons. The reasons include mismatch between the presumed and actual signal steering vector [11], [103], [104] and array imperfections such as non ideal array behavior, wave front distortion, array calibration errors, signal source spreading and distorted antenna shape [105]-[108]. Another cause of the performance degradation is the situation when the signal steering vector is known precisely but the training sample size is too small to estimate the correlation matrix $\mathbf{R}_y$ [73], [80], [109], [110].

Following are some simulation examples to show the performance degradation of MVDR Beamformer and GSC.

Example 1:

This example shows the performance degradation of MVDR Beamformer with DOA mismatch. A uniform linear array with 16 elements is used. The desired signal is presumed at $\theta_s = 0°$, while actual signal direction is along 3°, i.e. DOA mismatch is 3°. The interferences are placed at $\theta_{I1} = 40°$ and $\theta_{I2} = 70°$. SNR and INR are 10 dB and 30 dB respectively.

Fig. 4.9 (a) shows the performance of MVDR Beamformer without DOA mismatch. The performance of the beamformer is excellent at $\theta_s = 0°$ due to no error in signal look direction. Fig. 4.9 (b) shows the performance of MVDR Beamformer with DOA mismatch of 3°. The performance is degraded severely where the mismatch exists.

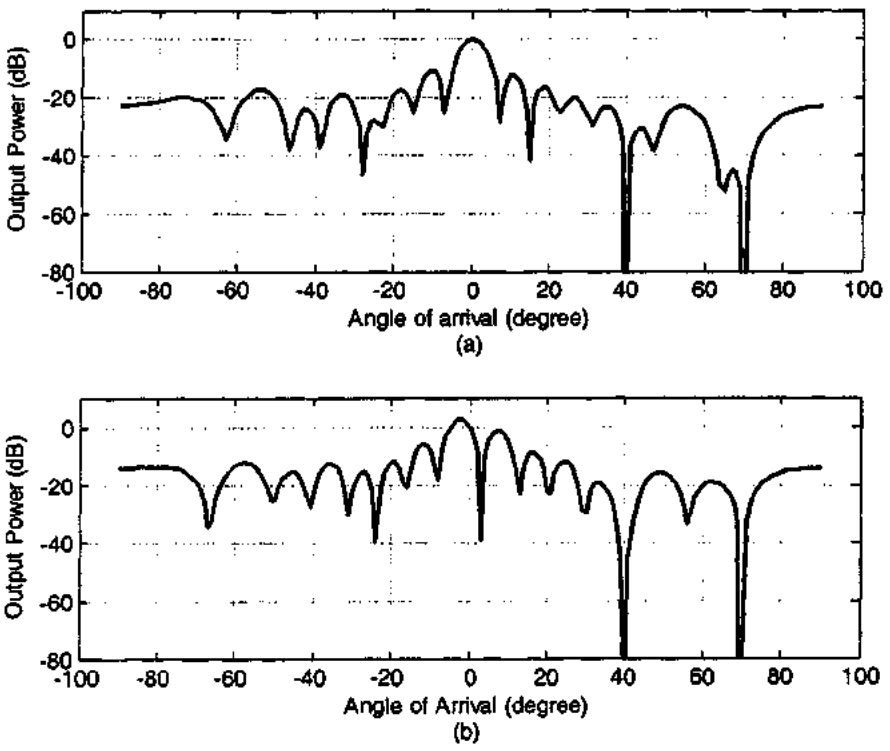

Figure 4.9: MVDR Beamformer (a) without DOA mismatch, (b) with DOA mismatch.

Example 2:

This example shows the SINR versus SNR for MVDR Beamformer with DOA mismatch equal to 3°. The desired signal is presumed at $\theta_s = 0°$ which actually exists at 3°, i.e. DOA mismatch of 3° is there. The interferences are placed at $\theta_{i1} = 30°$ and $\theta_{i2} = 60°$. INR is 30 dB. Fig. 4.10 shows the performance of the beamformer. It is clear from the figure that as the mismatched signal power increases, INR decreases. The reason is that the mismatched signal is also treated as interference.

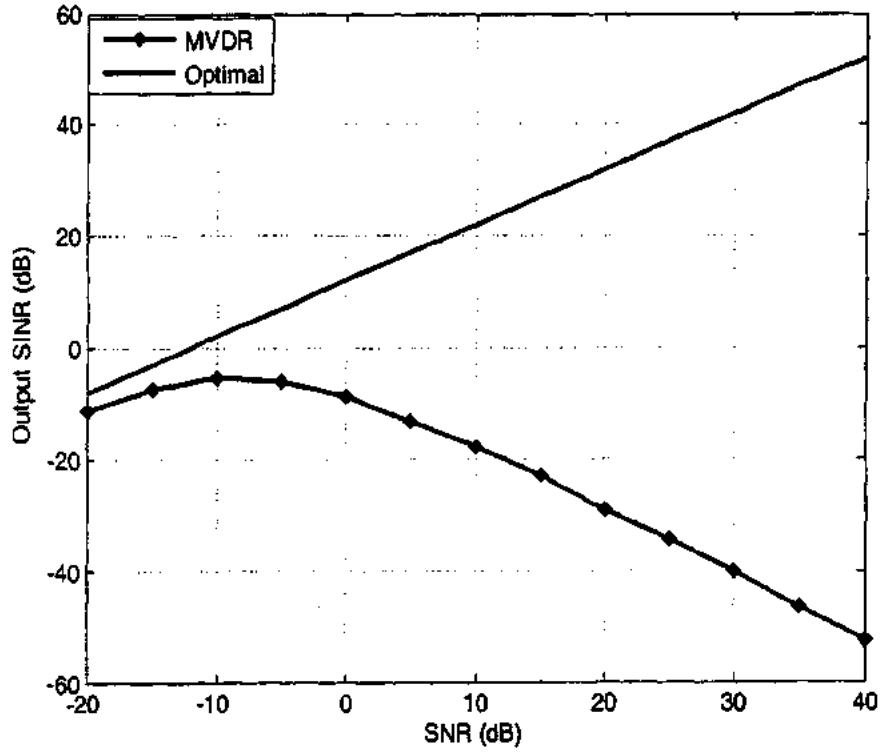

Figure 4.10: SINR versus SNR for MVDR Beamformer with DOA mismatch.

Example 3:

This example shows the performance degradation of GSC with DOA mismatch. A uniform linear array with 16 Omni-directional elements is used. The desired signal is presumed at $\theta_s = 0°$ while actual signal direction is along 3°, i.e. DOA mismatch is

3° . The interferences are placed at $\theta_{i1} = 40°$ and $\theta_{i2} = -70°$. SNR and INR are 10 dB and 30 dB respectively.

Fig. 4.11 (a) shows the performance of GSC without DOA mismatch where the null of a vector from blocking matrix, represented by the curve BM, is at 0°, and the desired signal falls inside this null. This is the reason that the performance of GSC is excellent in this situation.

Fig. 4.11 (b) shows the performance of GSC with DOA mismatch where the null for a vector from blocking matrix (BM) is at 0°, and the desired signal being at 3°, falls outside this null. This is the reason that the performance of GSC degrades severely in this situation at 3° which is -40 dB in Fig. 4.11 (b).

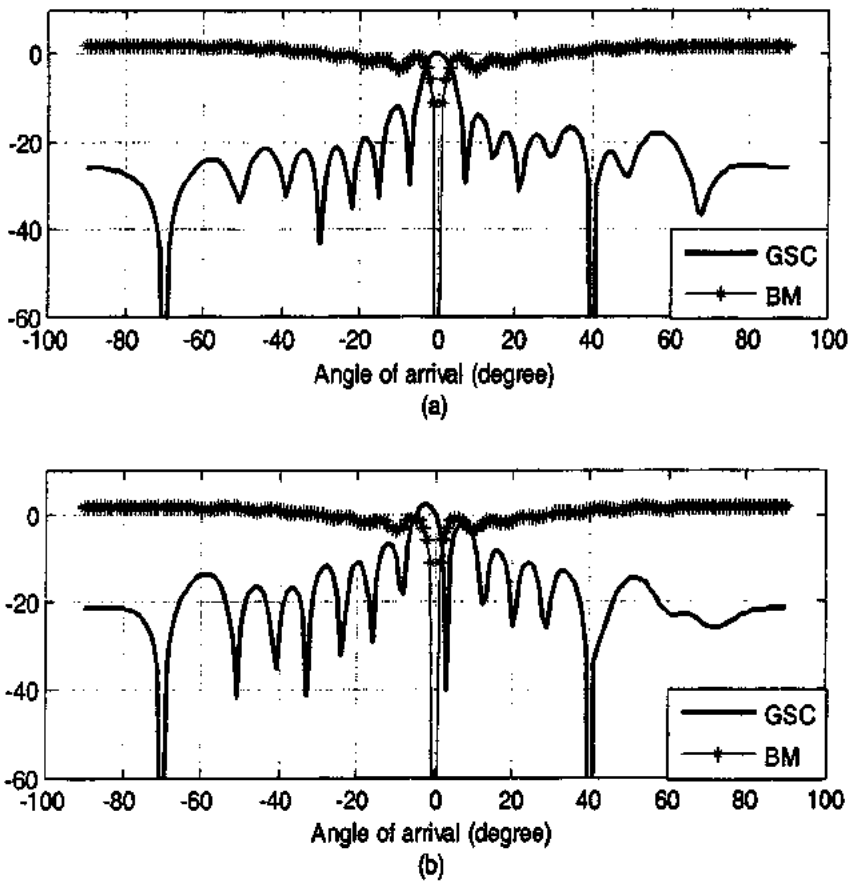

Figure 4.11: Performance of GSC (a) without DOA mismatch, (b) with DOA mismatch.

Example 4:

This example shows the SINR versus SNR for GSC with DOA mismatch equal to 3° . The desired signal is presumed at $\theta_s = 0°$ while actual signal direction is along $-3°$, i.e. DOA mismatch is 3°. The interferences are placed at $\theta_{i1} = 30°$ and $\theta_{i2} = 60°$. INR is 30 dB. Fig. 4.12 shows the performance of the beamformer. It is clear from the Fig. 4.12 that by increasing the power of mismatched signal INR decreases.

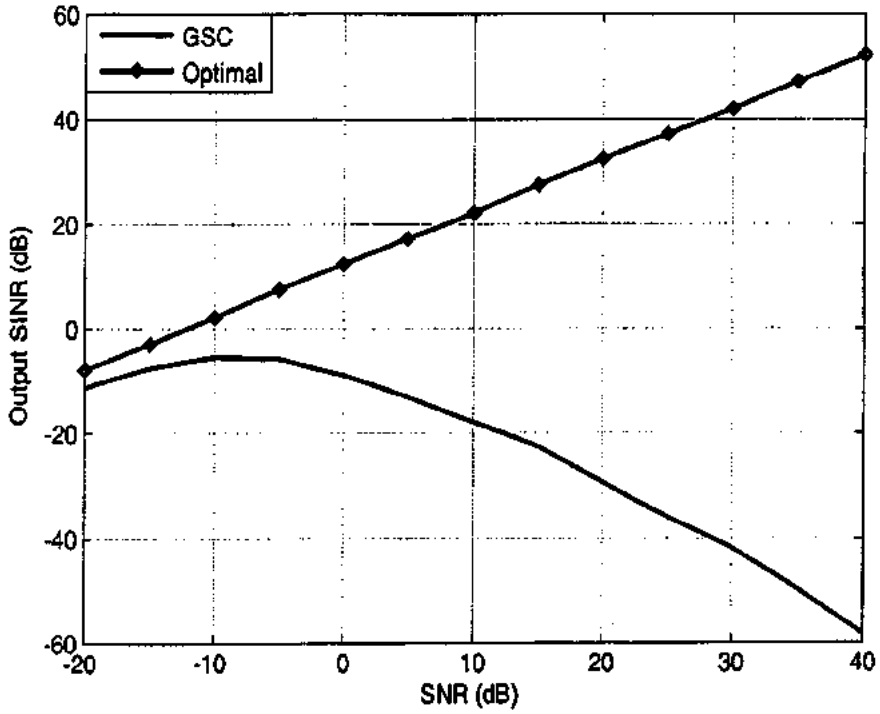

Figure 4.12: SINR versus SNR for GSC with DOA mismatch.

4.4 ROBUST ADAPTIVE BEAMFORMING ALGORITHMS

As mentioned in section 4.3, the performance of adaptive beamforming algorithms degrades severely when there is a mismatch between the presumed and actual signal direction. Lot of efforts has been made during the past three decades to overcome this problem.

Robust Linearly Constrained Minimum Variance (RLCMV) beamformer in fact achieves this robustness against signal look direction error by exploiting the linear constraints in the Minimum Variance Distortionless Response (MVDR) beamformer. However, the major drawback of these additional constraints is broadening of the main beam [87], [105].

Diagonal loading is a well known adaptive beamforming technique to alleviate DOA mismatch problem, yet with unavailability of the reliable criteria for choosing the optimal diagonal loading factor. Efforts are in progress even in recent years to develop reliable criterion for optimal diagonal loading level [81], [82], [111]. Robust adaptive beamforming using worst-case performance optimization is another popular approach for solving the signal look direction error problem [112]. However, the array performance of this method is very close to another simple algorithm known as diagonally loaded sample matrix inversion (LSMI) beamformer [80], [113].

Shahbazpanahi et al. developed general rank beamformer [86] by modeling DOA mismatch and array imperfections separately. This resulted in negative diagonal loading of desired signal covariance matrix and positive diagonal loading of sample data covariance matrix. The main problem of this algorithm is also the unavailability of the diagonal loading criterion.

In the following section the RLCMV beamformer and General-Rank beamformer are being discussed in detail.

4.4.1 RLCMV BEAMFORMER

This beamformer develops the constraint matrix $\tilde{\mathbf{C}}$ by incorporating left and right uncertainties $-\delta\theta$ and $+\delta\theta$ in the presumed signal steering vector $\mathbf{a}(\theta_s)$ for the robustness against signal DOA mismatch. The corresponding expression for matrix $\tilde{\mathbf{C}}$ is given by

$$\tilde{\mathbf{C}} = [\mathbf{a}(\theta_s - \delta\theta), \mathbf{a}(\theta_s), \mathbf{a}(\theta_s + \delta\theta)] \tag{4.4.1}$$

The gain vector corresponding to this matrix $\tilde{\mathbf{C}}$ is $\tilde{\mathbf{f}} = [1\ 1\ 1]^T$ and the LCMV beamforming problem is modified as [114]

$$\min_{\mathbf{w}} \mathbf{w}^H \mathbf{R}_y \mathbf{w} \text{ Subject to } \tilde{\mathbf{C}}^H \mathbf{w} = \tilde{\mathbf{f}} \tag{4.4.2}$$

The optimal weight vector for RLCMV beamformer, obtained by solving (4.4.2), is given by

$$\mathbf{w}_{LC} = \mathbf{R}_y^{-1} \tilde{\mathbf{C}} (\tilde{\mathbf{C}}^H \mathbf{R}_y^{-1} \tilde{\mathbf{C}})^{-1} \tilde{\mathbf{f}} \tag{4.4.3}$$

4.4.1.1 ROBUST LCMV BASED GSC

This GSC is an alternate way of finding RLCMV beamformer weight vector. The block diagram is shown below in Fig. 4.13. The parameters of RLCMV based GSC are given in expressions (4.4.4) through (4.4.7).

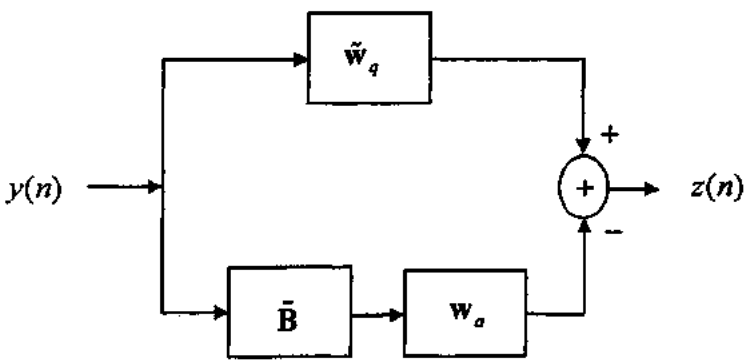

Figure 4.13: RLCMV Based Generalized Sidelobe Canceller

$$\tilde{\mathbf{w}}_q = \tilde{\mathbf{C}} (\tilde{\mathbf{C}}^H \tilde{\mathbf{C}})^{-1} \tilde{\mathbf{f}} \tag{4.4.4}$$

$$\tilde{\mathbf{B}} = null\{\tilde{\mathbf{C}}^H\} \tag{4.4.5}$$

$$\mathbf{w}_{ao} = (\tilde{\mathbf{B}}^H \mathbf{R}_y \tilde{\mathbf{B}})^{-1} \tilde{\mathbf{B}}^H \mathbf{R}_y \tilde{\mathbf{w}}_q \tag{4.4.6}$$

$$\tilde{\mathbf{w}}_{GSC} = \tilde{\mathbf{w}}_q - \tilde{\mathbf{B}} \tilde{\mathbf{w}}_{ao} \tag{4.4.7}$$

4.4.1.2 SIMULATION RESULTS FOR RLCMV BEAMFORMER

In this section three simulation examples are being presented to analyze the performance of RLCMV beamformer and RLCMV based GSC in the presence of signal look direction error. In all these examples, SNR and INR in a single sensor are equal to 10 dB and 30 dB respectively, and the desired signal is always present in the training data cell. AWGN with unit variance is also present along with signal and interferences.

Example 1:

This example shows the radiation pattern for RLCMV beamformer. A uniform linear array with 16 elements is considered. The desired signal is presumed at $\theta_S = 0°$ while actual signal direction is $\theta_{act} = 3°$ i.e. DOA mismatch is 3°.

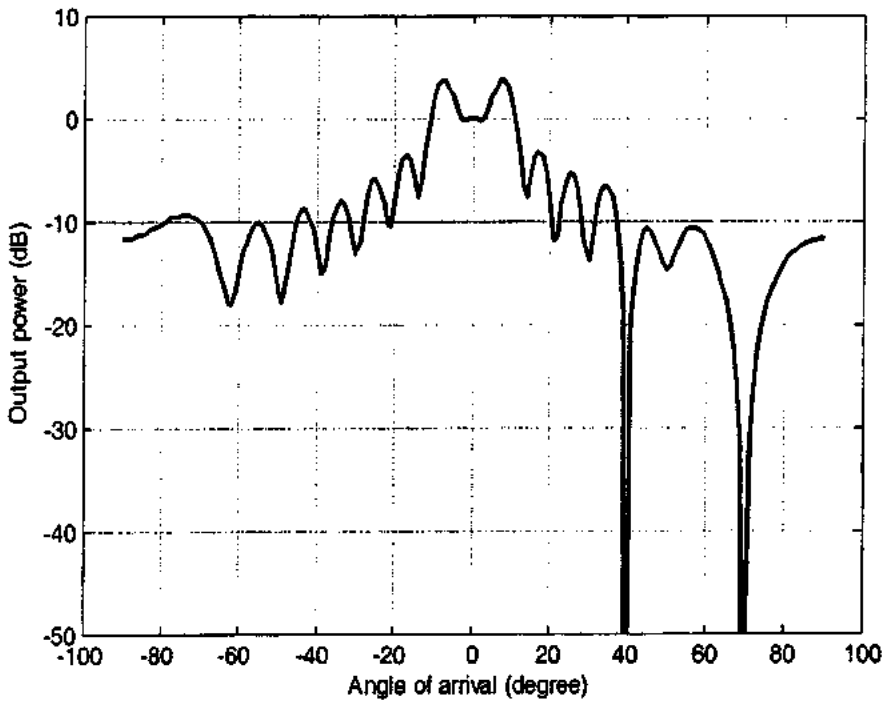

Figure 4.14: Pattern for RLCMV Beamformer and RLCMV Based GSC with $\theta_s = 0°$, $\theta_{act} = 3°$ and $\theta_i = \{40°, 70°\}$

Let the robustness is required within a region of ±3° around $\theta_S = 0°$ i.e. $\delta\theta = 3°$. The interferences are placed at $\theta_{i1} = 40°$ and $\theta_{i2} = 70°$.

Fig. 4.14 shows the performance of RLCMV beamformer and its equivalent GSC. For the robustness of this beamformer against the DOA mismatch of 3°, $\tilde{\mathbf{C}} = [\mathbf{a}(\theta_s - \delta\theta)\ \mathbf{a}(\theta_s)\ \mathbf{a}(\theta_s + \delta\theta)]$ and $\tilde{\mathbf{f}} = [1\,1\,1]^T$ have been used. Broadening of the main beam can clearly be observed in Fig. 4.14.

Example 2:

In this example SINR versus DOA mismatch is plotted for the beamformer of example 1. Two cases have been considered.

Case 1, with $\tilde{\mathbf{C}} = [\mathbf{a}(\theta_s - \delta\theta)\ \mathbf{a}(\theta_s)\ \mathbf{a}(\theta_s + \delta\theta)]$, $\tilde{\mathbf{f}} = [1\,1\,1]^T$ and $\delta\theta = 3°$.

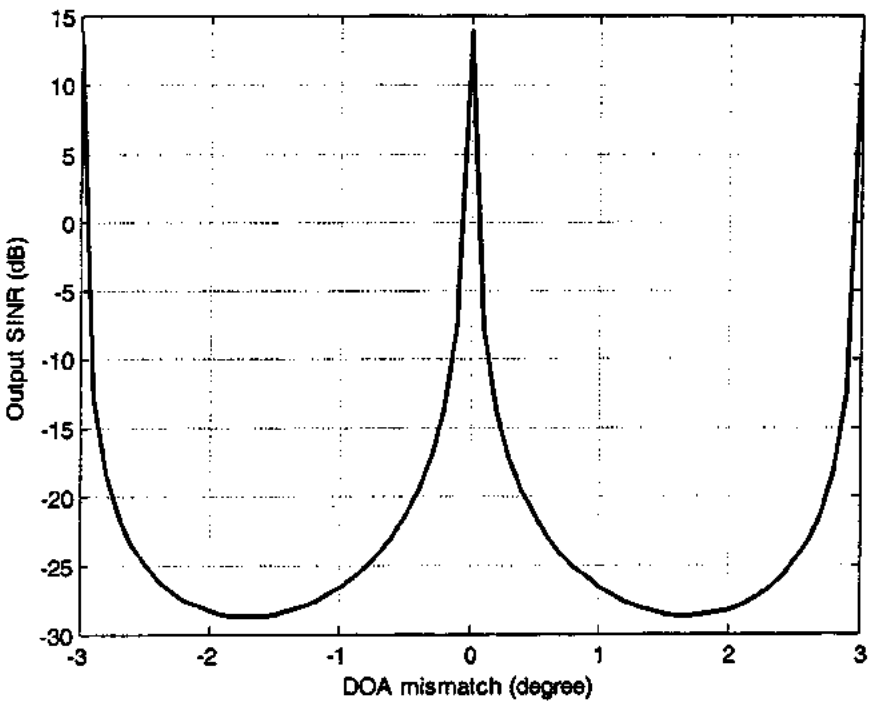

Figure 4.15: RLCMV beamformer and RLCMV based GSC with 3 steering vectors in $\tilde{\mathbf{C}}$. Output SINR versus DOA mismatch

This situation is shown in Fig. 4.15. It is clear from the Fig. that SINR is higher at angles whose steering vectors are contained in $\tilde{\mathbf{C}}$.

Case 2, with $\tilde{\mathbf{C}} = [\mathbf{a}(\theta_s - 2\delta\theta)\ \mathbf{a}(\theta_s - \delta\theta)\ \mathbf{a}(\theta_s)\ \mathbf{a}(\theta_s + \delta\theta)\ \mathbf{a}(\theta_s + 2\delta\theta)]$, $\tilde{\mathbf{f}} = [1\ 1\ 1\ 1\ 1]^T$ and $\delta\theta = 1.5°$. The performance for this situation is shown in Fig. 4.16.

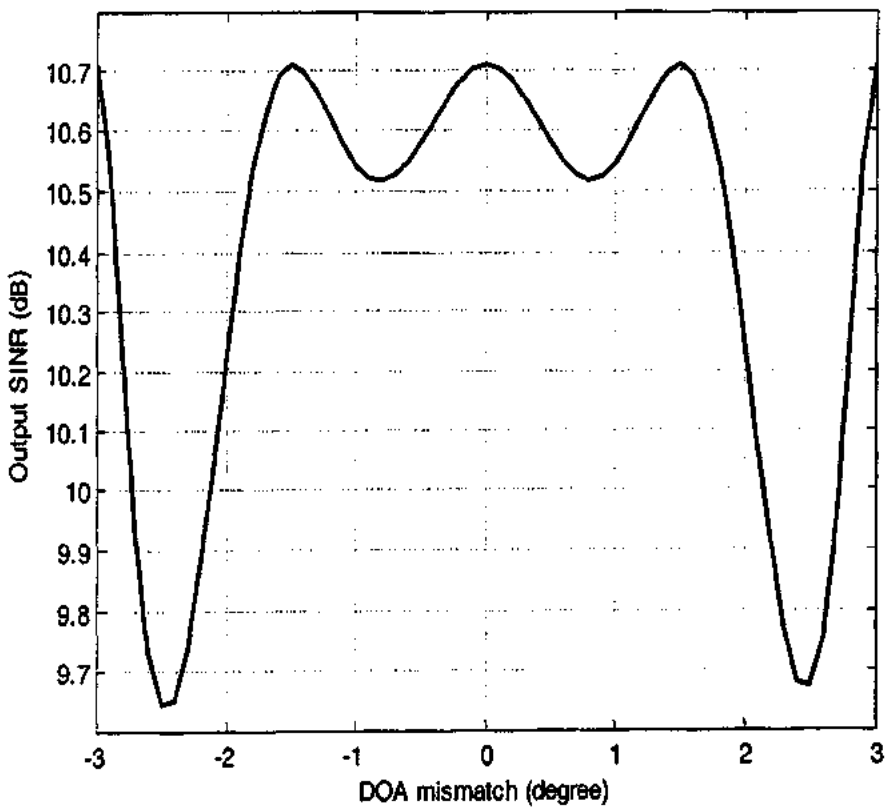

Figure 4.16: Output SINR versus DOA mismatch for RLCMV Beamformer and equivalent GSC with 5 steering vectors in $\tilde{\mathbf{C}}$

The comparison of the Fig. 4.15 and the Fig. 4.16, for the two cases, shows that the SINR in the mismatch region can be improved by increasing the number of steering vectors in $\tilde{\mathbf{C}}$.

Example 3:

In this example the desired signal is presumed at $\theta_S = 0°$ while actual signal direction is along 3°, i.e. DOA mismatch is 3°, and let $\delta\theta = 3°$. The interferences are placed at $\theta_{i1} = -45°$, $\theta_{i2} = 35°$ and $\theta_{i3} = 70°$. Fig. 4.17 shows the performance of RLCMV beamformer and its corresponding GSC.

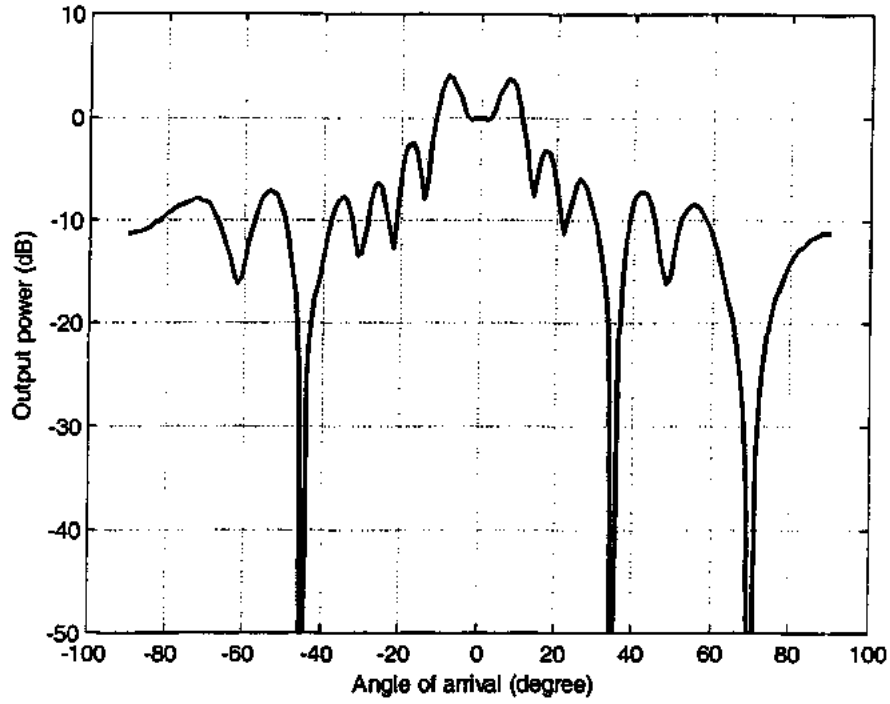

Figure 4.17: RLCMV Beamformer and RLCMV Based GSC with $\theta_s = 0°$, $\theta_{act} = 3°$ and $\theta_i = \{-45°, 35°, 70°\}$

4.4.2 ROBUST GENERAL RANK BEAMFORMER

Most of the robust adaptive beamforming techniques have been developed for point signal source model i.e., rank-one signal model. Shahbazpanahi et al. developed a beamformer for both rank-one and general-rank signal models. The general-rank signal models correspond to the situations with incoherently scattered sources and are

important for sonar and radio communications where signal sources can be dispersed in angle due to propagation effects.

4.4.2.1 MATHEMATICAL FRAMEWORK FOR RG-RANK BEAMFORMER

We start with SMI beamformer and end up with robust general-rank beamformer by modifying the constraints for robustness against signal look direction error and array imperfections given as below

SMI Beamformer

Consider a uniform linear array of M Omni-directional antenna elements with inter-element spacing $\lambda/2$. A plane wave impinging on the array making an angle θ with the normal to the array will have phase difference equal to $\pi \sin\theta$ on the consecutive elements, which generates the steering vector $a(\theta)$ .given as

$$\mathbf{a}(\theta) = \left[1 \; e^{j\pi\sin\theta} \; e^{j2\pi\sin\theta} \ldots \; e^{j(M-1)\pi\sin\theta}\right]^T$$

Similarly, desired signal steering vector is given as:

$$\mathbf{a}(\theta_s) = \left[1 \; e^{j\pi\sin\theta_s} \; e^{j2\pi\sin\theta_s} \ldots \; e^{j(M-1)\pi\sin\theta_s}\right]^T$$

Interference plus noise covariance matrix is denoted by $\mathbf{R}_{i+n}$ whereas the presumed signal covariance matrix is given by $\mathbf{R}_s$.

Output SINR maximization gives SMI beamformer i.e.

$$SINR = \frac{\mathbf{w}^H \mathbf{R}_s \mathbf{w}}{\mathbf{w}^H \mathbf{R}_{i+n} \mathbf{w}} \tag{4.4.8}$$

To maintain distortionless response from the desired direction $\mathbf{w}^H \mathbf{R}_s \mathbf{w} = 1$, and the output interference plus noise power is minimized. This gives SINR maximization and hence the optimization problem can be written as

$$\min_{\mathbf{w}} \mathbf{w}^H \mathbf{R}_{i+n} \mathbf{w} \text{ subject to } \mathbf{w}^H \mathbf{R}_s \mathbf{w} = 1 \tag{4.4.9}$$

The cost function for the above problem is as given below

$$J(\mathbf{w}) = \mathbf{w}^H \mathbf{R}_{i+n} \mathbf{w} + \lambda_L (\mathbf{w}^H \mathbf{R}_s \mathbf{w} - 1)$$

Where λ_L is Lagrange multiplier. Minimization of above cost function $J(\mathbf{w})$ is accomplished by differentiating it with respect to $\mathbf{w}$, i.e.

$$\frac{\partial J}{\partial \mathbf{w}^H} = \mathbf{R}_{i+n} \mathbf{w} - \lambda_L \mathbf{R}_s \mathbf{w}$$

And then for optimization

$$\mathbf{R}_{i+n} \mathbf{w} - \lambda_L \mathbf{R}_s \mathbf{w} = \mathbf{O}$$

Which gives

$$\mathbf{R}_{i+n} \mathbf{w} = \lambda_L \mathbf{R}_s \mathbf{w} \tag{4.4.10}$$

$$\mathbf{R}_{i+n}^{-1} \mathbf{R}_s \mathbf{w} = \frac{1}{\lambda_L} \mathbf{w} \tag{4.4.11}$$

One can observe the resemblance of this equation with Eigen value problem $\mathbf{A}\mathbf{x} = \lambda \mathbf{x}$ having $\mathbf{A} = \mathbf{R}_{i+n}^{-1} \mathbf{R}_s$, $\mathbf{x} = \mathbf{w}$ and $\lambda = \frac{1}{\lambda_L}$.

Per-multiplying expression (4.4.10) by $\mathbf{w}^H$ we get

$$\mathbf{w}^H \mathbf{R}_{i+n} \mathbf{w} = \lambda_L \mathbf{w}^H \mathbf{R}_s \mathbf{w}$$

$$\mathbf{w}^H \mathbf{R}_{i+n} \mathbf{w} = \lambda_L, \text{ Because } \mathbf{w}^H \mathbf{R}_s \mathbf{w} = 1$$

To fulfill the requirement for SINR maximization $\mathbf{w}^H \mathbf{R}_{i+n} \mathbf{w}$ should be minimized. This can be achieved if λ_L becomes minimum or equivalently $\lambda = \frac{1}{\lambda_L}$ becomes maximum.

The solution of equation (4.4.11) comes out to be [86]

$$\mathbf{w}_{opt} = P\left\{\mathbf{R}_{i+n}^{-1} \mathbf{R}_s\right\} \tag{4.4.12}$$

Where $P\{\cdot\}$ represents Principal Eigen vector corresponding to highest Eigen value. Actually, in practical situation the exact knowledge of $\mathbf{R}_{i+n}$ is not available because of the presence of desired signal in the data snapshots. As a result $\mathbf{R}_{i+n}$ is mixed with $\mathbf{R}_s$.

If in *SINR* expression, given by (4.4.8), $\mathbf{R}_{i+n}$ is replace by $\mathbf{R}_y$ where $\mathbf{R}_y = \mathbf{R}_s + \mathbf{R}_{i+n}$ then we get

$$\frac{\mathbf{w}^H\mathbf{R}_s\mathbf{w}}{\mathbf{w}^H\mathbf{R}_y\mathbf{w}} = \frac{\mathbf{w}^H\mathbf{R}_s\mathbf{w}}{\mathbf{w}^H\mathbf{R}_s\mathbf{w}+\mathbf{w}^H\mathbf{R}_{i+n}\mathbf{w}}$$
$$= \frac{1}{1+\mathbf{w}^H\mathbf{R}_{i+n}\mathbf{w}}$$

And $\min_{\mathbf{w}} \mathbf{w}^H\mathbf{R}_{i+n}\mathbf{w}$ subject to $\mathbf{w}^H\mathbf{R}_s\mathbf{w}=1$ will be same as

$\min_{\mathbf{w}} \mathbf{w}^H\mathbf{R}_y\mathbf{w}$ Subject to $\mathbf{w}^H\mathbf{R}_s\mathbf{w}=1$ Solution of both expressions results in SINR maximization. Accordingly equation (4.4.12) becomes

$$\mathbf{w}_{opt} = P\left\{\mathbf{R}_y^{-1}\mathbf{R}_s\right\} \tag{4.4.13}$$

In practical situation, $\mathbf{R}_y$ is replaced by the received data covariance matrix $\hat{\mathbf{R}}_y$ given by

$$\hat{\mathbf{R}}_y = \frac{1}{N}\sum_{n=1}^{N}\mathbf{y}(n)\mathbf{y}^H(n) \tag{4.4.14}$$

Where $\mathbf{y}(n)$ is the vector representing received data at the antenna elements for n^{th} snapshot and N is the number of snapshots. Replacing $\mathbf{R}_y$ by $\hat{\mathbf{R}}_y$ in (3.30) we get

$$\mathbf{w}_{SMI} = P\left\{\hat{\mathbf{R}}_y^{-1}\mathbf{R}_s\right\} \tag{4.4.15}$$

Above is the expression for *Sample Matrix Inversion (SMI) Beamformer*.

DOA Mismatch Problem

Let the DOA mismatch between the presumed and actual signal steering vectors causes an error $\mathbf{\Delta}_1$ in $\mathbf{R}_s$ and hence the received signal covariance matrix $\tilde{\mathbf{R}}_s$ can be expressed as

$$\tilde{\mathbf{R}}_s = \mathbf{R}_s + \mathbf{\Delta}_1 \tag{4.4.16}$$

Due to this adjustment the entire problem of SMI beamformer has to be reformulated given as follows.

Modified Problem

In order to overcome the DOA mismatch problem, the signal power in the mismatched region is constrained to be greater than or equal to unity, due to which expression (4.4.9) is modified as

$$\min_{\mathbf{w}} \mathbf{w}^H \mathbf{R}_y \mathbf{w} \text{ subject to } \mathbf{w}^H(\mathbf{R}_s + \Delta_1)\mathbf{w} \geq 1 \text{ with } \|\Delta_1\|_F \leq \varepsilon \tag{4.4.17}$$

Where $\|\Delta_1\|_F$ represents the Frobenius norm

First we shall give the solution for constraint as in expression (4.4.17). For worst case performance, we shall try to find Δ_1 that minimizes $\mathbf{w}^H(\mathbf{R}_s + \Delta_1)\mathbf{w}$ for $\|\Delta_1\|_F = \varepsilon$ and the problem becomes

$$\min_{\Delta_1} \mathbf{w}^H(\mathbf{R}_s + \Delta_1)\mathbf{w} \text{ subject to } \|\Delta_1\|_F^2 = \varepsilon^2 \tag{4.4.18}$$

Solution

The cost function corresponding to the expression (4.4.18) is given as under

$J(\Delta_1) = \mathbf{w}^H(\mathbf{R}_s + \Delta_1)\mathbf{w} + \lambda(\|\Delta_1\|_F^2 - \varepsilon^2)$ where λ is the Lagrange multiplier

$$\frac{\partial J}{\partial \Delta_1} = \frac{\partial}{\partial \Delta_1}\mathbf{w}^H\Delta_1\mathbf{w} - \lambda\frac{\partial}{\partial \Delta_1}tr(\Delta_1^2)\Big|\Delta_1^H = \Delta_1$$
$$= \mathbf{w}\mathbf{w}^H + 2\lambda\Delta_1$$

For optimization, $\mathbf{w}\mathbf{w}^H + 2\lambda\Delta_1 = \mathbf{O}$ which gives

$$\Delta_1 = -\frac{1}{2\lambda}\mathbf{w}\mathbf{w}^H \tag{4.4.19}$$

In order to find λ, multiplying (4.4.19) by Δ_1 and taking its trace

$$tr(\Delta_1^2) = tr\left(\left(-\frac{1}{2\lambda}\right)^2 \mathbf{w}\mathbf{w}^H\mathbf{w}\mathbf{w}^H\right)$$

Since $\Delta_1^H = \Delta_1$, therefore $tr(\Delta_1^2) = \|\Delta_1\|_F^2$ and the above expression becomes

$$\|\Delta_1\|_F^2 = \left(-\frac{1}{2\lambda}\right)^2 tr(\mathbf{w}\mathbf{w}^H\mathbf{w}\mathbf{w}^H)$$

$$\varepsilon^2 = \left(-\frac{1}{2\lambda}\right)^2 \|\mathbf{w}\|^4$$

$$\lambda = \frac{\|\mathbf{w}\|^2}{2\varepsilon}$$

Put value of λ in equation (4.4.19) we get

$$\Delta_1 = -\frac{\varepsilon \mathbf{w}\mathbf{w}^H}{\|\mathbf{w}\|^2}$$

Putting value of Δ_1 in modified optimization problem (4.4.17) we get

$$\min_{\mathbf{w}} \mathbf{w}^H \mathbf{R}_y \mathbf{w} \text{ Subject to } \mathbf{w}^H \left(\mathbf{R}_s - \frac{\varepsilon \mathbf{w}\mathbf{w}^H}{\|\mathbf{w}\|^2} \right) \mathbf{w} = 1 \text{ or equivalently}$$

$$\min_{\mathbf{w}} \mathbf{w}^H \mathbf{R}_y \mathbf{w} \text{ subject to } \mathbf{w}^H (\mathbf{R}_s - \varepsilon \mathbf{I}) \mathbf{w} = 1 \tag{4.4.20}$$

The solution comes out to be

$$\mathbf{w}_{rob} = P\left\{ \mathbf{R}_y^{-1} (\mathbf{R}_s - \varepsilon \mathbf{I}) \right\} \tag{4.4.21}$$

Replacing $\mathbf{R}_y$ by $\hat{\mathbf{R}}_y$ in equation (4.4.21) we get

$$\mathbf{w}_{rob,s} = P\left\{ \hat{\mathbf{R}}_y^{-1} (\mathbf{R}_s - \varepsilon \mathbf{I}) \right\} \tag{4.4.22}$$

Array Imperfections

These imperfections are caused by data nonstationarity, small training sample size and quantization errors and degrade the performance of the beamformer by affecting $\mathbf{R}_y$.

For the robustness of the beamformer against such errors we follow the procedure given as:

Let Δ_2 be the imperfection in $\mathbf{R}_y$ due to afore mentioned causes such that $\|\Delta_2\|_F \le \gamma$ then the problem for signal DOA mismatch and array imperfections becomes as given below.

$$\min_{\mathbf{w}} \mathbf{w}^H \left(\mathbf{R}_y + \Delta_2 \right) \mathbf{w} \text{ subject to } \mathbf{w}^H (\mathbf{R}_s + \Delta_1) \mathbf{w} \ge 1, \quad \text{with } \|\Delta_2\|_F \le \gamma, \|\Delta_1\|_F \le \varepsilon \tag{4.4.23}$$

Utilizing $\Delta_1 = -\frac{\varepsilon \mathbf{w}\mathbf{w}^H}{\|\mathbf{w}\|^2}$ for worst case DOA mismatch performance, expression (4.4.23) becomes

$$\min_{\mathbf{w}} \mathbf{w}^H \left(\mathbf{R}_y + \Delta_2\right)\mathbf{w} \text{ subject to } \mathbf{w}^H (\mathbf{R}_s - \varepsilon\mathbf{I})\mathbf{w} = 1, \text{ with } \|\Delta_2\|_F \le \gamma \qquad (4.4.24)$$

First we solve the objective function for the worst case performance i.e. we find Δ_2 that will maximize $\mathbf{w}^H \left(\mathbf{R}_y + \Delta_2\right)\mathbf{w}$ and the worst case performance optimization problem for object function of expression (4.4.24) becomes as

$$\max_{\Delta_2} \mathbf{w}^H (\mathbf{R}_y + \Delta_2)\mathbf{w} \text{ subject to } \|\Delta_2\|_F^2 = \gamma^2$$

Or equivalently

$$\min_{\Delta_2} -\mathbf{w}^H (\mathbf{R}_y + \Delta_2)\mathbf{w} \text{ subject to } \|\Delta_2\|_F^2 = \gamma^2 \qquad (4.4.25)$$

Solution

$J(\Delta_2) = -\mathbf{w}^H (\mathbf{R}_y + \Delta_2)\mathbf{w} + \lambda(\|\Delta_2\|_F^2 - \gamma^2)$ where λ is Lagrange multiplier

$$\frac{\partial J}{\partial \Delta_2} = -\frac{\partial}{\partial \Delta_2}\mathbf{w}^H \Delta_2 \mathbf{w} + \lambda \frac{\partial}{\partial \Delta_2} tr(\Delta_2^2) \text{ with } \Delta_2^H = \Delta_2$$

$$= -\mathbf{w}\mathbf{w}^H + 2\lambda\Delta_2$$

For optimization

$$-\mathbf{w}\mathbf{w}^H + 2\lambda\Delta_2 = \mathbf{O}$$
$$\Delta_2 = \frac{1}{2\lambda}\mathbf{w}\mathbf{w}^H \qquad (4.4.26)$$

To find out λ, multiply expression (4.4.26) by Δ_2 and taking trace

$$tr(\Delta_2^2) = tr\left(\left(\frac{1}{2\lambda}\right)^2 \mathbf{w}\mathbf{w}^H \mathbf{w}\mathbf{w}^H\right)$$

Since $\Delta_2^H = \Delta_2$, therefore $tr(\Delta_2^2) = \|\Delta_2\|_F^2$ and the above expression becomes

$\|\Delta_2\|_F^2 = \left(\frac{1}{2\lambda}\right)^2 tr(\mathbf{w}\mathbf{w}^H \mathbf{w}\mathbf{w}^H)$ Which gives

$\gamma^2 = \left(\frac{1}{2\lambda}\right)^2 \|\mathbf{w}\|^4$ And hence

$\lambda = \frac{\|\mathbf{w}\|^2}{2\gamma}$

Utilizing this λ in (4.4.26) we get

$$\Delta_2 = \frac{\gamma \mathbf{w}\mathbf{w}^H}{\|\mathbf{w}\|^2}$$

Put this value of Δ_2 in the optimization problem given in (4.4.24), we get

$$\min_{\mathbf{w}} \mathbf{w}^H \left(\mathbf{R}_y + \gamma \mathbf{I}\right)\mathbf{w} \text{ subject to } \mathbf{w}^H (\mathbf{R}_s - \varepsilon \mathbf{I})\mathbf{w} = 1 \tag{4.4.27}$$

The solution comes out to be

$$\tilde{\mathbf{w}}_{rob} = P\left\{\left(\mathbf{R}_y + \gamma \mathbf{I}\right)^{-1}(\mathbf{R}_s - \varepsilon \mathbf{I})\right\} \tag{4.4.28}$$

Replacing $\mathbf{R}_y$ by $\hat{\mathbf{R}}_y$ in expression (4.4.28) we get

$$\tilde{\mathbf{w}}_{rob,s} = P\left\{\left(\hat{\mathbf{R}}_y + \gamma \mathbf{I}\right)^{-1}(\mathbf{R}_s - \varepsilon \mathbf{I})\right\} \tag{4.4.29}$$

The beamformers given in expressions (4.4.28) and (4.4.29) are robust against signal DOA mismatch and array imperfections and is called robust general-rank (RG-Rank) beamformer.

4.4.2.2 Simulation Results for RG-Rank Beamformer

In this section, some simulation examples are given so as to demonstrate the performance of the Robust General-Rank Adaptive Beamformer.

A uniform linear array of 16 antenna elements has been used with inter element spacing $\lambda/2$. One desired signal with presumed direction along $\theta_s = 0°$ and two interferences at $\theta_{i1} = 30°$ and $\theta_{i2} = -60°$ are considered. The actual direction of the desired signal is at 3°. The INR is 30 dB. Simulations are carried out in MATLAB using 500 training snapshots except for example 5 where number of snapshots is variable.

Example 1:

In this example, we draw the beam pattern for SMI and robust general-rank beamformers when SNR is 10 dB and 15 dB. For the second beamformer $\varepsilon = 4$ and $\gamma = 10$. The results are shown in Fig 4.18 and 4.19.

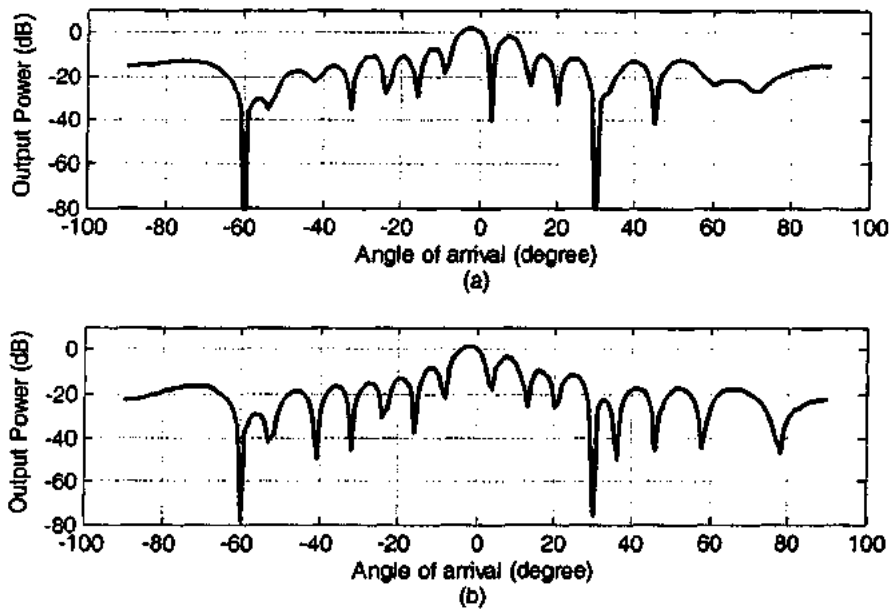

Figure 4.18: For SNR=10dB, $\theta_s = 0°$, actual AOA $= 3°$, with $\theta_{I1} = 30°$ and $\theta_{I2} = -60°$
(a) SMI beamformer (b) Robust-General Rank Beamformer with $\varepsilon = 4$ and $\gamma = 10$.

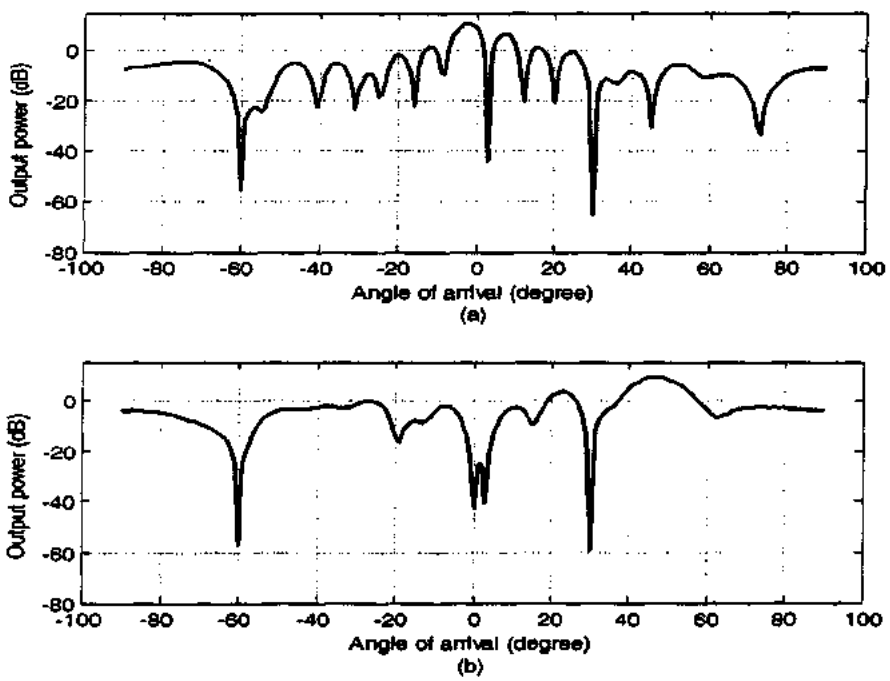

Figure 4.19: For SNR=15dB, $\theta_s = 0°$, actual AOA $= 3°$, with $\theta_{I1} = 30°$ and $\theta_{I2} = -60°$
(a) SMI beamformer (b) Robust-General Rank Beamformer with $\varepsilon = 4$ and $\gamma = 10$.

The performance degradation of SMI beamformer at 3° is obvious for both values of SNR due to signal DOA mismatch. The improved performance of general-rank beamformer for SNR=10 dB and the performance degradation at 15 dB is because $\mathbf{w}^H(\mathbf{R}_s - \varepsilon\mathbf{I})\mathbf{w}$ is greater than unity at SNR=10 dB while it is less than unity at SNR=10 dB as shown Fig. 4.18 (b) and 4.19 (b) respectively.

Example 2:

This example shows that the performance of Robust General-Rank Beamformer degrades severely as the value of $\mathbf{w}^H(\mathbf{R}_s - \varepsilon\mathbf{I})\mathbf{w}$ drops below 1. Two cases are considered. For the first case the values of ε and γ are the same as in example 1 i.e. $\varepsilon = 4$ and $\gamma = 10$. The performance for the first case is shown in Fig. 4.20 while the second case with $\varepsilon = 4$ and $\gamma = 300$ is shown in Fig. 4.21.

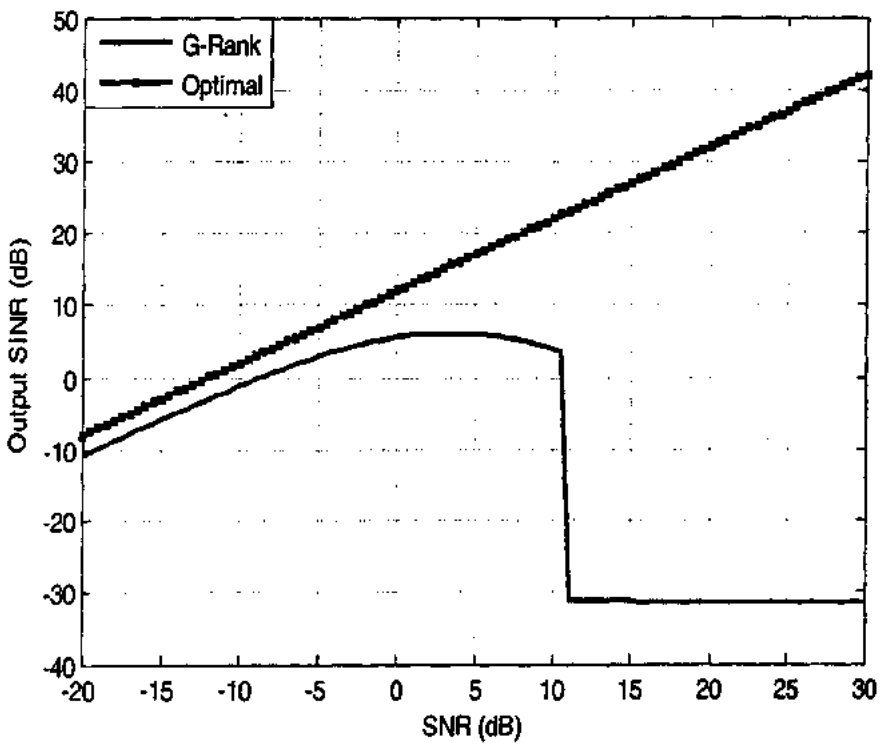

Figure 4.20: SINR versus SNR for Robust-General Rank Beamformer, with $\varepsilon = 4$ and $\gamma = 10$.

For both the cases, output SINR drops sharply as SNR approaches a certain critical value this is because at this value $\mathbf{w}^H(\mathbf{R}_x - \varepsilon\mathbf{I})\mathbf{w}$ becomes less than unity which is violation of the condition under which the algorithm is developed. It is further evident by the comparison of the two figures that for fixed value of ε as γ increases, the critical value of SNR for which performance degrades severely increases which is approximately 11 dB and 26 dB for the first second cases respectively.

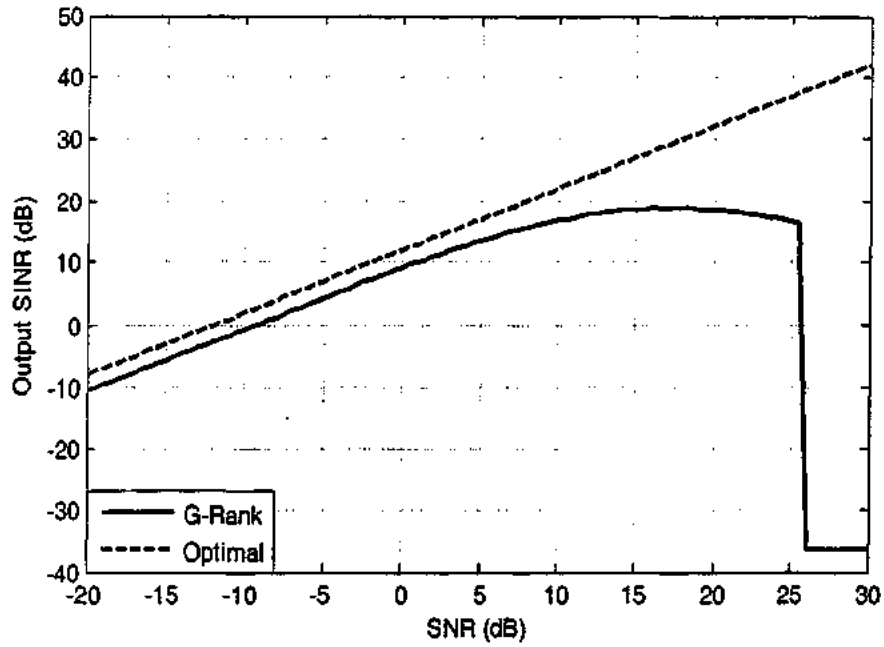

Figure 4.21: SINR versus SNR for Robust General-Rank Beamformer, with $\varepsilon = 4$ and $\gamma = 300$.

Example 3:

This example shows the effect of γ on output SINR for the fixed values of SNR, INR and ε. The performance of the beamformer in this context is shown in Fig. 4.22 for $\varepsilon = 7$, SNR=10 and INR=30. It is clear from the figure that as long as γ is below a critical value, output SINR is negligible because in this case $\mathbf{w}^H(\mathbf{R}_x - \varepsilon\mathbf{I})\mathbf{w} < 1$. However when γ attains a particular value, resulting $\mathbf{w}^H(\mathbf{R}_x - \varepsilon\mathbf{I})\mathbf{w} \geq 1$, the output SINR jumps to a higher level and remains approximately constant beyond that value.

This determines the critical level below which γ should never be dropped. However larger values of γ above threshold cause little change in output SINR. It is therefore suggested, in the absence any definite criterion, to use larger values of γ to ensure the value above threshold.

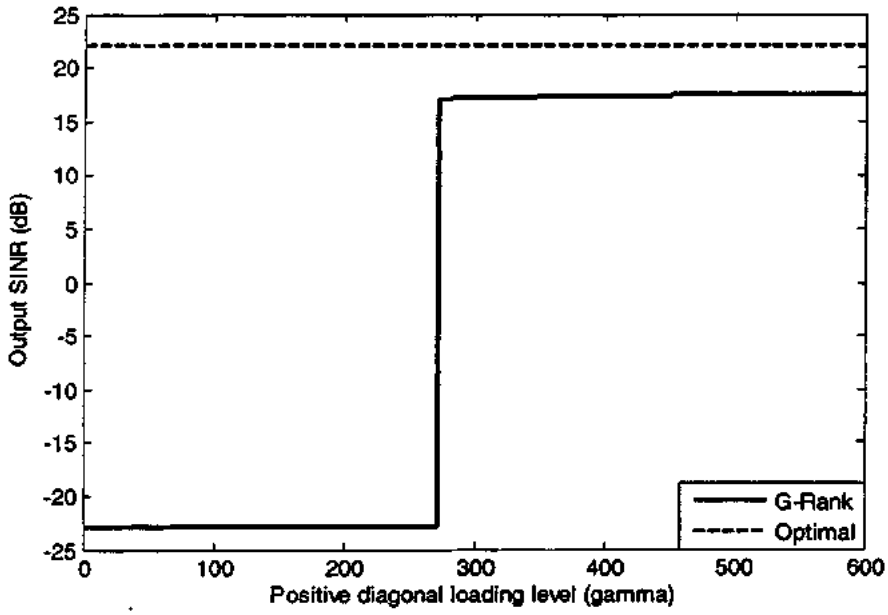

Figure 4.22: SINR versus γ for Robust General-Rank Beamformer, with $\varepsilon = 7$

Example 4:

This example shows the performance of the beamformer in terms of SNR versus ε with fixed value of γ. Fig. 4.23 depicts this scenario. The value of γ is chosen sufficiently large ($\gamma = 300$) to ensure the validity of the condition $\mathbf{w}^H(\mathbf{R}_x - \varepsilon\mathbf{I})\mathbf{w} \geq 1$.

Clearly it can be observed by the figure that as ε crosses a critical upper limit, SINR drops drastically. The reason may be the violation of one of the two conditions i.e., either $(\mathbf{R}_x - \varepsilon\mathbf{I})$ is not PSD or γ is not large enough to guarantee $\mathbf{w}^H(\mathbf{R}_x - \varepsilon\mathbf{I})\mathbf{w} \geq 1$. In Fig 4.23, even in the presence of DOA mismatch with $\varepsilon = 0$, the output SINR is sufficiently high. It is because of utilization of large value of γ.

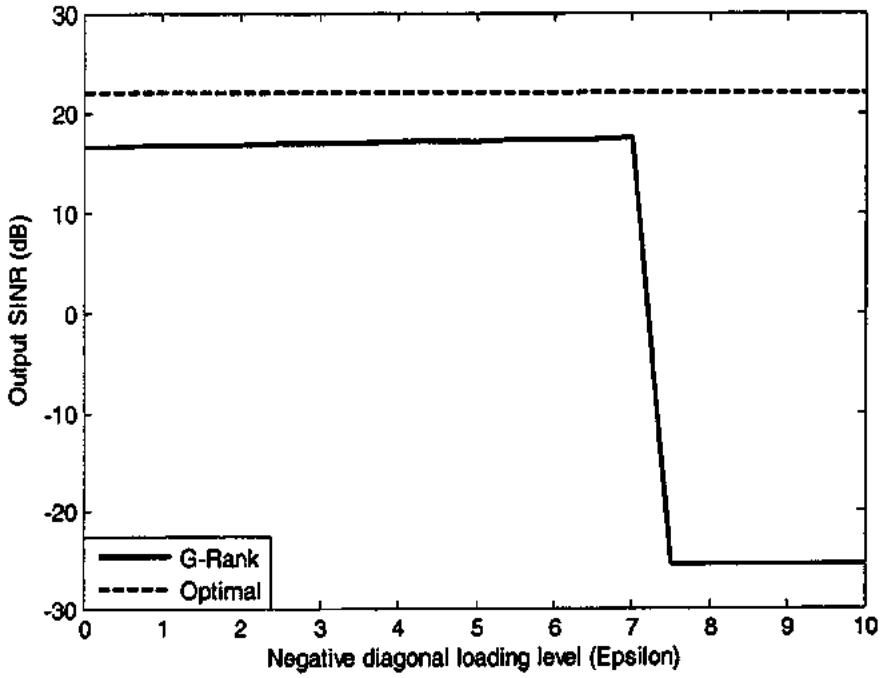

Figure 4.23: SINR versus ε for Robust General Rank Beamformer, with $\gamma = 300$

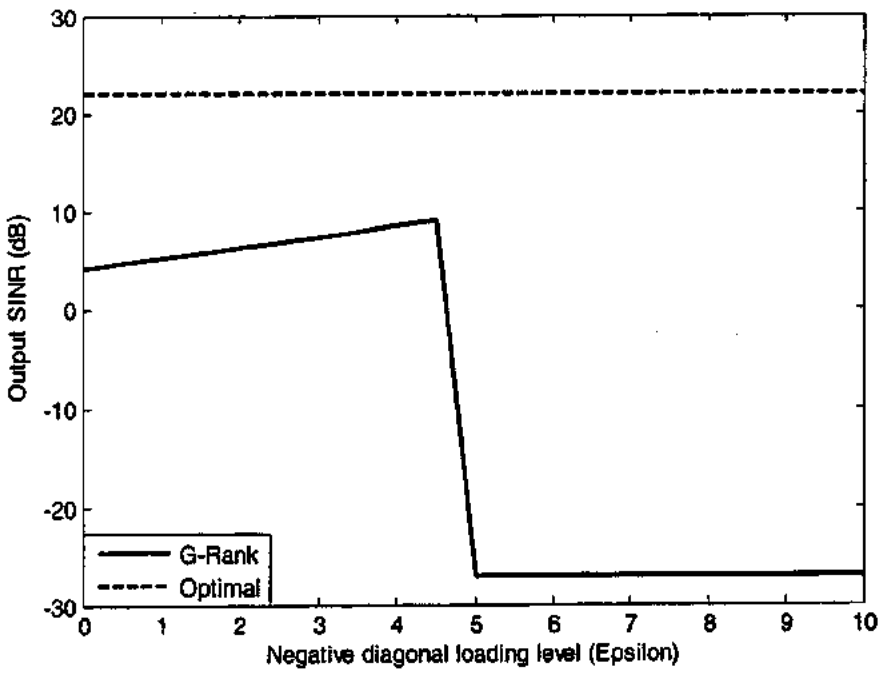

Figure 4.24: SINR versus ε for Robust General-Rank Beamformer, with $\gamma = 20$

Fig. 4.24 shows the beamformer performance with $\gamma = 20$ where SNR drops drastically for lower value of ε ($\varepsilon > 4$) as compare to Fig 4.23 where SNR drops down drastically for ($\varepsilon > 7$) due to difference of γ. From the comparison of these two figs, it is clear that the critical value of SNR is more sensitive to ε as compared to γ.

Example 5:

This example shows the Output SINR versus number of snapshots for the Robust General Rank Beamformer with $\varepsilon = 3.5$ and $\gamma =$ 180. Fig. 4.25 shows the performance of the beamformer where each point is averaged over 200 independent Monte Carlo trials. In the Fig. the optimal curve shows the performance under ideal conditions i.e., without DOA mismatch.

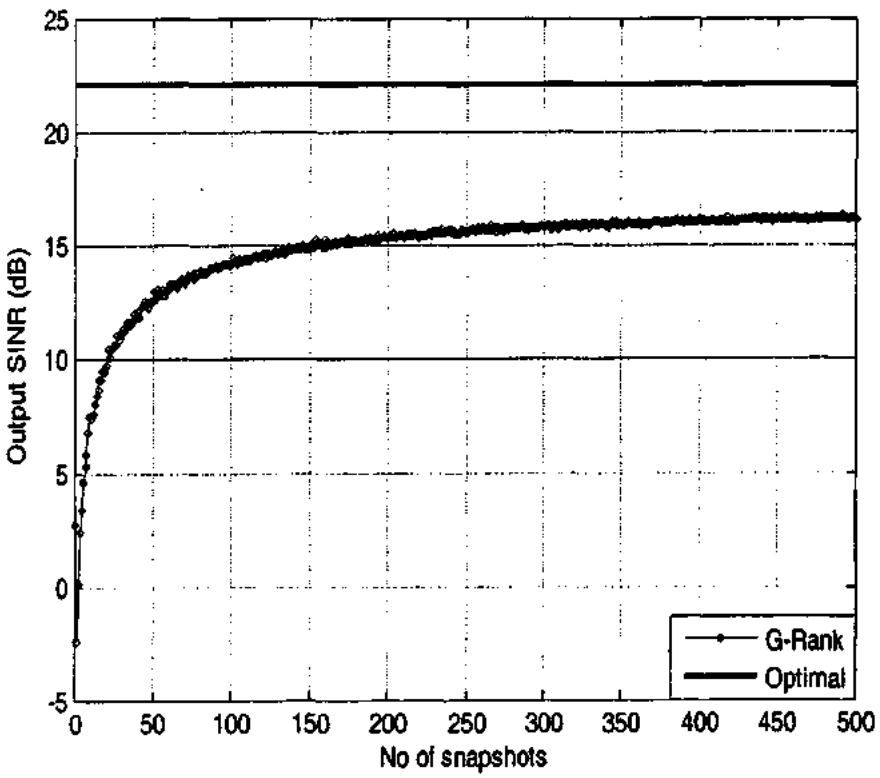

Figure 4.25: SINR versus No. of snapshots for Robust General-Rank Beamformer, with $\varepsilon = 3.5$ and $\gamma =$ 180

4.5 CONCLUSION

The features of the Optimum Adaptive Beamforming Algorithms discussed in this chapter are given below.

1. The only requirement for these beamformers is the knowledge of desired signal direction. They perform well if the perfect information of the direction of desired signal is available.
2. The performance of these beamformers degrades severely if there is mismatch between the presumed and actual signal direction in the data snapshots containing the desired signal.
3. If the linear constraints are added to LCMV beamformer, Robustness is achieved, however, at the cost of broadening of the main beam.
4. For Diagonal Loading Robust Beamforming Techniques, the criterion for diagonal loading is not available.
5. For Robust General-Rank Beamformer, there is no criterion for the selection of ε to maintain positive semi-definite (PSD) constraint on $(\mathbf{R}_x - \varepsilon\mathbf{I})$ intact.

CHAPTER 5

PROPOSED ROBUST ALGORITHMS IN OPTIMAL ADAPTIVE BEAMFORMING

We have already discussed two Robust Optimal Adaptive Beamforming Algorithms in section 4.4, chapter 4, which were RLCMV beamformer and Robust General Rank Adaptive Beamformer. RLCMV beamformer is robust against signal look direction error but faces the problem of broadening the main beam, which is desirable to as narrow as possible. Similarly the problem with the general rank beamformer is that we have to make it robust against DOA mismatch with the help of negative diagonal loading of desired signal covariance matrix. This diagonal loading is in tern the addition of artificial noise in the covariance matrix which prevents the gain in the signal mismatch region to be less than unity. The drawback with this algorithm is the absence of some well defined criteria to decide the amount of diagonal loading. The amount of diagonal loading is critical in this case. In case of excessive loading, it is quite possible that the covariance matrix involved in the weight vector computation may no more be positive definite which is against the basic assumption under which algorithm has been developed. Moreover the diagonal loading level affects the null depth in the pattern of the beamformer.

In this chapter a new generalized sidelobe canceller (GSC) is being introduced having two qualities:

1. It provides sidelobe cancellation without broadening the main beam
2. It is robust against signal look direction error.

The proposed GSC is based on exploitation of the standard GSC structure.

Most of the existing robust adaptive beamforming algorithms have been developed for point source signal models i.e., for rank-one signal models. In case of incoherently

scattered source and/or sources with randomly distorted (fluctuating) wave-fronts, the problem cannot be addressed directly by rank-one signal models. Such situations appear in wireless communications and SONAR where propagation effects cause the dispersion of the sources [115]-[120]. Such situations are addressed by higher rank signal models.

In wireless communications with a high base-station, incoherently scattered signal sources cause fast fading in the vicinity of mobile in rural and suburban areas [117]-[119]. In SONAR the signal propagation through randomly inhomogeneous channel causes loss in signal coherence [121]-[127].

Robust General-Rank Beamformer is applicable to both rank-one and higher-rank signal models because it incorporates signal look direction error for general-rank signal models and the array imperfections by explicit modeling of uncertainties in $\mathbf{R}_x$ and $\mathbf{R}_y$ respectively. This results in negative diagonal loading of $\mathbf{R}_x$ and positive diagonal loading of $\mathbf{R}_y$. However, the problem is that there is no reliable way to select proper diagonal loading level. Left right beam symmetry around the presumed signal direction is used in the literature for positive diagonal loading. We use this technique to select proper negative diagonal loading level of general-rank beamformer. This technique is presented in section 5.2.

5.1 Robust GSC for DOA Mismatch

We have discussed RLCMV based GSC in chapter 4. Although this GSC provides robustness against signal look direction error, yet it faces the main beam broadening problem similar to RLCMV beamformer. In the following we present RGSC that provides robustness against DOA mismatch without broadening the main beam.

5.1.1 Proposed Algorithm for RGSC

The traditional GSC contains two branches, one for the desired signal and for the interferences which is lower one in Fig 4.5. As discussed previously in chapter 4, $\mathbf{w}_q$

is the set of weights applied on the incoming signal to preserve the signal from desired direction as given by the steering vector $\mathbf{a}(\theta_s)$. This steering vector can be established using(4.1.3). Interference and noise signals are also weighted by $\mathbf{w}_q$ in this branch.

B is the matrix in the lower branch termed as the blocking matrix. It contains the set of vectors orthogonal to the vector $\mathbf{a}(\theta_s)$.Therefore, the signals falling in this orthogonal space are blocked in the lower branch and interference and noise signals are left there in this branch. Of course the final output $z(n)$ is the difference of the outputs of the two branches where adaptive weight vector $\mathbf{w}_a$ adjusts the interference and noise signals such that their effect is cancelled in the two branches. The performance of traditional GSC is very good in the absence of signal look direction error. However the major drawback is that it cannot stand with signal DOA mismatch scenario because the mismatched signal is treated as interference in this situation which is ideally assumed to be on single point θ_s with steering vector $\mathbf{a}(\theta_s)$.

RLCMV beamformer incorporates additional linear constraints in the signal mismatch region to cater for signal look direction error. The basic idea in this case was to utilize multiple steering vectors instead of single one as is the case with traditional GSC. Now in this case a set of closely spaced steering vectors in the vicinity of $\mathbf{a}(\theta_s)$ is established. This set of steering vectors extends the single point into a region for the desired signal. When this RLCMV is applied in the framework of GSC, RLCMV based GSC is resulted. Matrix **B** is updated accordingly and hence will become $\tilde{\mathbf{B}}$. Obviously, the number of vectors in $\tilde{\mathbf{B}}$ will be decreased in comparison with **B**. Similarly these multiple steering vectors also update $\mathbf{w}_q$ and hence will become $\tilde{\mathbf{w}}_q$

The drawback with RLCMV based GSC is that it causes broadening of the main beam due to utilization of $\tilde{\mathbf{w}}_q$. This broadening of the main beam is to be avoided.

Now the requirement is a GSC which provides the DOA mismatch capability without broadening the main beam. This requirement is fulfilled by our proposed GSC, i.e., it

provides the robustness against DOA mismatch without compromising on the width of the main beam. The basic idea in this case is to use the set of weights $\mathbf{w}_q$ of traditional GSC in the upper branch, however we use the blocking matrix $\tilde{\mathbf{B}}$ of RLCMV based GSC in the lower branch. Hence the proposed GSC is the combination of the previous two i.e., the traditional GSC and LCMV based GSC. We use single steering vector $\mathbf{a}(\theta_s)$ to evaluate $\mathbf{w}_q$ and a cluster of steering vectors with $\mathbf{a}(\theta_s)$ as center to evaluate $\tilde{\mathbf{B}}$. This results in broader null of $\tilde{\mathbf{B}}$ than $\mathbf{B}$ and the mismatched signal is blocked in the lower branch of proposed GSC. Hence we cater for DOA mismatch without compromising on the width of main beam.

In ideal situation, when there is no mismatch between the presumed and actual signal look direction, the LCMV beamforming problem given in (4.2.5) is reproduced here

$$\min_{\mathbf{w}} \mathbf{w}^H \mathbf{R}_y \mathbf{w} \text{ Subject to } \mathbf{C}^H \mathbf{w} = \mathbf{f} \tag{5.1.1}$$

Where $\mathbf{C} = \mathbf{a}(\theta_s)$

In chapter 4 we have already shown the LCMV beamforming problem in the framework of GSC see Fig 4.5. The other mapping GSC parameters on LCMV is given in table 5.1

Table 5.1: Relationship between parameters of GSC and LCMV beamformer

GSC parameters	Relationship with LCMV
$\mathbf{w}_q$	It is function of $\mathbf{C} = \mathbf{a}(\theta_s)$ and forms the main beam satisfying $\mathbf{f}$
$\mathbf{B}$	It forms nulls for the steering vectors contained in $\mathbf{C}$ to block the desired signal in the lower branch of GSC
$\mathbf{w}_q - \mathbf{B}\mathbf{w}_a$	It implements the object function with the help of $\mathbf{w}_a$ by cancelling the common signals in two branches and results in desired beam and nulls.

For ideal situation, when there is no mismatch in presumed and actual signal directions, $\mathbf{B}^H \mathbf{C} = \mathbf{B}^H \mathbf{a}(\theta_s) = \mathbf{O}$. The desired signal is blocked in the lower branch of GSC already shown in Fig 4.5 and is being reproduced here for convenience in Fig 5.1. The desired signal appears in upper branch only.

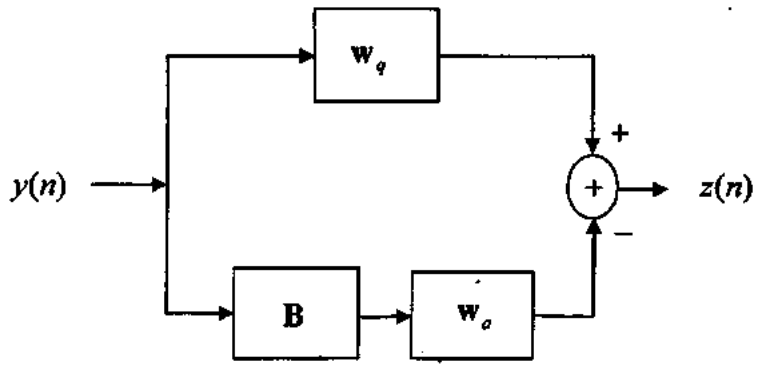

Figure 5.1: Generalized Sidelobe Canceller

Consider a mismatch in the presumed and actual signal direction. The actual signal direction is $\mathbf{a}(\theta_s + \delta\theta)$. For conventional GSC $\mathbf{B}^H\mathbf{a}(\theta_s) = \mathbf{O}$ because $\mathbf{B}$ has been derived such that it is orthogonal to $\mathbf{a}(\theta_s)$. However $\mathbf{B}^H\mathbf{a}(\theta_s + \delta\theta) \neq \mathbf{O}$ .because orthogonality between mismatched steering vector $\mathbf{a}(\theta_s + \delta\theta)$ and $\mathbf{B}$ has not been imposed due to uncertainty in $\delta\theta$. Thus the desired signal (mismatched signal) appears in the lower branch of GSC too. In this branch it is considered as interference and is cancelled through adaptive weight vector $\mathbf{w}_a$ at the output due to being common in the two branches. The other interferences also appear in both the branches and are cancelled at the output in the same manner. The basic problem is how to avoid the cancellation of desired signal with steering vector $\mathbf{a}(\theta_s + \delta\theta)$. The solution to this signal cancellation abnormality is the RLCMV with the optimization problem as stated under

$$\min_{\mathbf{w}} \mathbf{w}^H\mathbf{R}_y\mathbf{w} \text{ Subject to } \tilde{\mathbf{C}}^H\mathbf{w} = \tilde{\mathbf{f}} \tag{5.1.2}$$

While the extended constraint matrix $\tilde{\mathbf{C}}$ contains multiple steering vectors or alternatively a cluster of steering vectors from the signal mismatch region to address the uncertainty in presumed steering vector $\mathbf{a}(\theta_s)$ within a certain range. Similarly, the extended gain vector $\tilde{\mathbf{f}}$ contains gains corresponding to the steering vectors of $\tilde{\mathbf{C}}$.

RLCMV based GSC is obtained when this problem is applied in the framework of GSC. The block diagram of RLCMV based GSC is shown in Fig 5.2. Table 5.2 summarizes the features of RLCMV based GSC

Table 5.2: Parameter description of RLCMV based GSC

GSC parameters	Role in the performance
$\tilde{\mathbf{w}}_q$	It is function of $\tilde{\mathbf{C}}$ and forms the broader main beam, due to multiple steering vectors contained in $\tilde{\mathbf{C}}$, by satisfying $\tilde{\mathbf{f}}$
$\tilde{\mathbf{B}}$	It forms broad nulls in the region $\theta_s \pm \delta\theta$ due to the steering vectors contained in $\tilde{\mathbf{C}}$ and blocks the desired signal, from the region $\theta_s \pm \delta\theta$, in the lower branch of GSC.
$\tilde{\mathbf{w}}_q - \tilde{\mathbf{B}}\mathbf{w}_a$	It implements the object function with the help of $\mathbf{w}_a$ by cancelling the common signals in two branches and results in desired beam and nulls.

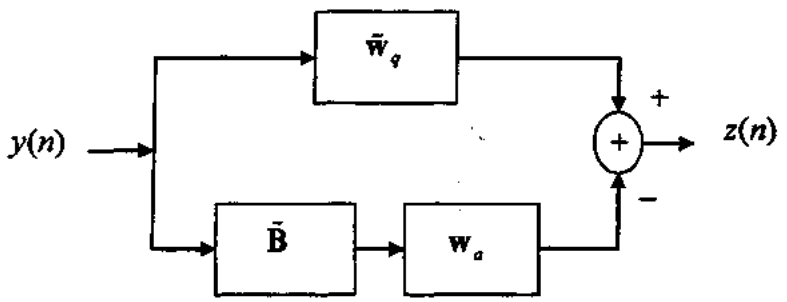

Figure 5.2: RLCMV Based Generalized Sidelobe Canceller

From table 5.1 and 5.2, it is clear that the broadening of the main beam can be avoided if the GSC utilizes $\mathbf{w}_q$, which is function of $\mathbf{C}$, rather than $\tilde{\mathbf{w}}_q$. Similarly, mismatched signal leakage in the lower branch can be avoided if $\mathbf{B}$ is replaced by $\tilde{\mathbf{B}}$, which is function of $\tilde{\mathbf{C}}$. It means robust GSC can avoid broadening of the main beam and provide robustness against signal look direction error by exploiting both $\mathbf{C}$ and $\tilde{\mathbf{C}}$ for $\mathbf{w}_q$ and $\tilde{\mathbf{B}}$ respectively.

GSC structure is adopted for this purpose because, the optimization problem analogous to expression (5.1.2), that utilizes both $\mathbf{C}$ and $\tilde{\mathbf{C}}$, cannot be formed. The block diagram of RGSC is shown in Fig 5.3.

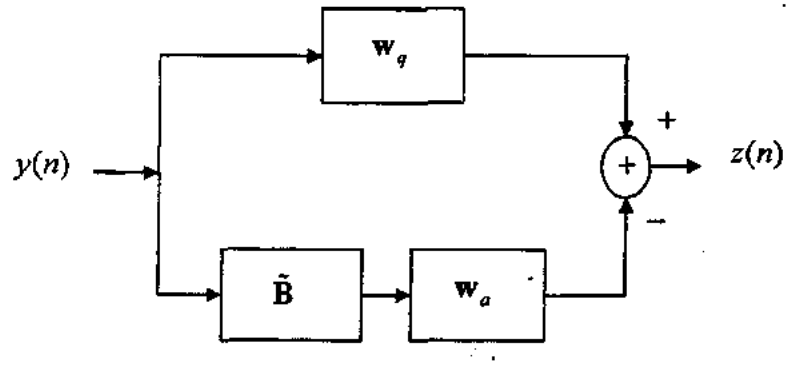

Figure 5.3: Robust Generalized Sidelobe Canceller

For RGSC, we define the constraint matrix, $\mathbf{C} = \mathbf{a}(\theta_s)$ and the gain vector, $\mathbf{f} = 1$.

Whereas $\mathbf{w}_q$ is the same for both the traditional and RGSC i.e.,

$$\mathbf{w}_q = \mathbf{C}(\mathbf{C}^H\mathbf{C})^{-1}\mathbf{f} \tag{5.1.3}$$

Similarly, for the robustness against signal look direction error, the condition on blocking matrix $\tilde{\mathbf{B}}$ is given as

$$\tilde{\mathbf{B}}^H\mathbf{a}(\theta) = \mathbf{O} \text{ for } \theta_s - \frac{\Delta\theta}{2} \le \theta \le \theta_s + \frac{\Delta\theta}{2} \tag{5.1.4}$$

Where the angular region of mismatch is continuous from $\theta_s - \frac{\Delta\theta}{2}$ to $\theta_s + \frac{\Delta\theta}{2}$ having length $\Delta\theta$ and contains infinite angles.

In order to discretize this angular region $\Delta\theta$ into p number of angles, we define a new parameter θ_n given as

$$\theta_n = \theta_s + n\delta, \ \forall n \in Z, -(\frac{p-1}{2}) \le n \le (\frac{p-1}{2}) \tag{5.1.5}$$

Where $\delta = \frac{\Delta\theta}{p-1}$

The p steering vectors corresponding to the angles given in (5.1.5) are placed in extended constraint matrix $\bar{\mathbf{C}}$ as given below

$$\tilde{\mathbf{C}} = \left[\mathbf{a}(\theta_{-(P-1)/2}),\ldots,\mathbf{a}(\theta_{-1}),\mathbf{a}(\theta_0),\mathbf{a}(\theta_1),\ldots,\mathbf{a}(\theta_{(P-1)/2})\right] \tag{5.1.6}$$

Where in this case $\mathbf{a}(\theta_0) = \mathbf{a}(\theta_s)$. In order to find out the matrix $\tilde{\mathbf{B}}$, the matrix $\tilde{\mathbf{C}}$ is utilized as given below

$$\tilde{\mathbf{B}} = null\{\tilde{\mathbf{C}}^H\} = null\left\{\left[\mathbf{a}(\theta_{-(P-1)/2}),\ldots,\mathbf{a}(\theta_{-1}),\mathbf{a}(\theta_0),\mathbf{a}(\theta_1),\ldots,\mathbf{a}(\theta_{(P-1)/2})\right]^H\right\} \tag{5.1.7}$$

In order to derive the expression for optimum adaptive weight vector $\mathbf{w}_a$ of RGSC we proceed as under.

Let the RGSC receives the desired signal with an error in the presumed direction i.e.

$$\mathbf{y}(n) = s(n)\mathbf{a}(\theta_s + \delta\theta), \quad -\frac{\Delta\theta}{2} \le \delta\theta \le \frac{\Delta\theta}{2} \tag{5.1.8}$$

Where $s(n)$ is the desired signal and $\mathbf{a}(\theta_s + \delta\theta)$ is the steering vector corresponding to the direction of the desired signal.

Then the output will become

$$\begin{aligned} z(n) &= s(n)(\mathbf{w}_q - \tilde{\mathbf{B}}\mathbf{w}_a)^H \mathbf{a}(\theta_s + \delta\theta) \\ &= s(n)\mathbf{w}_q{}^H \mathbf{a}(\theta_s + \delta\theta) - s(n)\mathbf{w}_a{}^H \tilde{\mathbf{B}}^H \mathbf{a}(\theta_s + \delta\theta) \\ &= s(n)\mathbf{w}_q{}^H \mathbf{a}(\theta_s + \delta\theta) \end{aligned} \tag{5.1.9}$$

That means, when the RGSC receives the desired signal from mismatch region, its output becomes a weighted value of the desired signal.

Next we consider the situation when the beamformer receives interference from sidelobe region i.e.

$$\mathbf{y}(n) = i(n)\mathbf{a}(\theta), \quad \theta_s + \frac{\Delta\theta}{2} \le \theta \le \theta_s - \frac{\Delta\theta}{2} \tag{5.1.10}$$

Then in this case the output is given as

$$\begin{aligned} z(n) &= i(n)(\mathbf{w}_q - \tilde{\mathbf{B}}\mathbf{w}_a)^H \mathbf{a}(\theta) \\ &= i(n)\mathbf{w}_q{}^H \mathbf{a}(\theta) - i(n)\mathbf{w}_a{}^H \tilde{\mathbf{B}}^H \mathbf{a}(\theta) \end{aligned} \tag{5.1.11}$$

Now the situation, in which the beamformer receives both the desired signal with steering vector error and the interference signal from sidelobe region along with noise

vector $\mathbf{v}(n)$, can be expressed mathematically by utilizing (5.1.8) and (5.1.10) as given below

$$\mathbf{y}(n) = s(n)\mathbf{a}(\theta_s + \delta\theta) + i(n)\mathbf{a}(\theta) + \mathbf{v}(n) \tag{5.1.12}$$

Where

$$\theta_s + \frac{\Delta\theta}{2} \le \theta \le \theta_s - \frac{\Delta\theta}{2}, \; -\frac{\Delta\theta}{2} \le \delta\theta \le \frac{\Delta\theta}{2}$$

In (5.1.12) $i(n)$ is the interference signal and $\mathbf{a}(\theta)$ is the steering vector corresponding to the direction of the interference. The beamformer output in this case will become

$$\begin{aligned} z(n) &= (\mathbf{w}_q - \tilde{\mathbf{B}}\mathbf{w}_a)^H \mathbf{y}(n) \\ &= s(n)(\mathbf{w}_q - \tilde{\mathbf{B}}\mathbf{w}_a)^H \mathbf{a}(\theta_s + \delta\theta) + i(n)(\mathbf{w}_q - \tilde{\mathbf{B}}\mathbf{w}_a)^H \mathbf{a}(\theta) + (\mathbf{w}_q - \tilde{\mathbf{B}}\mathbf{w}_a)^H \mathbf{v}(n) \\ &= s(n)\mathbf{w}_q{}^H \mathbf{a}(\theta_s + \delta\theta) + i(n)(\mathbf{w}_q - \tilde{\mathbf{B}}\mathbf{w}_a)^H \mathbf{a}(\theta) + (\mathbf{w}_q - \tilde{\mathbf{B}}\mathbf{w}_a)^H \mathbf{v}(n) \end{aligned} \tag{5.1.13}$$

Now, the average output power of the beamformer is given by

$$\begin{aligned} E[z(n)z^*(n)] &= E[(\mathbf{w}_q - \tilde{\mathbf{B}}\mathbf{w}_a)^H \mathbf{y}(n)\mathbf{y}^H(n)(\mathbf{w}_q - \tilde{\mathbf{B}}\mathbf{w}_a)] \\ &= (\mathbf{w}_q - \tilde{\mathbf{B}}\mathbf{w}_a)^H E[\mathbf{y}(n)\mathbf{y}^H(n)](\mathbf{w}_q - \tilde{\mathbf{B}}\mathbf{w}_a) \\ &= (\mathbf{w}_q - \tilde{\mathbf{B}}\mathbf{w}_a)^H \mathbf{R}_y (\mathbf{w}_q - \tilde{\mathbf{B}}\mathbf{w}_a) \end{aligned} \tag{5.1.14}$$

Where $E[\cdot]$ denote statistical expectation. An equivalent expression for the average output power of the beamformer is obtained if statistical expectation is applied on the end result of expression (5.1.13) i.e.

$$\begin{aligned} E[z(n)z^*(n)] &= E[s(n)\mathbf{w}_q{}^H \mathbf{a}(\theta_s + \delta\theta)\mathbf{a}^H(\theta_s + \delta\theta)\mathbf{w}_q s^*(n)] \\ &\quad + E[i(n)(\mathbf{w}_q - \tilde{\mathbf{B}}\mathbf{w}_a)^H \mathbf{a}(\theta)\mathbf{a}^H(\theta)(\mathbf{w}_q - \tilde{\mathbf{B}}\mathbf{w}_a)i^*(n)] \\ &\quad + E[(\mathbf{w}_q - \tilde{\mathbf{B}}\mathbf{w}_a)^H \mathbf{v}(n)\mathbf{v}^H(n)(\mathbf{w}_q - \tilde{\mathbf{B}}\mathbf{w}_a)] \\ &= \mathbf{w}_q{}^H E[s(n)s^*(n)]\mathbf{a}(\theta_s + \delta\theta)\mathbf{a}^H(\theta_s + \delta\theta)\mathbf{w}_q \\ &\quad + (\mathbf{w}_q - \tilde{\mathbf{B}}\mathbf{w}_a)^H E[i(n)i^*(n)]\mathbf{a}(\theta)\mathbf{a}^H(\theta)(\mathbf{w}_q - \tilde{\mathbf{B}}\mathbf{w}_a) \\ &\quad + (\mathbf{w}_q - \tilde{\mathbf{B}}\mathbf{w}_a)^H E[\mathbf{v}(n)\mathbf{v}^H(n)](\mathbf{w}_q - \tilde{\mathbf{B}}\mathbf{w}_a) \end{aligned}$$

$$
\begin{aligned}
&= \mathbf{w}_q{}^H \sigma_s^2 \mathbf{a}(\theta_s + \delta\theta)\mathbf{a}^H(\theta_s + \delta\theta)\mathbf{w}_q \\
&\quad + (\mathbf{w}_q - \tilde{\mathbf{B}}\mathbf{w}_a)^H \sigma_i^2 \mathbf{a}(\theta)\mathbf{a}^H(\theta)(\mathbf{w}_q - \tilde{\mathbf{B}}\mathbf{w}_a) \\
&\quad + (\mathbf{w}_q - \tilde{\mathbf{B}}\mathbf{w}_a)^H \sigma_v^2 \mathbf{I}(\mathbf{w}_q - \tilde{\mathbf{B}}\mathbf{w}_a) \\
&= \mathbf{w}_q{}^H \mathbf{R}_{mis}\mathbf{w}_q + (\mathbf{w}_q - \tilde{\mathbf{B}}\mathbf{w}_a)^H \mathbf{R}_i(\mathbf{w}_q - \tilde{\mathbf{B}}\mathbf{w}_a) \\
&\quad + (\mathbf{w}_q - \tilde{\mathbf{B}}\mathbf{w}_a)^H \mathbf{R}_v(\mathbf{w}_q - \tilde{\mathbf{B}}\mathbf{w}_a) \\
&= \mathbf{w}_q{}^H \mathbf{R}_{mis}\mathbf{w}_q + (\mathbf{w}_q - \tilde{\mathbf{B}}\mathbf{w}_a)^H (\mathbf{R}_i + \mathbf{R}_v)(\mathbf{w}_q - \tilde{\mathbf{B}}\mathbf{w}_a) \\
&= \mathbf{w}_q{}^H \mathbf{R}_{mis}\mathbf{w}_q + (\mathbf{w}_q - \tilde{\mathbf{B}}\mathbf{w}_a)^H \mathbf{R}_{iv}(\mathbf{w}_q - \tilde{\mathbf{B}}\mathbf{w}_a)
\end{aligned} \tag{5.1.15}
$$

In order to minimize the output power of the beamformer, we utilize expression (5.1.14) to develop the cost function J given as

$$J(\mathbf{w}_a) = (\mathbf{w}_q - \tilde{\mathbf{B}}\mathbf{w}_a)^H \mathbf{R}_y (\mathbf{w}_q - \tilde{\mathbf{B}}\mathbf{w}_a)$$

Taking its derivative with respect to $\mathbf{w}_a$ we get

$$
\begin{aligned}
\frac{\partial J}{\partial \mathbf{w}_a{}^H} &= -\tilde{\mathbf{B}}^H \mathbf{R}_y (\mathbf{w}_q - \tilde{\mathbf{B}}\mathbf{w}_a) \\
&= -\tilde{\mathbf{B}}^H \mathbf{R}_y \mathbf{w}_q + \tilde{\mathbf{B}}^H \mathbf{R}_y \tilde{\mathbf{B}}\mathbf{w}_a
\end{aligned} \tag{5.1.16}
$$

For optimization $\frac{\partial J}{\partial \mathbf{w}_a{}^H} = \mathbf{O}$ and the optimized adaptive weight vector is denoted by $\mathbf{w}_{ao}$ i.e.,

$$
\begin{aligned}
&-\tilde{\mathbf{B}}^H \mathbf{R}_y \mathbf{w}_q + \tilde{\mathbf{B}}^H \mathbf{R}_y \tilde{\mathbf{B}}\mathbf{w}_{ao} = \mathbf{O} \\
&\tilde{\mathbf{B}}^H \mathbf{R}_y \tilde{\mathbf{B}}\mathbf{w}_{ao} = \tilde{\mathbf{B}}^H \mathbf{R}_y \mathbf{w}_q \\
&\mathbf{w}_{ao} = \left(\tilde{\mathbf{B}}^H \mathbf{R}_y \tilde{\mathbf{B}}\right)^{-1} \tilde{\mathbf{B}}^H \mathbf{R}_y \mathbf{w}_q
\end{aligned} \tag{5.1.17}
$$

We shall use (5.1.15) to develop the cost function given as

$$J(\mathbf{w}_a) = \mathbf{w}_q{}^H \mathbf{R}_{mis}\mathbf{w}_q + (\mathbf{w}_q - \tilde{\mathbf{B}}\mathbf{w}_a)^H \mathbf{R}_{iv}(\mathbf{w}_q - \tilde{\mathbf{B}}\mathbf{w}_a) \tag{5.1.18}$$

Observing this cost function, it is clear that adaptive weight vector $\mathbf{w}_a$ is multiplied with interference plus noise covariance matrix $\mathbf{R}_{iv}$ and the optimum value of adaptive weight vector will minimize the interference plus noise power at the output of the beamformer without affecting the desired signal power $\mathbf{w}_q{}^H \mathbf{R}_{mis}\mathbf{w}_q$.

For optimization, if we use the cost function given above in (5.1.18) we get

$$J(\mathbf{w}_a) = \mathbf{w}_q{}^H \mathbf{R}_{mis} \mathbf{w}_q + (\mathbf{w}_q - \tilde{\mathbf{B}}\mathbf{w}_a)^H \mathbf{R}_{iv} (\mathbf{w}_q - \tilde{\mathbf{B}}\mathbf{w}_a)$$

The derivative of this cost function with respect to $\mathbf{w}_a$ is given as

$$\begin{aligned} \frac{\partial J}{\partial \mathbf{w}_a} &= -\tilde{\mathbf{B}}^H \mathbf{R}_{iv} (\mathbf{w}_q - \tilde{\mathbf{B}}\mathbf{w}_a) \\ &= -\tilde{\mathbf{B}}^H \mathbf{R}_{iv} \mathbf{w}_q + \tilde{\mathbf{B}}^H \mathbf{R}_{iv} \tilde{\mathbf{B}} \mathbf{w}_a \end{aligned} \tag{5.1.19}$$

For optimization put $\frac{\partial J}{\partial \mathbf{w}_a} = \mathbf{O}$. Consequently the optimized adaptive weight vector $\mathbf{w}_{ao}$ will be taken as

$$\begin{aligned} &-\tilde{\mathbf{B}}^H \mathbf{R}_{iv} \mathbf{w}_q + \tilde{\mathbf{B}}^H \mathbf{R}_{iv} \tilde{\mathbf{B}} \mathbf{w}_{ao} = \mathbf{O} \\ &\tilde{\mathbf{B}}^H \mathbf{R}_{iv} \tilde{\mathbf{B}} \mathbf{w}_{ao} = \tilde{\mathbf{B}}^H \mathbf{R}_{iv} \mathbf{w}_q \\ &\mathbf{w}_{ao} = \left(\tilde{\mathbf{B}}^H \mathbf{R}_{iv} \tilde{\mathbf{B}}\right)^{-1} \tilde{\mathbf{B}}^H \mathbf{R}_{iv} \mathbf{w}_q \end{aligned} \tag{5.1.20}$$

In above expressions, we have considered single interference. The expressions for multiple interferences can be obtained simply by adding the covariance matrices of individual interference due to the reason that interferences are considered to be statistically independent.

In actual situation desired signal, interference signals and noise are mixed at the array and it is easy to get $\hat{\mathbf{R}}_y$ rather than $\mathbf{R}_{iv}$. This is the reason that expression (5.1.17) is used by replacing $\mathbf{R}_y$ with $\hat{\mathbf{R}}_y$ instead of (5.1.20) in practice.

Now we shall analyze the effect of multiple steering vectors of $\tilde{\mathbf{C}}$

In case of traditional GSC, the constraint matrix is given as $\mathbf{C} = \mathbf{a}(\theta_s)$ and accordingly the blocking matrix is given by

$$\mathbf{B} = null\{\mathbf{C}^H\} \tag{5.1.21}$$

Since $\tilde{\mathbf{C}}$ contains cluster of p uniformly spaced steering vectors from signal mismatch region with presumed signal steering vector $\mathbf{a}(\theta_s)$ at the centre. The traditional matrix $\mathbf{C}$ contains only $\mathbf{a}(\theta_s)$, hence the matrix $\mathbf{B}$ corresponding to the traditional GSC

causes a single sharp null along θ_s. This null results due to utilization of $\mathbf{C}$ in expression (5.1.21). However on the other hand broad nulls are resulted by using $\tilde{\mathbf{B}}$ which is due to the cluster of steering vectors in $\tilde{\mathbf{C}}$ given by (5.1.6) [128], [129]. These broad nulls will be in better position to block the signal from mismatch region in the lower branch of RGSC.

That is quite understandable by (5.1.7), that is

$$\tilde{\mathbf{B}}^H\tilde{\mathbf{C}}=\mathbf{O} \tag{5.1.22}$$

The null matrix in above equation is of order $M-p$ by p, therefore p must be less than M i.e. the number of steering vectors contained in $\tilde{\mathbf{C}}$ should be less than the number of elements in the array. This condition will make the problem over determine and will be easy to solve to give the unique solution mathematically.

5.1.2 SIMULATION RESULTS FOR RGSC

A uniform linear array having 16 Omni-directional elements has been considered for simulation. The inter-element spacing has been kept λ/2. Spatially white Gaussian noise with unit variance is assumed to be added at the sensor inputs. Five different examples are being presented here to generate a comparison of performance of traditional GSC, RLCMV based GSC with the proposed one that is RGSC. In all examples, INR in a single sensor is kept equal to 30 dB and the desired signal is always present in the snapshot data. In these examples, we have used 500 snapshots averaged over 300 independent trials.

In the literature [82], [130], expression for beam width is given as under

$$\theta_{nd}=\frac{50.7\lambda}{Md} \tag{5.1.23}$$

With λ, M and d being the wave length, number of antenna elements and the inter-element spacing respectively. Using (5.1.23), the half power beam width for the traditional beamformer utilizing this linear array comes out to be 6.2° that is from -3.1° to 3.1°. That is why in the following examples, GSC has been made robust for

DOA mismatch up to 6° i.e., from $\theta_s - 3°$ to $\theta_s + 3°$. The proposed RGSC is robust for the arbitrary DOA mismatches in this range.

Example1:

This example shows the effect of DOA mismatch on beamformer performance.

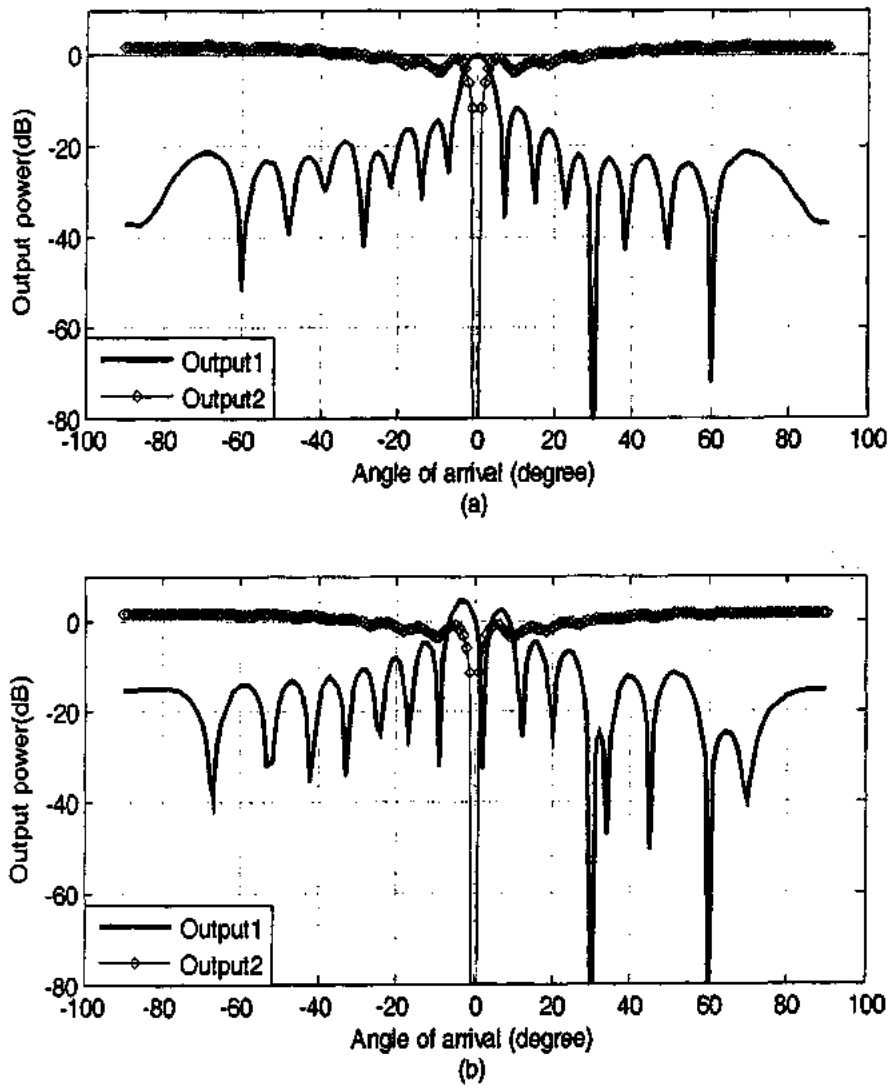

Figure 5.4: Generalized Sidelobe Canceller (a) Without DOA mismatch (b) With DOA mismatch

Two interferences are considered at $\theta_{i1}=30°$ and $\theta_{i2}=60°$ along with the above mentioned desired signal. SNR is kept at 10 dB. First the performance of traditional GSC without any DOA mismatch has been computed and is shown in Fig 5.4 (a). In this case the 'Output 1' is for traditional GSC and 'Output 2' is for a vector from its blocking matrix. Clearly the null corresponding to the vector from blocking matrix is along the presumed signal direction i.e. at 0° and the desired signal falls in the range of this null, obviously, there is no mismatch. Same is true for the behavior of the nulls corresponding to the remaining vectors of the blocking matrix. Fig 5.4 (b) indicates the situation for DOA mismatch of 3°. The null corresponding to each vector of the blocking matrix is at 0° i.e. along the presumed direction while the desired signal being at 3° falls outside these nulls. In the Fig 5.4 (b), 'Output 2' and 'Output 1' are corresponding to a vector from blocking matrix and GSC respectively. Clearly the Output 1 is degraded severely at 3° due to the DOA mismatch problem.

Example 2:

This example presents the beam-width comparison for the proposed algorithm and the robust LCMV based GSC. Same signals as in previous example have been considered. The constraint problem for the RLCMV beamformer is as under:

$$\min_{\mathbf{w}} \mathbf{w}^H \mathbf{R}_y \mathbf{w} \text{ Subject to}$$
$$\mathbf{a}^H(\theta_s-\delta\theta)\mathbf{w}=1, \mathbf{a}^H(\theta_s)\mathbf{w}=1, \mathbf{a}^H(\theta_s+\delta\theta)\mathbf{w}=1$$

Therefore, for RLCMV beamformer

$\tilde{\mathbf{C}}=[\mathbf{a}(\theta_s-\delta\theta) \quad \mathbf{a}(\theta_s) \quad \mathbf{a}(\theta_s+\delta\theta)]$ and $\tilde{\mathbf{f}}=[1 \quad 1 \quad 1]^T$

To cover up the complete DOA mismatch region of 6°. The parameters for the proposed robust GSC are given as:

$\mathbf{C}=[\mathbf{a}(\theta_s)]$, $\tilde{\mathbf{C}}=[\mathbf{a}(\theta_s-\delta\theta) \quad \mathbf{a}(\theta_s) \quad \mathbf{a}(\theta_s+\delta\theta)]$, $\mathbf{f}=\mathbf{1}$

Fig. 5.5 shows the results of two algorithms. A clear difference in beam width for the two algorithms is there. The proposed algorithm is outperforming in this case.

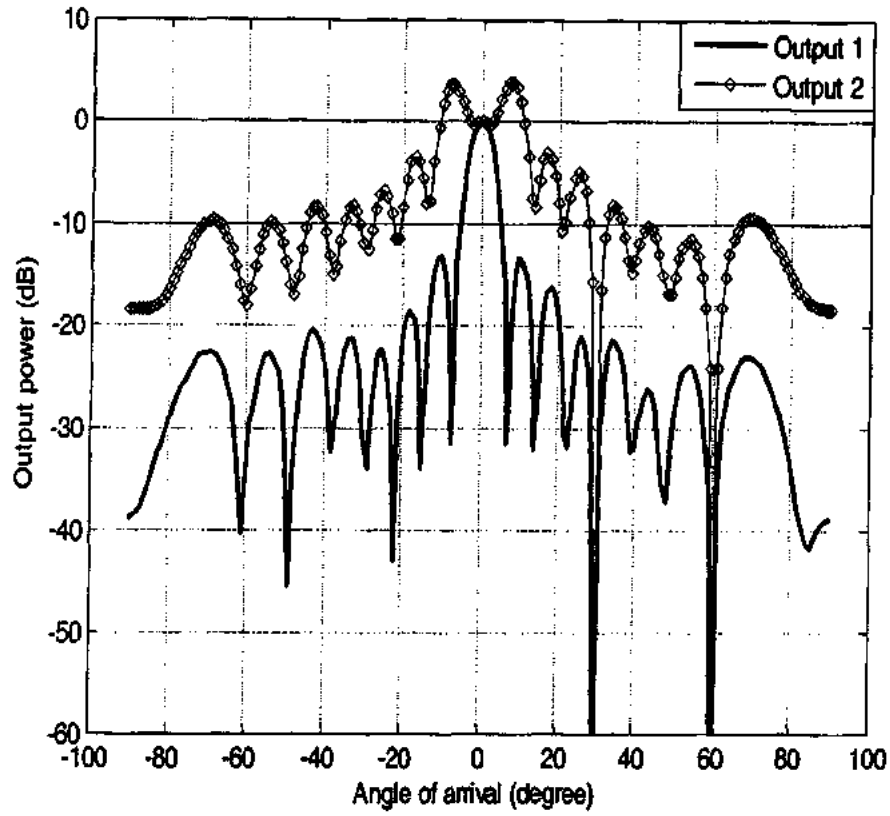

Figure 5.5: Beam-width comparison. Output 1: RGSC, Output 2: RLCMV based GSC

Example 3:

This example shows the effect of number of steering vectors on the null depth of the blocking matrix and hence the performance of RGSC. It can be seen from Fig 5.6 (a) and Fig. 5.6 (b) that the null depth is not uniform through the signal mismatch region. On the other hand depth corresponding to the steering vector angles of the modified constraint matrix $\bar{C}$ is excellent. Troughs can be seen there which are shifted at some other angles. The signal leakage in the lower branch of GSC along these troughs is higher than the angles corresponding to the steering vectors of $\bar{C}$ i.e. in other words these troughs can affect the performance of the GSC. Fig 5.6 (a) and 5.6 (b) are for $\bar{C}$ with three steering vectors along -3°, 0° and 3° and five steering vectors along -3°, -1.5°, 0°, 1.5° and 3° respectively.

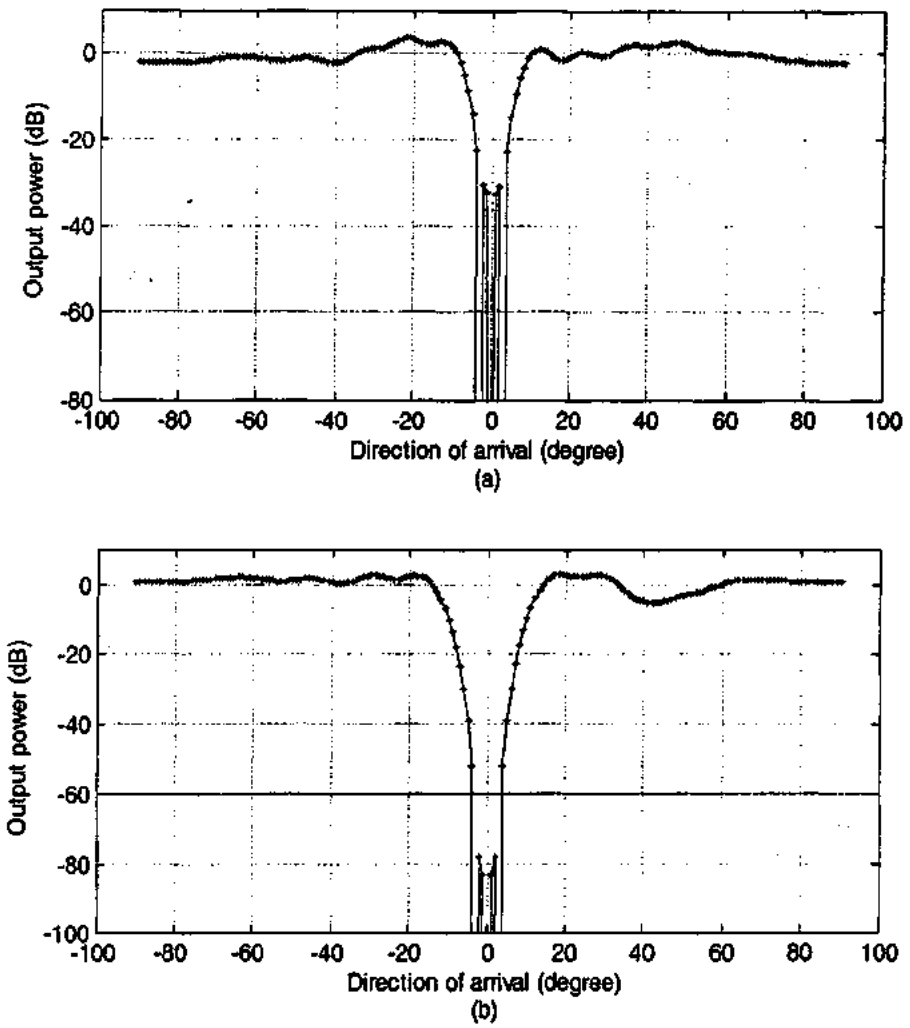

Figure 5.6: Effect of number of steering vectors on null depth. (a) For $\bar{C}$ with steering vectors along -3°, 0°, 3°. (b) For $\tilde{C}$ with steering vectors along -3°, -1.5°, 0°, 1.5°, 3°.

Fig 5.7 indicates the performance of GSC for both cases mentioned in figure 5.6 (a) and (b), where the desired signal appears at 2°.

In Fig 5.7 (b) the null depth at 2° is better than that in Fig 5.7 (a), which is the reason for performance degradation of the beamformer given in Fig 5.7 (a). In the Fig 'Output 1' shows the RGSC performances while 'Output 2' represents the output power of a vector from modified blocking matrix.

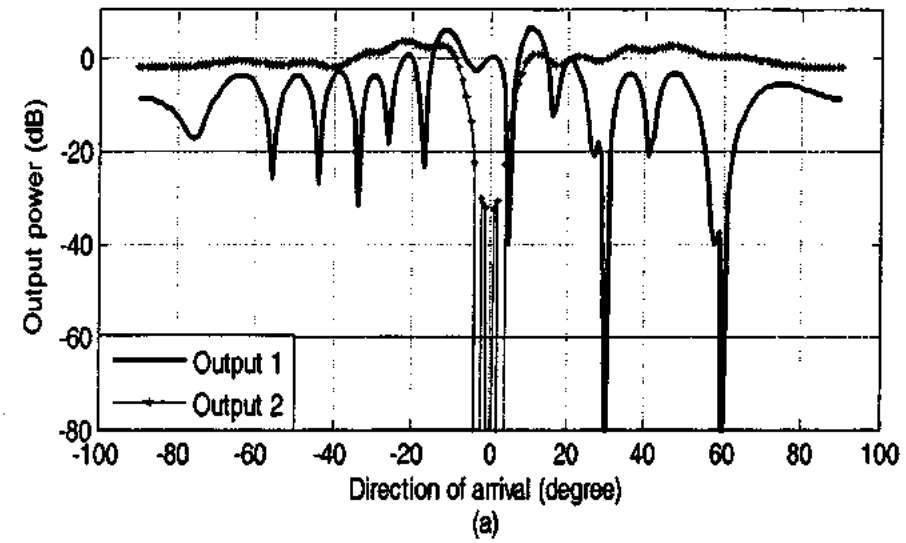

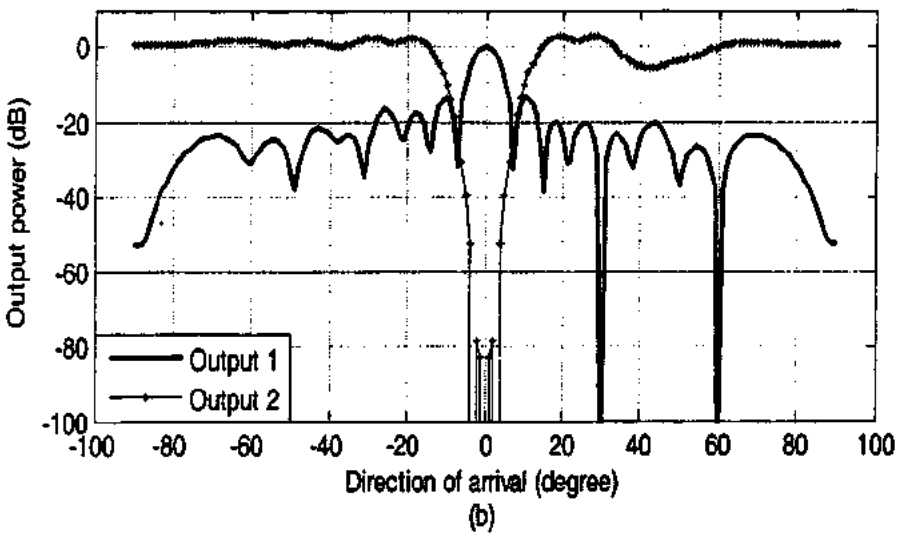

Figure 5.7: Effect of crest height on beamformer performance. (a) For $\tilde{C}$ with three steering vectors, high trough at 2°. (b) For $\tilde{C}$ with five steering vectors, relatively low trough appears at 2°.

Example 4:

In this example, it is shown that the crest height depends upon the number of steering vectors in the cluster contained in $\tilde{C}$. Fig 5.8 shows the trough height in the signal mismatch region when $\tilde{C}$ contains 3, 5, 7 and 9 steering vectors.

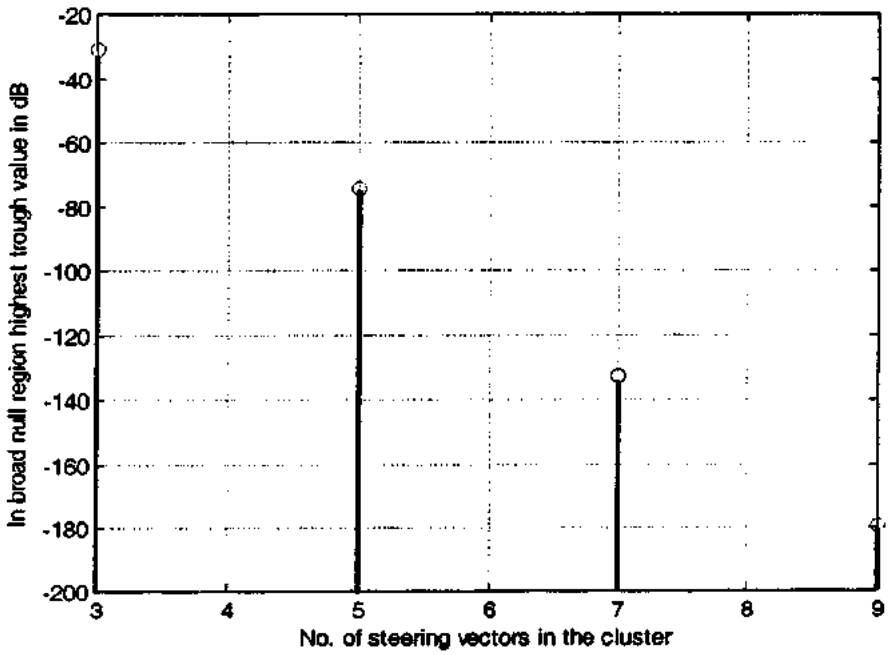

Figure 5.8: Crest height versus number of steering vectors contained in $\check{C}$.

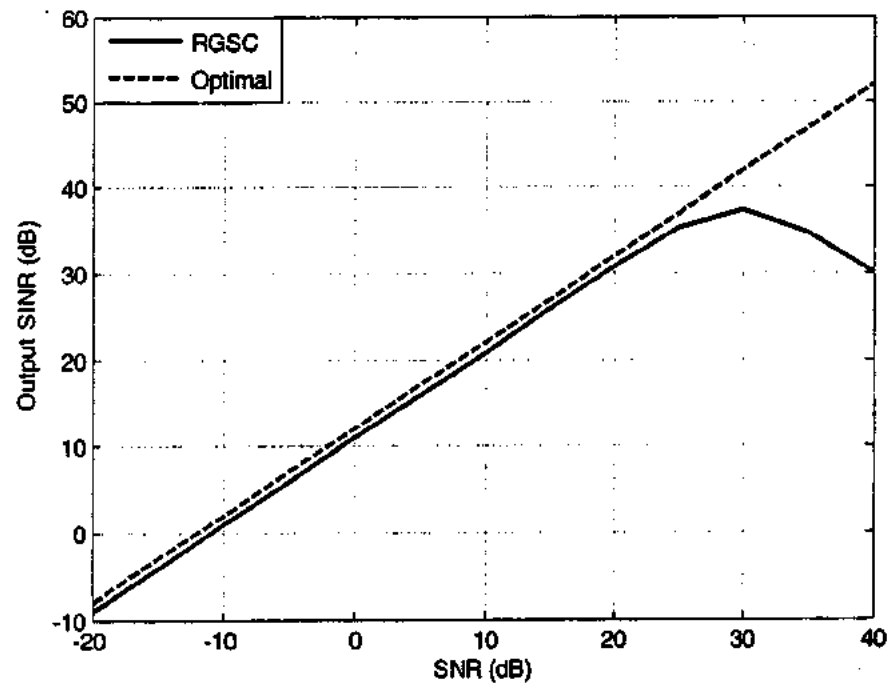

Figure 5.9: SINR versus SNR for proposed RGSC under ideal signal and interference conditions.

Example 5:

In this example, we compare the performance of RLCMV based GSC and the proposed algorithm in terms of output SINR versus SNR.

The presumed source signal is considered at 3°. The interferences are placed at 30° and 60°. The actual direction of the source signal is 2°. Fig 5.9 shows the comparative performance of the two algorithms.

5.2 DL OF RG-RANK BEAMFORMER FOR DOA MISMATCH

In the literature, a positive diagonal loading (DL) technique is available that utilizes the increasing diagonal loading value for the movement of the peak of the main beam, towards the presumed signal direction [82].

The general-rank beamformer utilizes negative diagonal loading for robustness against signal DOA mismatch. For this beamformer, the negative diagonal loading level cannot exceed beyond a certain level at which the diagonally loaded signal covariance matrix becomes negative definite. Similarly, positive diagonal loading level of received signal covariance matrix cannot be below a certain value otherwise the constraint given in expressions (4.4.23) and (4.4.24) will be violated.

Following, is an iterative approach being presented for the diagonal loading (DL) of robust general-rank beamformer RG-Rank Beamformer).

5.2.1 PROPOSED ALGORITHM FOR DL OF RG-RANK BEAMFORMER

The weight vector for robust general-rank beamformer is given in expression (4.4.29) and is being reproduced here for convenience.

$$\tilde{\mathbf{w}}_{rob,s} = P\left\{\left(\hat{\mathbf{R}}_y + \gamma\mathbf{I}\right)^{-1}\left(\mathbf{R}_s - \varepsilon\mathbf{I}\right)\right\} \tag{5.2.1}$$

In case of DOA mismatch if $\gamma = 0$ and $\varepsilon = 0$ then RG-Rank beamformer becomes SMI beamformer and faces the signal cancellation problem as discussed in previous section. By increasing the diagonal loading level the peak of the main beam moves towards the presumed signal direction. This reduces the signal and interference

cancellation capabilities of the beamformer. Proper diagonal loading level can be achieved by increasing ε iteratively and monitoring the left-right beam symmetry around the presumed signal direction.

For a uniform linear array of M antenna elements, the beam width is given by (5.1.23). The maximum value of ε will result in the weight vector for which the peak of the main beam will move at a position that results in the left-right beam symmetry about the presumed signal direction i.e.

$$\left|\tilde{\mathbf{w}}_{rob,s}\mathbf{a}(\theta_s+\delta\theta)\right|-\left|\tilde{\mathbf{w}}_{rob,s}\mathbf{a}(\theta_s-\delta\theta)\right|=0 \tag{5.2.2}$$

Where $0<\delta\theta\le\frac{1}{2}\theta_{nd}$

Let $m_1=\left|\tilde{\mathbf{w}}_{rob,s}\mathbf{a}(\theta_s+\delta\theta)\right|$ and $m_2=\left|\tilde{\mathbf{w}}_{rob,s}\mathbf{a}(\theta_s-\delta\theta)\right|$ and imposing the condition on beam symmetry i.e., the difference about the desired signal direction to remain below a certain specified value $\mu>0$ i.e.

$$|m_1-m_2|\le\mu \tag{5.2.3}$$

In above equation, μ is the trade off parameter that controls the robustness against DOA mismatch and the interference suppression capability.

An expression for ε as available in the literature is given below [87].

$$\varepsilon=\max_{\theta_s-\delta\theta\le\theta\le\theta_s+\delta\theta}\left\|\mathbf{a}(\theta)-\mathbf{a}(\theta_s)\right\| \tag{5.2.4}$$

Where $\theta_s-\delta\theta\le\theta\le\theta_s+\delta\theta$ represents the specified region for signal DOA mismatch. The maximum value of ε may exist outside this region. The value of ε within the specified region is named as ε_{min} which is

$$\varepsilon_{min}=\max_{\theta_s-\delta\theta\le\theta\le\theta_s+\delta\theta}\left\|\mathbf{a}(\theta)-\mathbf{a}(\theta_s)\right\| \tag{5.2.5}$$

The ε_{max} can be found by expanding the mismatch region iteratively. During this expansion a stage will be reached beyond which the value of ε stops to increase and becomes constant. This value will be ε_{max} and is expressed as

$$\varepsilon_{max} = \max_{\theta_s - \delta\theta - n\frac{\Delta\theta}{2} \le \theta \le \theta_s + \delta\theta + n\frac{\Delta\theta}{2}} \|\mathbf{a}(\theta) - \mathbf{a}(\theta_s)\| \qquad (5.2.6)$$

Where $\Delta\theta$ is the step size for expansion of region.

Following is the working sequence of the proposed algorithm.

Step 1: Initialization

In initialization, the minimum and maximum values of diagonal loading levels ε and γ are provided. Same is also indicated in the flowchart.

Step 2: Evaluation of weight vector

Based on initial values of ε and γ, expression (5.2.1) is utilized to find out the weight vector. $\mathbf{w} = \tilde{\mathbf{w}}_{rob,s}$

Step 3: Check the condition

Validity of the constraint given in expressions (4.4.23), (4.4.24) is checked at this stage whether they are fulfilled or not.

Step 4: Evaluation of m_1 and m_2

If the condition in step 3 is satisfied, then evaluate m_1 and m_2 otherwise, increase γ with step increment $\delta\gamma$ and go to step 3 until the condition in step 3 is satisfied.

Step 5: Beam Symmetry comparison

Find out $|m_1 - m_2|$ and if the condition in (5.2.3) is satisfied then stop otherwise increase ε with increment $\delta\varepsilon$ and go back to step 2. If condition in (5.2.3) is not satisfied even with ε_{max} then stop with the message "Array Calibration is required".

Since $\tilde{\mathbf{w}}_{rob,s}$ is evaluated for minimum possible values of ε and γ, hence better null depth in addition to the robustness against signal look direction error is achieved.

5.2.2 FLOWCHART FOR DL OF RG-RANK BEAMFORMER

The flowchart for the proposed algorithm is shown in Fig 5.10

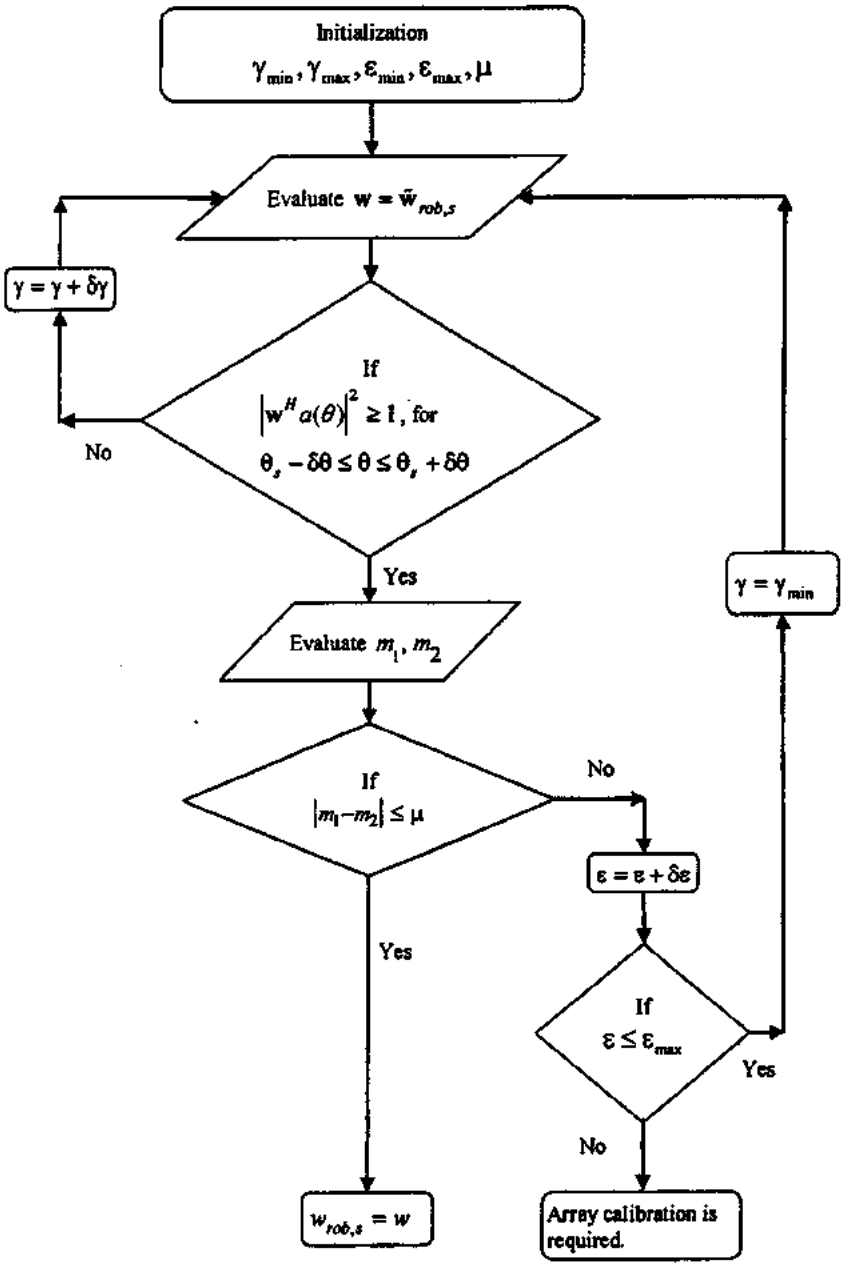

Figure 5.10: Flowchart for diagonal loading of robust general-rank beamformer.

5.2.3 SIMULATION RESULTS

In this section, simulations results are presented. Simulations are performed in MATLAB to verify the validity of proposed algorithm. For this purpose, we have considered a uniform linear array of 15 Omni-directional elements with inter-element spacing equal to $\lambda/2$. The presumed signal direction is 0° while the actual direction is 3°. Two interferences are placed at 35° and 70°. The values of SNR and INR have been taken as 10 dB and 30 dB respectively.

Example 1:

In this example, effect of ε is being observed on the beam symmetry. The results in table 5.3 are obtained by increasing ε while keeping γ constant. Higher value of γ is used to satisfy the constraints given by expression (4.4.17). All the corresponding values of ε shown in first column of the table except the first one where $\varepsilon = 0$ and $\gamma = 0$. That is SMI beamformer with DOA mismatch of 3°. It is clear from the table that the beam symmetry improves as ε increases.

Table 5.3: Difference in beam symmetry with increasing values of ε.

S. No.	ε	γ	Difference at ±3°	Difference at ±2°	Difference at ±1°
1	0	0	35.5dB	11 dB	4.80 dB
2	2	280	2.30 dB	1.4 dB	0.70 dB
3	4	280	1.93 dB	1.2 dB	0.57 dB
4	6	280	1.52 dB	0.9 dB	0.46 dB

Example 2:

In this example, effect of γ is observed on the beam symmetry. The results in table 5.4 are obtained by increasing γ while keeping ε constant. It can be seen from the table that beam symmetry improves as γ increases.

Comparison of table 5.3 and table 5.4 shows that beam symmetry is more sensitive to ε than γ. This is due to obvious reason that small change in ε has more effect on beam symmetry than the small change in γ.

Table 5.4: Difference in beam symmetry with increasing values of γ.

S. No.	ε	γ	Difference at ±3°	Difference at ±2°	Difference at ±1°
1	4	30	8.94 dB	5.13 dB	2.38 dB
2	4	60	6.10 dB	3.63 dB	1.71 dB
3	4	90	4.69dB	2.83 dB	1.34 dB
4	4	120	3.84 dB	2.33 dB	1.11 dB
5	4	150	3.25 dB	1.99 dB	0.95 dB
6	4	180	2.82 dB	1.72 dB	0.82 dB
7	4	210	2.49 dB	1.53 dB	0.73 dB
8	4	240	2.23 dB	1.37 dB	0.66 dB
9	4	270	2.01 dB	1.24 dB	0.59 dB

Example 3:

This example shows the effect of diagonal loading level on null depth. The results are shown in table 5.5 where the null depth decreases by increasing values of diagonal loading level while the desired signal strength is also improved.

Table 5.5: Comparison of Null depth with increasing values of ε and γ

S. No	γ	ε	Signal (dB)	Null_1 (dB)	Null_2 (dB)
1	5	1	-12.0	-69.93	-74.32
2	5	2	-10.7	-68.60	-72.90
3	5	3	-8.85	-66.49	-70.01
4	25	4	1.31	-55.01	-59.47
5	50	4	4.15	-50.92	-56.27
6	50	4.5	4.50	-50.20	-55.87

5.3 CONCLUSION

In this chapter, two algorithms have bee presented. These algorithms are robust and adaptive for direction of arrival mismatch. The features of these algorithms are summarized below.

1. RGSC provides the robustness against signal look direction error without broadening the main beam.

2. For RGSC, the capability of the beamformer to implement more constraints is reduced by an amount equal to the number of steering vectors contained in the extended constraint matrix $\tilde{\mathbf{C}}$.

3. The diagonal loading technique presented for General-Rank beamformer utilizes beam symmetry as a criterion to select diagonal loading level.

4. The only area which needs improvement is the technique for diagonal loading. Currently the proposed diagonal loading technique is based on iterative computations, which is time consuming. A more efficient algorithm may be given to make it proficient.

CHAPTER 6

CONCLUSION AND FUTURE WORK

6.1 SUMMARY OF THE WORK

In this thesis we have investigated two categories of beamformers. First category is based on DOA, hence is named as DOA based Beamformers. The second category is named as Optimal Adaptive Beamformers. These categories have been discussed in part-I and part-II of the dissertation respectively.

We have started part-I with mathematical model for DOA Based Beamformers using uniform linear array as mentioned in chapter-2. The chapter also includes the initial setup with some relevant existing time efficient algorithms lying in this category. The main problem with these existing algorithms is the smaller number of steerable nulls specifically less than half of the number of antenna elements. Another problem is that the radiation pattern for these algorithms may have high sidelobe levels and main beam may not be symmetric about the desired signal direction.

These problems with existing algorithms have been addressed Chapter 3. Three different new algorithms have been contributed to rectify each of the above mentioned problems specifically. All of them lie in the domain of DOA Based Beamforming algorithms and are mentioned as under

a. *INS by Decoupling Complex Weights:*

   This algorithm provides independent weight control for each null and is capable of steering the maximum available nulls.

b. *INS with Suppressed SLs:*

   This is another independent weight control technique for each null and provides sidelobe suppression in addition to the independent null steering.

However, the extra feature, i.e., the suppression of sidelobes is achieved at the cost of reduced number of steerable nulls.

c. *INS with Suppressed SLs and Symmetric Beam:*

This is the third contribution in this category. The main beam symmetry may get disturbed while going through the INS algorithm mentioned above. That symmetry has been improved as well in this case. The proposed algorithm improves the main beam symmetry for 'INS with Suppressed SLs'.

The second category of beamformers i.e., Optimal Adaptive Beamformers have been discussed in chapter 4 and chapter 5. Chapter 4 presents Mathematical model for optimal adaptive beamformers and the effect of signal DOA mismatch on these beamformers. Some existing robust techniques against signal DOA mismatch are also given in this chapter. The problem with LCMV based robust algorithm is that it causes the broadening of main beam. Diagonal loading techniques have also been discussed which have the deficiency that there is no reliable method to select amount of diagonal loading level.

In chapter 5 we have contributed toward Robust Generalized Sidelobe Canceller in the form of algorithm that provides robustness against signal look direction error without broadening the main beam. Another contribution included in this chapter is towards the diagonal loading criterion for Robust General-Rank Beamformer. Previously no criteria existed to decide the amount of diagonal loading level. The proposed technique presents an iterative approach to select diagonal loading level on the basis of difference in left-right beam levels around the presumed signal direction.

6.2 FUTURE WORK

The INS algorithms with independent weight control presented in chapter 3 are meant for single beam. The independent null steering algorithms with multiple beam scenarios will be a potential area of research in the near future. Of course the work will be more challenging, however, its utility specifically in smart antennas cannot be

denied. In short it will be more demanding and a good contribution in DOA based adaptive beamformers.

The sidelobe levels depend upon the relative position of the interferences. The sidelobe level control by steering of some forced nulls can be a better choice than that of weight control. The problem is how to find out the number and the position of forced nulls for sidelobe control. Solution to this problem i.e., finding the number and position of sidelobes is another area of research which can be taken in future.

In case of robust LCMV based beamformer the null depth is smoothened by increasing the number of steering vectors in the cluster to modify the blocking matrix of RGSC. However, it also increases the computational complexity. There must be a threshold level to which the smoothening is required. To develop a criterion for number of steering vectors in the cluster to modify the blocking matrix of RGSC is a topic of research. It will be a contribution towards robust LCMV based beamformers.

The proposed approach for diagonal loading is iterative which takes some time to reach the optimal value. Development of a closed form solution for diagonal loading of Robust General-Rank Beamformer will be a valuable contribution as an alternate to iterative approach presented in chapter 5.

References

[1] F. R. Farrokhi, K. J. R. Liu, and Leandros, "Transmit beamforming and power control for cellular wireless systems," *IEEE J. Selected Areas Comm.*, vol. 16, no. 8, pp. 1437-1450, Oct. 1998.

[2] M. Bengtsson, and B. Ottersten, "Optimal downlink beamforming using Semidefinite optimization," In Proc. of 37th *annual Allerton Conf. on Comm., Control, and Computing*, pp. 987-996, Sep. 1999.

[3] V. Sharma, I. Wajid, A. B. Gershman, H. Chen, and S. Lambotharan, "Robust Downlink Beamforming Using Positive Semi-definite covariance constraints," *IEEE Int. ITG Workshop on smart antennas (WSA 2008)*, pp. 36-41.

[4] L. E. Brennan, J. D. Mallet, and I. S. Reed, "Adaptive Arrays in Airborne MTI radar," *IEEE Trans. Antennas Prop.*, vol. 24, pp. 607-615, Sept. 1976.

[5] T. Hong, M. –Z. Song, and X.-Y. Sun, "Design of a sparse antenna array for communication and direction finding applications based on the Chinese remainder theorem," *PIER 98*, pp. 119-136, 2009.

[6] D. M. Byrne, O' Halloran, E. Jones, and M. Galvin, "Transmitter-grouping robust Capon beamforming for breast cancer detection," *PIER 108*, pp. 401-416, 2010.

[7] G. Liang, W. Gong, H. Liu, and J. Yu, "Development of 61-channel digital beamforming (DBF) transmitter array for mobile satellite communication," *PIER 97*, pp. 177-195, 2009.

[8] K. Guney and A. Akdagli, "Null Steering of Linear Antenna Arrays Using a Modified TABU Search Algorithm," *PIER 33*, pp. 167–182, 2001.

[9] D. J. Chapman, "Partial Adaptivity for the Large Array," *IEEE Trans. Antennas Prop.*, AP-24, no. 5, pp. 685-696, Sep. 1976.

[10] B. Friedlander and B. Porat, "Performance Analysis of a Null-Steering Algorithm Based on Direction of Arrival Estimation," *IEEE Trans. Acoust. Speech, Sig. Process.*, vol. 37, no 4, pp. 461-466, Apr. 1989.

[11] H. Cox, "Resolving power and sensitivity to mismatch of optimum array processors," *J. Acoust. Soc. Amer.*, vol. 54, no. 3, pp. 771–785, 1973.

[12] C. A. Balanis, *Antenna Theory Analysis and Design*, third ed., John Wiley & Sons, New York, NY, USA, 2005.

[13] R. 0. Schmidt, "Multiple emitter location and signal parameter estimation," in *Proc. RADC Spectrum Estimcition Workshop.* Griffiths AFB, New York, 1979, pp. 243-258; reprinted in *IEEE Trans. Antennas Prop.*, vol. AP-34. pp. 276-280, Mar. 1986.

[14] R. Roy, and T. Kailath, "ESPIRIT-estimation of signal parameters via rotational invariance technique," *IEEE Trans. Acoust. Speech, Signal Processing*, vol. 37, no. 7, pp. 984-995, Jul 1989.

[15] B. D. Rao, and K. V. S. Hari, "Performance analysis of Root-Music," *IEEE Trans. Acoust. Speech, Signal Processing*, vol. 37, no 12, pp.1939-1949, Dec. 1989.

[16] F. Zaman, I. M. Qureshi, A. Naveed, and Z. U khan, "Real Time Direction of Arrival Estimation in Noisy Environment Using Particle Swarm Optimization with Single Snapshot," *R. J. Applied Sc., Eng. Tech.*, 4(13): pp. 1949-1952, Jul 2012.

[17] T. K. Sarkar, and O. Pereira, "Using the matrix pencil method to estimate the parameters of a sum of complex exponentials," *IEEE Antennas Prop.*, vol. 37, no. 1, pp. 48-55, Feb 1995.

[18] N. Yilmazer, J. Koh, and T.K. Sarkar, "Utilization of a unitary transform for efficient computation in the matrix pencil method to find the direction of arrival," *IEEE Trans. Antenna Prop.*, vol. 54, no. 1, pp. 175-181, Jan 2006.

[19] M. F. Khan, and M. Tufail, "Beamspace matrix pencil method for direction of arrival estimation," *IEICE Electron. Express*, vol. 6, no. 16, pp. 1168-1173, Aug 2009.

[20] H. Karim, and M. Viberg, "Two Decades of Array Signal Processing Research: The parametric approach," *IEEE Signal processing Mag.*, vol. 13, no. 4, pp. 67-94, Jul. 1996.

[21] H. M. Pour, Z. Atlasbaf, and M. Hakkak, "Performance of Neural Network Trained with Genetic Algorithm for Direction of Arrival Estimation," *Proc. 1st IEEE int. conf. Mobile Computing & Wireless Comm.*, 17-20 Sep. 2006, pp. 197-202,.

[22] F. Zaman, I. M. Qureshi, A. Naveed, J. A. Khan, and R. M. A. Zahoor, "Amplitude and Directiona of Arrival estimation: comparison between different techniques," *PIER B*, vol. 39, pp. 319-335, 2012.

[23] F. Zaman, I.M. Qureshi, A. Naveed, and Z.U. Khan, "Joint estimation of amplitude, direction of arrival and range of near field sources using memetic computing," *PIER C*, vol. 31, pp. 199-213, 2012.

[24] T. H. Ismail, and M. M. Dawoud, "Null steering in phased arrays by controlling the element positions," *IEEE Trans. Antennas Prop.*, vol. Ap-39, no. 11, pp. 1561-1566, Nov. 1991.

[25] M. M. Dawoud, and T. H. Ismail, "Experimental verification of null steering by element position perturbations," *IEEE Trans. Antennas Prop.*, vol. Ap-40, no. 11, pp. 1431-1434, Nov. 1992.

[26] J. A. Hejres, "Null steering in phased arrays by controlling the positions of selected elements," *IEEE Trans. Antenna Prop.*, vol. 52, no. 11, pp. 2891 - 2895, Nov 2004.

[27] J. A. Hejres, A. Peng, and J. Hijres, "Fast Method for Sidelobe Nulling in a Partially Adaptive Linear Array Using the Elements Positions," *IEEE Antenna Wireless Prop., Letters*, vol. 6, pp. 332 - 335, 2007.

[28] P. Sattari, and N. Hejazi, "Array pattern null steering using genetic algorithm by element position perturbations," *IEEE Conf. Elect. Comp. Eng.* 4-7 May, 2008, pp. 000423-000428.

[29] M. T. Alsharaa, M. A. Mangoud, and H. M. Elragal, "Null control by position perturbation of selected elements for phased antenna array using hybrid EPSO/DE optimization," *IEEE Int. Conf. Comm. Systems* 17-19 Nov. 2010, pp. 621-624.

[30] S. A. Schelkunoff, "A mathematical theory of linear arrays," *Bell Syst. Tech. J.*, vol. 22, pp. 80-107, Jan. 1943.

[31] E. Mendelovicz, and E. T. A. Oestreich, "Phase-only adaptive nulling with discrete value," *Proc. IEEE*, vol. 17, pp. 193–198, Jun. 1979.

[32] R. Giusto, and P. DE Vincenti, "Phase-only optimization for the generation of wide deterministic nulls in the radiation pattern of phased arrays," *IEEE Trans. Antennas Prop.*, AP-31, no. 5, pp. 814-817, Sep 1983.

[33] H. Steyskal, "Simple method for Pattern Nulling by Phase Perturbation," *IEEE Trans. Antennas Prop.*, AP-31, no. 1, pp. 163-166, Jan 1983.

[34] R. A. Shore, "Nulling at Symmetric Pattern Location with Phase-Only Weight Control," *IEEE Trans. Antennas Prop.*, AP-32, no. 5, pp. 530-533, May 1984.

[35] C. –W. Su, "Synthesis of array patterns with deep nulls by use of one couple phases," *Antennas and Prop. Society Int. Symp.*, 24-28 Jun 1991, vol.3, pp. 1412-1415.

[36] D.-C. Chang, C. –I. Hung, H.-T. Chen, T.-M. Lee, and K. T. Ho, "A Novel Phase-Only Nulling in a Monopulse Phased Array Antenna," *Proc. IEEE*, vol. 2, pp. 1035–1038, Jul. 1992.

[37] D. S. Hicks, "Null steering in linear arrays by using amplitude control of signals in the feeder network," *Electronics Letters*, vol. 13, no. 7, pp. 198-199, Mar 1977.

[38] T. B. Vu, "Method of null steering without using phase shifters," *Inst. Elec. Eng. Proc.*, vol. 131, pt. H, no. 4, pp. 242-245, Aug. 1984.

[39] T. B. Vu, "Simultaneous Nulling in Sum and Difference Patterns by Amplitude Control," *IEEE Trans. Antennas Prop.*, AP-34, no. 2, pp. 214-218, Feb 1986.

[40] H. M. Ibrahim, "Null Steering by Real-Weight Control-A Method of Decoupling the Weights," *IEEE Trans. Antennas Prop.*, AP-39, no. 11, pp. 1648-1650, Nov 1991.

[41] Z. U. Khan, A. Naveed, I. M. Qureshi, and F. Zaman, "Independent Null Steering by Decoupling Complex Weights," *IEICE Electronics Express*, vol. 8, no. 13, pp. 1008-1013, July 10, 2011.

[42] D. Marcano, and F. Duran, "Synthesis of Antenna Array Using Genetic Algorithms," *IEEE Antennas Prop. Mag.*, vol. 42, no. 3, pp. 12-20, Jun 2000.

[43] W. P. Liao, and F. L. Chu, "Array pattern synthesis with null steering using genetic algorithms by controlling only the current amplitudes," *Int. J. Electronics*, vol. 86, no. 4, pp. 445–457, 1999.

[44] K. Guney, B. Babayigit, and A. Akdagli, "Position only pattern nulling of linear antenna arrays by using a clonal selection algorithm (CLONALG)," *Electrical Engineering*, vol. 90, issue 2, pp. 147–153, Dec. 2007.

[45] A. Tennant, M.M. Dawoud, and A.P. Anderson, "Array pattern nulling by element position perturbations using a genetic algorithm," *Electronics Letters*, vol. 30, no. 3, pp. 174-176, 3 Feb1994.

[46] F. Tokan, and F. Gunes, "Interference suppression by optimizing the positions of selected elements using generalized pattern search algorithm," *IET Microwaves, Antennas Prop.*, vol. 5, no. 2, pp. 127–135, 2011.

[47] M. A. Mangoud, and H. M. Elragal, "Antenna Array Pattern Synthesis and Wide Null Control Using Enhanced Particle Swarm Optimization," *PIER B*, vol. 17, pp. 1-14, 2009.

[48] J. C. Liberti Jr., and T. S. Rappaport, *Smart Antenna for Wireless Comm.: IS-95 and Third Generation CDMA Applications*, Prentice Hall PTR, Upper Saddle River, NJ, 1999.

[49] Special Issue on Active and Adaptive Antennas, *IEEE Trans. Antennas Prop.*, vol. AP-12, Mar. 1964.

[50] C. A. Belfi, C. Rothenberg, L. Schwartzman, R. E. Tilley, and A. Wills, "A Satellite Data Transmission Antenna," *IEEE Trans. Antennas Prop.*, AP-12, pp. 200-206, Mar 1964.

[51] C. Pon, "Retrodirective array using the heterodyne technique," *IEEE Trans. Antennas Prop.*, AP-12, pp. 176-180, Mar 1964.
[52] Y. C. Guo, X. W. Shi, and L. Chen, "Retrodirective Array Technology," *PIER B*, vol. 5, pp. 153–167, 2008.
[53] P. Howells, "Intermediate Frequency Side-Lobe Canceller," *U. S. Patent 3202990*, Aug. 24, 1965.
[54] S. P. Applebaum, "Adaptive Arrays," *IEEE Trans. Antennas Prop.*, vol. AP-24, no. 5, pp. 585-598, Sept. 1976.
[55] M. W. Ganz, "Rapid convergence by cascading Applebaum adaptive arrays," *IEEE Trans. Aerosp. Elect. Syst.*, vol. 30, no.2, pp. 298-306, Apr. 1994.
[56] KM Lee and DS Han, "AGC Applebaum Array for Rejection of Eigenvalue Spread Interferences," *IEICE Trans. Comm.*, E84-B(6), pp. 1674-1679, 2001.
[57] B. Widrow, P. E. Mantey, L. J. Griffiths, and B. B. Goode, "Adaptive antenna systems," *Proc. IEEE*, vol. 55, pp. 2143-2159, Dec. 1967.
[58] L. J. Griffiths, "A simple adaptive algorithm for real-time processing in antenna arrays," *Proc. IEEE*, vol. 57, pp. 1696-1704, Oct. 1969.
[59] O. L. Frost, III, "An algorithm for linearly constrained adaptive array processes," *Proc. IEEE*, vol. 60. pp. 926-935, Aug. 1972.
[60] J. Capon, "High-resolution frequency-wavenumber spectrum analysis," *Proc. IEEE*, vol. 57, 1408–1418, Aug. 1969.
[61] K. Takao, H. Fujita, and T. Nishi, "An adaptive array under directional constraint," *IEEE Trans. Antennas Prop.*, vol. AP-24, no. 5, pp. 662–669, Sep. 1976.
[62] G. S. Liao, H. Q. Liu, and J. Li, "A Subspace-based Robust Adaptive Capon Beamforming," *PIER Symp.*,March 26-29, 2006, Cambridge, USA, pp. 374-379.
[63] I. S. Reed, J. D. Mallett, and L. E. Brennan, "Rapid convergence rate in adaptive arrays," *IEEE Trans. on Aerosp. Elect. Syst.*, vol. 10, no. 6, pp. 853–863, Nov. 1974.
[64] L. J. Griffiths and C. W. Jim, "An alternative approach to linearly constrained adaptive beamforming," *IEEE Trans. on Antennas and Prop.*, vol. 30, no. 1, pp. 27–34, Jan. 1982.
[65] B. D. Van Veen, and K. M. Beukley, "Beamforming: A Versatile Approach to Spatial Filtering," *IEEE ASSP Mag.*, pp. 4-24, Apr. 1988.
[66] H. Singh and R. M. Jha, "Trends in Adaptive Array Processing," *Int. J. Antennas Prop.*, Article ID 361768, 20 pages, 2012.
[67] Special Issue on Adaptive Antennas, *IEEE Trans. Antennas Prop.*, vol. AP-24, Sept. 1976.
[68] W. F. Gabriel, "Adaptive Processing Array Systems," *Proc. IEEE*, vol. 80, no. 1, pp. 152-162, Jan. 1992.
[69] X. Mestre, and M. A. Lagunas, "Finite sample size effect on minimum variance beamformers: optimum diagonal loading factor for large arrays," *Proc. IEEE Trans. Sig. Process.*, vol. 54, no. 1, pp. 69-82, Jan, 2006.
[70] S. P. Applebaum, and D. J. Chapman, "Adaptive arrays with main beam constraints," *IEEE Trans. Antennas Prop.*, vol. AP-24, no. 5, pp. 650–662, Sep. 1976.
[71] K. M. Buckley, and L. J. Griffiths, "An adaptive generalized sidelobe canceller with derivative constraints," *IEEE Trans. Antennas Prop.*, vol. AP-34, no. 3, pp. 311–319, Mar. 1986.

[72] K. Takao, and C. S. Boon, "Importance of the exclusion of the desired signal from the control of a generalized sidelobe canceller," *IEE Proc. Radar Sig. Process.*, vol. 139, no. 4, pp. 265–272, Aug. 1992.

[73] D. D. Feldman, and L. J. Griffiths, "A projection approach for robust adaptive beamforming," *IEEE Tran. Sig. Process.*, vol. 42, no. 4, pp. 867-876, Apr. 1994.

[74] L. Chang, and C. C. Yeh, "Performance of DMI and eigen space-based beamformers," *IEEE Trans. Antennas Prop.*, vol. 40, no. 11, pp. 1336-1347, Nov. 1992.

[75] R. G. Lorentz, and S. P. Boyd, "Robust Minimum Variance Beamforming," *IEEE Trans. Sig. Process.*, vol. 53, no. 5, pp. 1684–1696, May, 2005.

[76] Z. U. Khan, A. Naveed, I. M. Qureshi, and F. Zaman, "Robust generalized sidelobe canceller for direction of arrival mismatch," *Archives Des Sc.*, vol. 65, no. 11, pp. 483–497, Nov. 2012.

[77] K. L. Bell, Y. Ephraim, and H. L. Van Trees, "A Bayesian approach to robust adaptive beamforming," *IEEE Trans. Sig. Process.*, vol. 48, no. 2, pp. 386-398, Feb. 2000.

[78] B. D. Van Veen, "Minimum variance beamforming with soft response constraints," *IEEE Trans. Sig. Process.*, vol. 39, no. 9, pp. 1964-1972, Sep. 1991.

[79] N. K. Jablon, "Adaptive beamforming with the generalized sidelobe canceller in the presence of array imperfections," *IEEE Trans. Antennas Prop.*, vol. 34, no. 8, pp. 996-1012, Aug. 1986.

[80] B. D. Carlson, "Covariance matrix estimation errors and diagonal loading in adaptive arrays," *IEEE Trans. Aerosp. Elect. Syst.*, vol. 24, no. 4, pp. 397-401, Jul. 1988.

[81] A. Elnashar, S. M. Elnoubi, and H. A. El-Mikati, "Further Study on Robust Adaptive Beamforming With Optimum Diagonal Loading," *IEEE Trans. Antennas Prop.*, vol. 54, no. 12, pp. 3647-3658, Dec. 2006.

[82] W. Wang, R. Wu, and J. Liang, "A Novel Diagonal Loading Method for Robust Adaptive Beamforming," *PIER C*, vol. 18, pp. 245-255, 2011.

[83] A. B. Gershman, "Robust Adaptive Beamforming in sensor arrays," *AEU-Int. J. Elect. Comm.*, vol. 53, no. 6, pp. 305-314, Dec. 1999.

[84] A. M. Vural, "Effects of perturbations on the performance of optimum/adaptive arrays," *IEEE Trans. Aerosp. Elect. Syst.*, vol. 15, no. 1, pp. 76-87, Jan. 1979.

[85] A. B. Gershman, C. F. Mecklenbrauker, and J. F. Bohme, "Matrix fitting approach to direction of arrival estimation with imperfect spatial coherence of wavefronts," *IEEE Trans. Sig. Process.*, vol. 45, pp. 1894-1899, July 1997.

[86] S. Shahbazpanahi, A. B. Gershman, Z.-Q. Luo, and K. M. Wong, "Robust adaptive beamforming for general-rank signal models," *IEEE Trans. Sig. Process.*, vol. 51, pp.2257-2269, Sept. 2003.

[87] C-Y. Chen, and P. P. Vaidyanathan, "Quadratically Constrained Beamforming Robust against Direction-of-Arrival Mismatch," *IEEE Trans. Sig. Process.*vol. 55, no. 8, pp. 4139-4150, Aug. 2007.

[88] Z. U. Khan, A. Naveed, A.Safeer, and F. Zaman, "Diagonal loading of robust general-rank beamformer for direction of arrival mismatch," *R. J. Applied Sc., Eng., Tech.* vol. 5, no. 17, pp. 4257-4263, May, 2013.

[89] L. C. Godara, *Smart Antennas,* CRC Press, 2004.

[90] R. Elliott, "Array Pattern Synthesis," *IEEE Antennas Prop. Society Newsletter*, vol. 27, no. 5, pp. 4-9, Oct. 1985.

[91] S. Boyd and L. Vandenbergh, *Convex Optimization*, Cambridge University Press, 2004.

[92] J. F. Sturm, Using SeDuMi 1.02, a MATLAB toolbox for optimization over symmetric Cones. *Methods and Software, Special issue on Interior Point Methods.* 11-12: pp. 625-633, 1999.

[93] R. L. Haupt, "An introduction to genetic algorithms for electromagnetics," *IEEE Antennas Prop. Mag.*, vol. 37, pp. 7–15, Apr. 1995.

[94] A. Monorchio, S. Genovesi, U. Serra, A. Brizzi, and G. Manara, "A novel technique to optimize nonuniformly spaced arrays with low sidelobe level using a genetic algorithm," in *2005 IEEE Antennas Prop. Soc. Int. Symp. Dig.*, Jul. 2005, vol. 2B, pp. 275–278.

[95] R. A. Monzingo, and T. W. Miller, *Introduction to Adaptive Arrays.* John Wiley & Sons, New York, 1980.

[96] J. E. Hudson, *Adaptive Array Principles.* Stevenage, U.K.: Peregrinus, 1981.

[97] Z. U. Khan, A. Naveed, I. M. Qureshi, and F. Zaman, "Comparison of Adaptive Beamforming algorithms robust against direction of arrival mismatch," *J. Space Tch.*, vol. 1, no.1, pp. 28-31, Jul, 2012.

[98] A-C. Chang, C-W. Jen, and I-J. Su, " Robust Adaptive Array Beamforming Based on Independent Component Analysis with Regularized Constraints," *IEICE Trans. Comm.*, vol. E90-B, no. 7, pp. 1791-1800, Jul, 2007.

[99] J. Liu, A. B. Gershman, Z-Q. Luo, and K. M. Wong, "Adaptive Beamforming with Sidelobe Control: A Second-Order Cone Programming Approach," *IEEE Sig. Process. Letters*, vol. 10, no. 11, pp. 331-334, Nov. 2003.

[100] Y. Zhang, B. P. Ng., and Q. Wan, "Sidelobe suppression for adaptive beamforming with sparse constraint on beam pattern," *Electronics Letters*, vol. 44, no. 10, pp. 615-616, 8th May, 2008.

[101] C-Y. Tseng, and L. J. Griffiths, "A Unified Approach to the Design of Linear Constraints in Minimum Variance Adaptive Beamformers," *IEEE Trans. Antennas Prop.*, Vol. 40, No. 12, 1533-1542, Dec. 1992.

[102] L. J. Griffiths, and K. M. Buckley, "Quiescent pattern control in linearly constrained adaptive arrays," *IEEE Trans. Acoust., Speech, Sig. Proces.*, vol. ASSP-35, pp. 917-926, July 1987.

[103] C. C. Lee, and J. H. Lee, "Robust Adaptive Array Beamforming Under Steering Vector Errors," *IEEE Trans. Antennas Prop.*, vol. 45, no. 1, pp. 168-175, Jan. 1997.

[104] A. B. Gershman, "Robustness issues in adaptive beamforming and high-resolution direction finding," Chapter in the book *High-Resolution and Robust Signal Processing*. Y. Hua, A. B. Gershman, and Q. Cheng, Eds., Marcel Dekker, 2003.

[105] J. Li and P. Stoica, Eds., *Robust Adaptive Beamforming*, New York: Wiley, 2006.

[106] Z. L. Yu, W. Ser, M. H. Er, Z. Gu, and Y. Li, " Robust Adaptive Beamformers Based on Worst-Case Optimization and Constraints on Magnitude Response," *IEEE Trans. Sig. Process.*, vol. 57, no. 7, pp. 2615-2627, Jul. 2009.

[107] J. R. Guerci, *Space-Time Adaptive Processing.* Norwood, MA: Artech House, 2003.

[108] S. Valaee, B. Champagne, and P. Kabal, "Parametric Localization of Distributed Sources," *IEEE Trans. Sig. Process.*, vol. 43, no. 9, pp. 2144-2153, Sep. 1995.

[109] E. K. Hung, and R. M. Turner, "A Fast Beamforming Algorithm for Large Arrays," *IEEE Trans. Aerosp. Elect. Syst.* vol. 24, pp. 397-401, Jul. 1988.

[110] ——, "Performance Analysis of the Minimum Variance Beamformer," *IEEE Trans. Sig. Process.*, vol. 44, no. 4, pp. 928-937, Apr. 1996.

[111] L. Du, J. Li, and P. Stoica, "Fully Automatic Computation of Diagonal Loading Levels for Robust Adaptive Beamforming," *IEEE Trans. Aerosp. Elect. Syst.*, vol. 46, pp. 449-458, 2010.

[112] S. A. Vorobyov, A. B. Gershman, & Z. Q. Luo, "Robust Adaptive Beamforming Using Worst-Case Performance Optimization: A Solution to the Signal Mismatch Problem," *IEEE Trans. Sig. Process.*, vol. 52, pp. 313-324, 2003.

[113] Y. I. Abramovich, "Controlled method for adaptive optimization of filters using the criterion of maximum SNR," *Radio Eng. Elect. Physics*, vol. 26, pp. 87-95, March 1981.

[114] H. L. Van Trees, *Optimum Array Processing*, John Wiley & Sons, New York, USA, 2002.

[115] Y. Meng, P. Stoica, and K. M.Wong, "Estimation of the directions of arrival of spatially dispersed signals in array processing," *Proc. Inst. Elect. Eng. Radar, Sonar Navigat.*, vol. 143, pp. 1–9, Feb. 1996.

[116] T. Trump, and B. Ottersten, "Estimation of nominal direction of arrival and angular spread using an array of sensors," *Sig. Process.*, vol. 50, pp. 57–69, Apr. 1996.

[117] K. I. Pedersen, P. E. Mogensen, and B. H. Fleury, "Spatial channel characteristics in outdoor environments and their impact on BS antenna system performance," in *Proc. 48th IEEE Veh. Tech. Conf.*, 18-21 May 1998, vol. 2, pp. 719–723.

[118] K. I. Pedersen, P. E. Mogensen, and B. H. Fleury, "A stochastic model of the temporal and azimuthal dispersion seen at the base station in outdoor propagation environments," *IEEE Trans. Veh. Technol.*, vol. 49, pp. 437–447, Mar. 2000.

[119] O. Besson, and P. Stoica, "Decoupled estimation of DOA and angular spread for a spatially distributed source," *IEEE Trans. Sig. Process.*, vol. 48, pp. 1872–1882, July 2000.

[120] S. Shahbazpanahi, S. Valaee, and M. H. Bastani, "Distributed source localization using ESPRIT algorithm," *IEEE Trans. Sig. Process.*, vol. 49, pp. 2169–2178, Oct. 2001.

[121] H. Cox, "Line array performance when the signal coherence is spatially dependent," *J. Acoust. Soc. Amer.*, vol. 54, pp. 1743–1746, June 1973.

[122] E. Y. Gorodetskaya, A. I. Malekhanov, A. G. Sazantov, and N. K. Vdovicheva, "Deep-water acoustic coherence at long ranges: Theoretical prediction and effects on large-array signal processing," *IEEE J. Ocean Eng.*, vol. 24, no.2, pp. 156–171, Apr. 1999.

[123] W. Carey, "Measurement of down-slope sound propagation from a shallow source to a deep ocean receiver," *J. Acoust. Soc. Amer.*, vol. 79, pp. 49–59, Jan. 1986.

[124] J. Ringelstein, A. B. Gershman, and J. F. Böhme, "Direction finding in random inhomogeneous media in the presence of multiplicative noise," *IEEE Sig. Process. Letters*, vol. 7, pp. 269–272, Oct. 2000.

[125] D. R. Morgan, and T. M. Smith, "Coherence effects on the detection performance of quadratic array processors with application to large-array matched-field beamforming," *J. Acoust. Soc. Amer.*, vol. 87, no. 2, pp. 737–747, Feb. 1988.

[126] O. Besson, F. Vincent, P. Stoica, and A. B. Gershman, "Maximum likelihood estimation for array processing in multiplicative noise environments," *IEEE Trans. Sig. Process.*, vol. 48, no. 9, pp. 2506–2518, Sept. 2000.

[127] A. Paulraj, and T. Kailath, "Direction of arrival estimation by eigenstructure methods with imperfect spatial coherence of wave fronts," *J. Acoust. Soc. Amer.*, vol. 83, no. 3, pp. 1034–1040, Mar. 1988.

[128] R. J. Mailloux, "Covariance matrix augmentation to produce adaptive array pattern troughs," *Elect. Letters*, vol. 31, no. 10, 771-772, May 1995.

[129] M. Zatman, "Production of adaptive array troughs by dispersion synthesis", *Elect. Letters*, vol. 31, no. 25, pp. 2141–2142, Dec. 1995.

[130] P. Stoica, and R. L. Moses, *Introduction to Spectral Analysis*, Prentice-Hall, Englewood Cliffs, NJ, 1997.